Identification of a novel synaptic G protein-coupled receptor controlling nicotine dependence and withdrawal

Inaugural-Dissertation

to obtain the academic degree

Doctor rerum naturalium (Dr. rer. nat.)

Submitted to the Department of Biology, Chemistry and Pharmacy

of the Freie Universität Berlin

by

Beatriz Antolin Fontes

from Girona, Spain

Berlin, March 2014

This work was carried out in the period from June 2010 until March 2014 under the supervision of Dr. Inés Ibañez-Tallon and Prof. Dr. Constance Scharff at the Max-Delbrück-Center for Molecular Medicine (MDC) in Berlin and at The Rockefeller University in New York.

1st Reviewer: Dr. Inés Ibañez-Tallon

2nd Reviewer: Prof. Dr. Constance Scharff

Date of defense: 18.06.2014

Scientific Acknowledgments

I would like to express my sincere gratitude to all the people who made this thesis possible:

- My supervisor Dr. Inés Ibañez-Tallon: For your advice, support and supervision throughout the years. Thank you for believing in me from the first moment, for giving me the opportunity to do research in different outstanding environments and specially, for transmitting always motivation and inspiration. I could not wish for a better supervisor.
- My supervisor Prof. Dr. Constance Scharff from the Freie Universität Berlin: For your supervision and advice.
- Prof. Dr. Nathaniel Heintz: For your valuable support and for so many useful and constructive recommendations on this project.
- My fellow lab members, both current and past: Dr. Silke Frahm-Barske, Dr. Marta Slimak, Dr. Jessica Ables, Dr. Andreas Görlich, Dr. Sebastian Auer, Branka Kampfrath, Cuidong Wang, Syed Shehab, Dr. Martin Laqua, Dr. Julio Santos-Torres, Susanne Wojtke, Monika Schwarz-Harsi, and all Prof. Heintz lab members: For your help, not only in carrying out the research but also in creating such a great social work environment.
- Dr. Kunihiro Uryu and Dr. Nadine Soplop: For introducing me to the fascinating world of electron microscopy. Thank you so much for teaching me and helping me, for your advice and patience. It's been such an enjoyable experience that I am actually considering to work in this field in the future.
- Timkehet Teffera: For your invaluable assistance.
- The Max Delbrück Center for Molecular Medicine, particularly the International Program MolNeuro and its coordinator Dr. Jana Droese; Freie Universität and The Rockefeller University: For the financial, academic and technical support during these years.
- NICHD Brain and Tissue Bank for Developmental Disorders at the University of Maryland, Baltimore, MD: For providing us with human brain samples.

Personal Acknowledgments

- To great friends I met in Berlin and New York. Thank you for helping me get through the difficult times, for all the emotional support, friendship, entertainment, and caring you provided.
- Als amics/amigues de tota la vida, per ser el que sou, amics de tota la vida.
- To Jeff, Josefina and Lola: For making this roommate experience so fun and easy.
- A mi família, sobretodo a mis padres y hermanos. Gracias por el apoyo incondicional continuo, por hacerme quien soy, por animarme a dar cada uno de los pasos que necesitaba para empezar y acabar la tesis, por seguirme por la mitad del planeta y venir a visitarme incluso durante las peores tormentas de nieve. Gracias por estar siempre tan cerca y por las incontables horas en Skype.
- Al meu amor: First of all, thank you for encouraging me to make a step forward to move to Berlin. Second, thank you Dr. Perrinjaquet for being my personal consultant in western blots, immunoprecipitations and general molecular biology. Thank you for listening to all my Gpr151 stories and for giving me great advice. I el més important de tot, moltíssimes gràcies per haver-te casat amb mi dues vegades i voler casar-te amb mi moltes vegades més.

Contents

1. INTRODUCTION 8

1.1 The habenular nucleus and its output to the midbrain 8

1.1.1 Medial habenula 10

1.1.1.1 Medial habenula connectivity 10

1.1.1.2 Behavioral functions mediated by the medial habenula 12

1.1.2 Lateral habenula 15

1.1.2.1 Lateral habenula connectivity 15

1.1.2.2 Behavioral functions mediated by the lateral habenula 16

1.2 G protein-coupled receptors 18

1.2.1 Classical model of GPCR signaling 18

1.2.2 Non-canonical mechanisms of GPCR signaling 21

1.2.3 Orphan G-protein-coupled receptors 22

1.2.3.1 Ligand independent functions or constitutively active orphan receptors 22

1.3 Gpr151, also known as PGR7, GPCR-2037 or Galanin-receptor like 4 23

1.4 TRAP analysis of cholinergic MHb neurons reveals enrichment of Gpr151 25

1.5 Aims of this work 27

1.5.1 To determine the distribution of the Gpr151 protein in mouse and human brain. 27

1.5.2 To assess the subcellular ultrastructural localization of Gpr151 at habenular axonal terminals in the IPN. 27

1.5.3 To determine the signaling pathway activated by Gpr151. 28

1.5.4 To identify putative ligands of Gpr151. 28

1.5.5 To elucidate the contribution of Gpr151 to the function of the habenula using genetically modified mice. 28

2. MATERIALS AND METHODS 30

2.1 Preface 30

2.1.1 Animals 30

2.1.2 Chemicals 30

2.1.3 Buffers and solutions 32

2.1.3.1 General buffers and solutions 32

2.1.3.2 Culture media 33

2.1.3.3 Solutions for behavioral experiments 33

2.1.4 Molecular biology reagents 33

2.1.4.1 Bacteria strains 33

2.1.4.2 Cell lines 33

2.1.4.3 Plasmids 33

2.1.4.4 Primers 34

2.1.4.5 Oligonucleotides used for shRNA cloning 34

2.1.4.6 Enzymes 35

2.1.4.7 Kits 35

2.1.4.8 Antibodies 35

2.1.4.9 Peptides used for cell-based second messenger assays 36

2.1.5 Equipment and software 36

2.1.6 Statistical analyses 38

2.2 Molecular Biology protocols 38
2.2.1 Vector construction 38
2.2.2 Oligonucleotides design 39
2.2.3 Amplification of DNA fragments by PCR 39
2.2.4 Agarose gel electrophoresis 40
2.2.5 DNA purification from agarose gels 40
2.2.6 Restriction digest and subcloning 41
2.2.7 Transformation 41
2.2.8 Glycerol stock preparation 41
2.2.9 Plasmid DNA extraction 41
2.2.10 Sequencing 42
2.3 Cell culture protocols 42
2.3.1 Cell culture of HEK293T cells 42
2.3.2 Preparation of cryostocks of HEK293T for long term storage 42
2.3.3 Thawing of HEK293T cryostocks for culturing 42
2.3.4 Lentivirus production 43
2.3.5 Lentivirus concentration 43
2.3.6 Lentivirus titration 43
2.3.7 FACS analysis 44
2.3.8 Protein extraction of transfected HEK293T cells 44
2.3.9 SDS-PAGE and Western blotting 44
2.3.10 Mouse habenular primary cultures 45
2.4 Cell-Based Second Messenger Assays 46
2.4.1 Assay to measure cAMP levels 46
2.4.2 Assay to measure calcium levels 46
2.5 cAMP ELISA 47
2.6 Mouse brain stereotactic injections 48
2.7 Behavioral analysis 48
2.7.1 Conditioned Place Preference 48
2.7.2 Elevated Plus maze 49
2.7.3 Open field and light/dark test 49
2.7.4 Prepulse Inhibibition 50
2.7.5 Nicotine treatment 50
2.7.6 Nicotine Withdrawal Assessment. 51
2.8 Immunohistochemistry 51
2.8.1 Perfusion of mice 51
2.8.2 Cryosections of perfused mouse brains 51
2.8.3 Immunohistochemistry of mouse sections 51
2.8.4 Immunohistochemistry of human samples 52
2.9 Electron microscopy 52
2.9.1 Perfusion of mice 52
2.9.2 Pre-embedding immunocytochemistry 53
2.9.3 High pressure freezing and freeze substitution 54
2.9.4 Post-embedding immunocytochemistry 54
2.10 Comparative modeling and molecular docking 55

3. RESULTS 56

3.1 Gpr151 is localized at the axonal projections of habenular neurons in the mouse brain. 56
3.2 Gpr151 is expressed in the human brain with the same specific axonal compartimentalization as in mice 65
3.3 Ultrastructural sub-localization of Gpr151 in the interpeduncular nucleus. 67
3.3.1 Ultrastructure of the IPN is not altered in Gpr151-KO mice 70
3.4 Analysis of the Gpr151 signaling pathway 72
3.5 Approaches used to identify Gpr151 ligands 75
3.5.1 Cell-based assays to test the activity of galanin, galanin-like peptides and tachykinin-like peptides 75
3.5.2 Use of habenular primary cultures as a source of the ligand 77
3.5.3 Bioinformatics approach to simulate *in silico* docking of Gpr151 with a lead-like structural library of synthetic compounds 80
3.6 Contribution of Gpr151 to habenular-related behaviors 82
3.6.1 Gpr151 knockout mice showed normal locomotor activity, no anxiety-like behaviors and regular sensorimotor gating. 82
3.6.2 Gpr151 modulates nicotine reward and nicotine withdrawal 83
3.6.3 Downregulation of Gpr151 in the medial habenula increases sensitivity to nicotine 85

4. DISCUSSION 89

4.1 Gpr151 is localized at the axonal projections from habenular neurons in the mouse and the human brain. 89
4.2 Ultrastructural localization of Gpr151 at habenular presynaptic terminals in the IPN 92
4.3 Gpr151 modulates nicotine conditioned reward 95
4.4 Gpr151 modulates nicotine withdrawal 99
4.5 Gpr151 modulates cAMP levels at habenular terminals 101
4.6 Gpr151 as a novel target for smoking cessation therapies 103
4.7 Deorphanizing Gpr151 105

5. CONCLUSIONS 108

6. APPENDIX 114

6.1 Abbreviations 114
6.2 Plasmid maps 118
6.3 Index of figures 121
6.4 Index of tables 122
6.5 Publication and presentation list 124
6.6 Curriculum Vitae 125

7. REFERENCES 127

1. Introduction

According to the World Health Organization, cigarette smoking is a global health problem affecting one third of the population. The success rates for smoking cessation without pharmacological treatment are less than 5% (Stead et al., 2008). Progress has been made over the last decade in our understanding of the brain areas and circuits involved in reward and withdrawal, leading to models of addiction that assign different addictive behaviors to distinct, yet overlapping, neural circuits. Recently the habenula-interpeduncular (Hb-IPN) midbrain pathway has emerged as a new critical crossroad that influences the brain's response to nicotine. The aim of this thesis is to unveil the biological function of a novel habenular specific G protein-coupled receptor (GPCR) named Gpr151. Gpr151, also known as PGR7, GPCR-2037 or Galanin-receptor like 4 (GALR4) displays several typical features of family A type of GPCRs. Previous to the presented studies there were only reports of gene expression in the rat brain by *in situ* hybridization showing that Gpr151 mRNA expression was particularly prominent in the habenular nucleus (Berthold et al., 2003; Ignatov et al., 2004). In this thesis I present my work on the subcellular and ultrastructural localization of this receptor in habenular neurons, on the functional contribution of this receptor to habenular-related behaviors in mice deficient for Gpr151, and on the elucidation of the Gpr151 signaling pathway. I will first introduce the anatomy and connectivity of the habenula as well as the behaviors that have been ascribed to the habenula. Second, I will introduce the structure and classification of GPCRs, and the classical as well as novel mechanisms of GPCR signaling. Further, I will briefly introduce the concept of orphan GPCR and some of the limitations of the current deorphanization strategies. Finally, I will introduce how we discovered Gpr151 and present the current publications in this emerging field.

1.1 The habenular nucleus and its output to the midbrain

The habenula is a small bilateral structure located in the epithalamic region of the diencephalon. Together with its associated afferent and efferent tracts, it forms part of the dorsal diencephalic conduction system, which connects the limbic forebrain with nuclei in the midbrain and hindbrain (Sutherland, 1982). The habenula is phylogenetically highly conserved across vertebrates. In fishes, amphibian, and

reptiles, the right and left sides of the habenula exhibit a remarkable asymmetry in size, molecular properties, connectivity and associated behaviors (Aizawa et al., 2005; Concha and Wilson, 2001; Dadda et al., 2010).

In birds and mammals, the habenula is located on the posterior medial end of the dorsal thalamus, adjacent to the third ventricle (Fig. 1). It has been subdivided into the medial habenula (MHb) and the lateral habenula (LHb) (Andres et al., 1999), each having different anatomical connections and serving different functions (Herkenham and Nauta, 1977, 1979; Klemm, 2004; Lecourtier and Kelly, 2007).

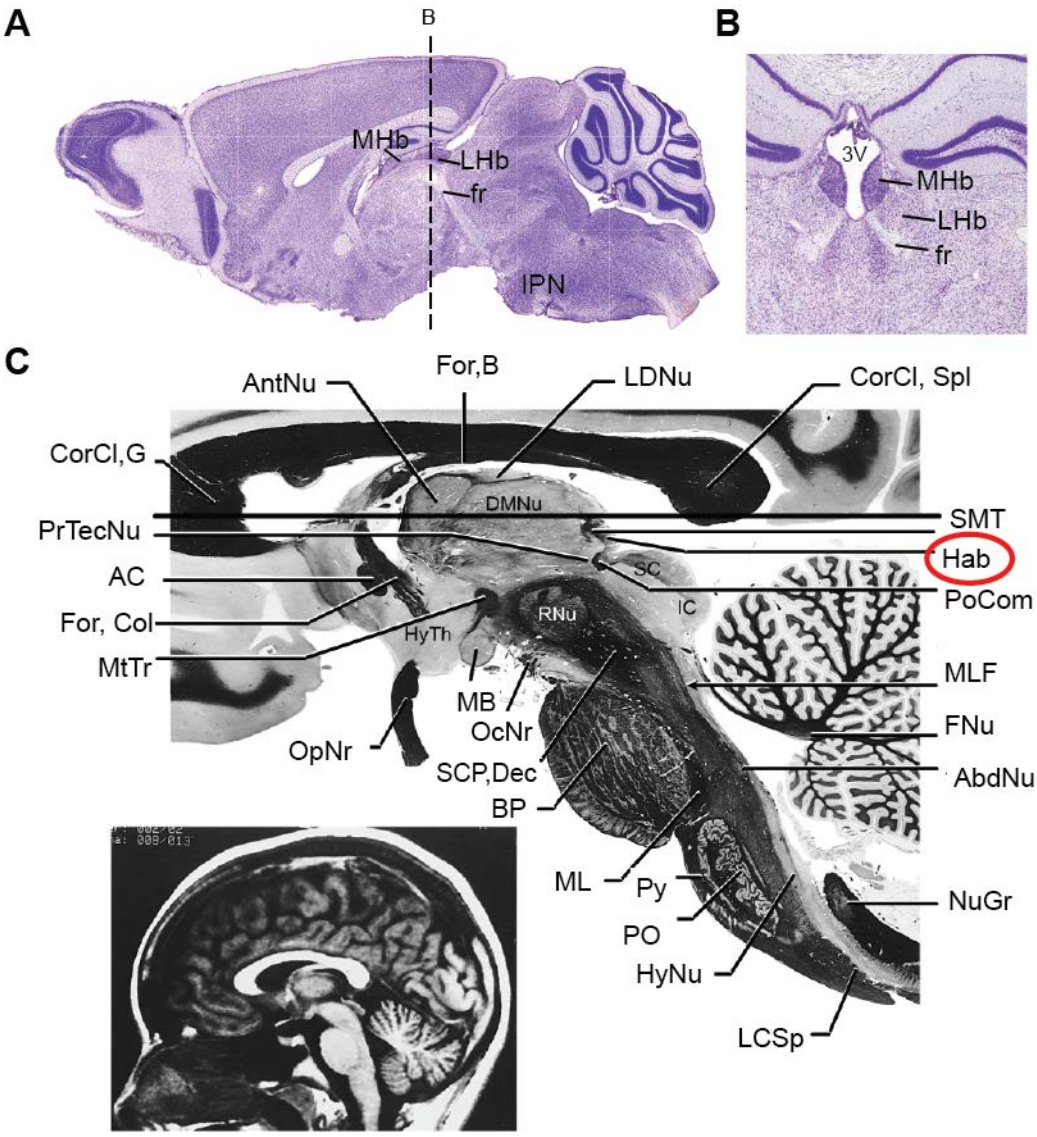

Figure 1. Habenula neuroanatomy.

(A) Sagittal section of a mouse brain showing the medial habenula (MHb), lateral habenular (LHb), fasciculus retroflexus (fr) and interpeduncular nucleus (IPN). (B) Coronal section of a mouse brain at the coordinates indicated with a dashed line in A. A-B are taken from images by (Paxinos and Franklin, 2001). (C) Sagittal section of a human brain and a corresponding T1-weigthed magnetic resonance image. Images are taken from (Haines, 2000). AbdNu, abducens nucleus; AC, anterior commissure; AntNu, anterior nucleus of thalamus; BP, basilar pons; CorCl,G, corpus callosum, genu;

CorCl,Spl, corpus callosum, splenium; DMNu, dorsomedial nucleus of thalamus; FNu, fastigial nucleus; For,B, fornix, body; For,Col, fornix, column; Hab, habenular nuclei; HyNu, hypoglossal nucleus; HyTh, hypothalamus; IC, inferior colliculus; LCsp, lateral corticospinal tract; LDNu, lateral dorsal nucleus; MB, mammillary body; ML, medial lemniscus; MLF, medial longitudinal fasciculus; MtTr, mammillothalamic tract; NuGr, nucleus gracilis; OcNr, oculomotor nerve; OpNr, optic nerve; PO, principal olivary nucleus; PoCom, posterior commissure; PrTecNu, pretectal nuclei; Py, pyramid; RNu, red nucleus; SC, superior colliculus; SCP,Dec, superior cerebellar peduncle, decussation; SMT, stria medullaris thalami; TroNr, trochlear nerve.

1.1.1 Medial habenula

1.1.1.1 Medial habenula connectivity

The MHb receives input mainly from the septum through the stria medularis (SM) and projects to the interpeduncular nucleus (IPN) through the fasciculus retroflexus (FR) (Herkenham and Nauta, 1979; Qin and Luo, 2009; Swanson and Cowan, 1979).

MHb afferents derive mostly from the posterior septum (Fig. 2), specifically from the septofimbrial nucleus (SFi), the triangular septum (TS) and the bed nucleus of the anterior commissure (BAC) (Herkenham and Nauta, 1977). Topographic connections have been revealed from the TS and the BAC to the ventral and dorsal subnuclei of the medial habenula (vMHb and dMHb) respectively (Yamaguchi et al., 2013). The MHb also receives input from the medial septum (MS) and nucleus of diagonal band (NDB) in the basal forebrain; from the interfascicular nucleus of the ventral tegmental area (VTA)(Phillipson and Pycock, 1982) and from the mesencephalic raphe in the midbrain (Herkenham and Nauta, 1977; Staines et al., 1988). Tracing and genetic studies showed that the MHb receives GABAergic input from the MS and NDB and glutamatergic and ATP-ergic input from the TS (Qin and Luo, 2009; Robertson and Edwards, 1998). In addition, the input from the posterior septum is likely to be cholinergic (Contestabile and Fonnum, 1983).

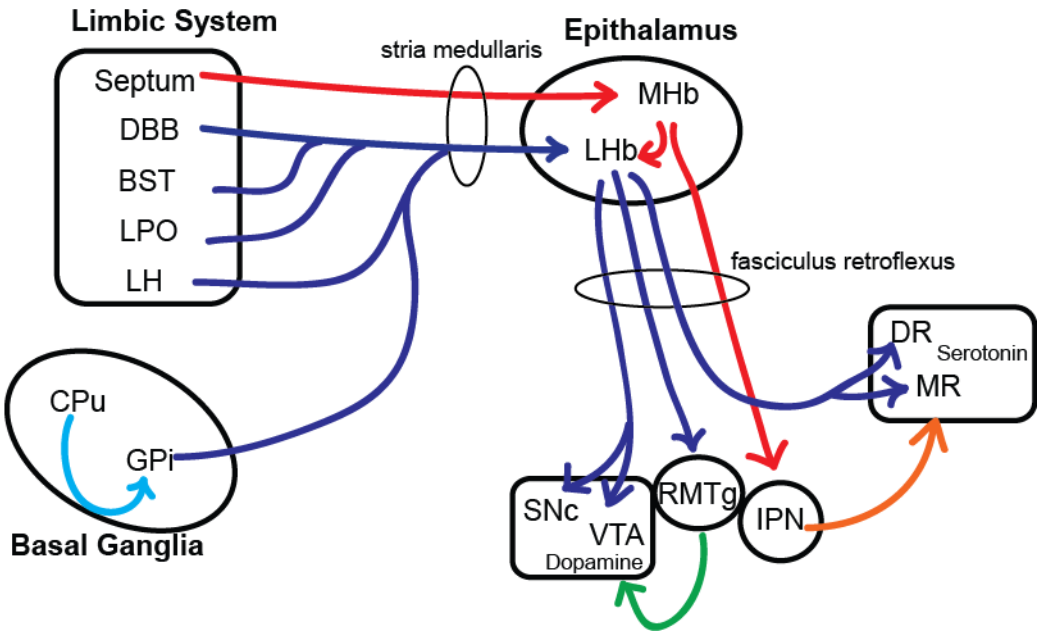

Figure 2. Connectivity of the habenula.

The MHb receives inputs mainly from the limbic system and sends outputs to the interpeduncular nucleus (IPN), which projects to the raphe nuclei. The LHb receives inputs mostly from the basal ganglia and sends outputs to brain structures that contain dopaminergic and serotonergic neurons, partly through the rostromedial tegmental nucleus (RMTg). Red and blue lines indicate the axonal connections associated with the MHb and LHb, respectively. BST, Bed Nucleus of Stria Terminalis; CPu, caudate and putamen; DBB, diagonal band of Broca; DR, dorsal raphe; GPi, globus pallidus internus; LPO, lateral preoptic area; LH, lateral hypothalamus; MR, median raphe; PFC, prefrontal cortex; SNc, substantia nigra pars compacta; VTA, ventral tegmental area. Modified from (Hikosaka, 2010).

The MHb has been subdivided in the ventral (vMHb) and the dorsal (dMHb) parts which display different molecular markers and connectivity. Neurons in the dMHb express the neuropeptide Tachykinin 1 (substance P: SP) (Contestabile et al., 1987; Cuello et al., 1978) and project to the rostral and lateral subnuclei of the IPN (Contestabile et al., 1987), while neurons in the vMHb express the acetylcholine synthesizing enzyme choline acetyltransferase (ChAT) and project to the central and intermediate subnuclei of the IPN (Contestabile et al., 1987).

A small subpopulation of MHb neurons does not project to the IPN but has been shown to innervate the LHb and medial dorsal thalamic nucleus (Kim and Chang, 2005). Kim et al., filled habenular cells with biocytin and analyzed their morphology and branching. They found two distinct intrinsic circuits in the MHb, one projecting selectively to the medial dorsal thalamic nucleus and the other one to the LHb, suggesting a medial-to-lateral connection in the habenula (Kim and Chang, 2005).

In addition, the MHb and the pineal gland have been observed to have reciprocal connections (Ronnekleiv and Moller, 1979).

1.1.1.2 Behavioral functions mediated by the medial habenula

The MHb and its major target, the IPN, have emerged as key regions in the regulation of nicotine dependence and withdrawal (Fowler et al., 2011; Frahm et al., 2011; Salas et al., 2009). In addition a growing number of reports suggests that the MHb plays an important role in stress (Lecourtier et al., 2004; Mathuru and Jesuthasan, 2013), depression (Shumake et al., 2003) and memory (Kobayashi et al., 2013).

As part of my thesis aims to analyze the functional contributions of Gpr151 to nicotine-mediated behaviors, I will introduce in detail the neuronal circuits mediating nicotine addiction and the contribution of our group and the laboratory of Paul Kenny to the first demonstration that modulation of nicotinic acetylcholine receptors (nAChR) in the habenula resulted in altered nicotine consumption and self-administration (Fowler et al., 2011; Frahm et al., 2011; Gorlich et al., 2013; Slimak et al., 2014).

1.1.1.2.1 Neuronal circuits involved in nicotine addiction and the emerging role of the MHb-IPN tract

The reinforcing properties of nicotine have been shown to be mediated by the mesocorticolimbic dopamine system, specially by activation of nAChRs containing α4β2 and α7 subunits located in VTA dopaminergic neurons (Corrigall et al., 1992; Ikemoto et al., 2006; Maskos et al., 2005; Picciotto et al., 1998; Tapper et al., 2004). Activation of dopaminergic neurons in the VTA induces an increase of forebrain dopamine transmission, particularly in the shell region of the nucleus accumbens (NAc). The increase of dopamine in the NAc shell is considered to contribute to the reinforcing properties of addictive drugs (Iyaniwura et al., 2001; Nisell et al., 1997; Pontieri et al., 1996). Besides mediating reward and behavioral reinforcement, the mesocorticolimbic dopamine pathway is also critical for the aversive effects of nicotine. Two different populations of dopaminergic neurons in the VTA have been found to encode reward and aversion separately: the population that receives cholinergic inputs from the laterodorsal tegmental nucleus and projects to the NAc shell contributes to the reward behavior; whereas the population that receives inputs from the LHb and projects to the medial prefrontal cortex contributes to signaling aversive effects (Lammel et al., 2012).

In addition to the mesocorticolimbic dopamine system, cumulative evidence suggests that the MHb-IPN pathway plays an important role in nicotine intake, nicotine aversion and nicotine withdrawal. MHb and IPN neurons express high levels of the α5, α3 and β4 nAChR subunits (Gorlich et al., 2013; Hsu et al., 2013; Sheffield et al., 2000). Noteworthy genome-wide association studies (GWAS) have linked single nucleotide polymorphisms (SNP) within the gene cluster CHRNA5-CHRNA3-CHRNB4 (that encodes the α5, α3 and β4 nAChR subunits) to heavy smoking, nicotine dependence, and smoking related diseases in humans (Berrettini et al., 2008; Bierut et al., 2008; Lips et al., 2010; Liu et al., 2010; Ware et al., 2011). Strikingly, the polymorphism in CHRNA5 (rs16969968) that results in the amino acid substitution aspartic acid to asparagine (D398N) in the α5 subunit, more than doubles the risk of tobacco dependence in those carrying two copies of the risk allele (Berrettini et al., 2008; Bierut et al., 2008; Grucza et al., 2008; Stevens et al., 2008). We demonstrated that transgenic mice for this gene cluster, overexpressing the β4 nAChR subunit (called Tabac mice), display enhanced sensitivity to the aversive properties of nicotine and reduced nicotine consumption (Frahm et al., 2011). Molecularly, β4 is rate-limiting and competes with α5 to form pentameric α3β4α5 nAChRs, thus β4 overexpression leads to increased density of α3β4* receptors at the plasma membrane, as well as to potentiation of α3β4* currents in vitro and in habenular neurons of Tabac mice (Frahm et al., 2011). Importantly, the nicotine aversion observed in Tabac mice overexpressing β4, is reversed upon viral-mediated expression in the MHb of the α5 D398N variant associated to heavy smoking in humans (Frahm et al., 2011). In addition, we recently confirmed that viral-mediated overexpression of β4 in the MHb is sufficient to produce nicotine aversion (Slimak et al., 2014). By analyzing the nicotine-mediated currents in Xenopus oocytes and hippocampal cultures, and the behavioral consequences of overexpressing different β4 SNPs in the habenula of wildtype mice, we found that increased β4-mediated nAChR currents increase aversion to nicotine, while decreased currents decrease aversion (Slimak et al., 2014). Altogether, these studies establish that the β4 subunit in the MHb-IPN pathway limits nicotine consumption (Frahm et al., 2011; Slimak et al., 2014).

In agreement with these findings, mice with null mutation in the α5 nAChR subunit gene were shown to continue to self-administer nicotine at doses that normally elicit aversion in wildtype animals. Nicotine self-administration returned to wildtype levels

when the α5 nAChR subunit was re-expressed in the MHb or the IPN (Fowler et al., 2011). Moreover, viral-mediated knockdown of α5 nAChR subunits in the MHb–IPN tract did not alter the reward-enhancing properties of lower doses of nicotine, but significantly diminished the aversive effects of higher doses in rats (Fowler et al., 2011).

In summary, animal studies and human genetic data point to nAChRs-containing α5 and β4 subunits in the MHb-IPN axis, as critical regulators to limit nicotine consumption. This has led to suggest a model in which nicotine reward and nicotine aversion are mediated by separate circuits (Fowler and Kenny, 2014): the VTA to NAc dopaminergic transmission would regulate the positive reinforcing effects of nicotine; while the MHb-IPN pathway would mediate the nicotine aversion. Moreover it has been suggested that low doses of nicotine would activate the high-affinity α4α6β2β3* nAChR subtype (Grady et al., 2007) in the mesoaccumbens pathway leading to reward; whereas high doses of nicotine would activate the lower affinity α3β4* or α5* nAChRs in the MHb-IPN tract leading to aversion (Fowler and Kenny, 2014).

In addition to nicotine aversion, the MHb-IPN axis has been involved in nicotine withdrawal. The withdrawal syndrome after chronic tobacco use manifests as a collection of affective and somatic symptoms. In humans, this includes affective symptoms such as irritability, anxiety, depressed mood, difficulty concentrating, disrupted cognition and nicotine craving; and somatic symptoms such as bradycardia, gastrointestinal discomfort and increased appetite accompanied by weight gain (reviewed in (Dani and De Biasi, 2013)). In rodent models, somatic symptoms include increased scratching, rearing, jumping, head nods, and body shakes (Damaj et al., 2003; Grabus et al., 2005), whereas affective symptoms include anxiety-like behaviors, withdrawal-induced contextual fear conditioning and withdrawal-induced conditioned place aversion (Jackson et al., 2008). Mice lacking α5 or β4 nAChR subunits show decreased somatic and affective nicotine withdrawal symptoms (Salas et al., 2004). Moreover, microinjection of the nAChR antagonist mecamylamine into the habenula and IPN is sufficient to precipitate nicotine withdrawal symptoms in mice chronically treated with nicotine (Salas et al., 2009). A recent study in mice showed that induction of somatic nicotine withdrawal signs activates GABAergic neurons in the IPN and that this activation is likely to be mediated by glutamate release from MHb terminals. Moreover, optogenetic stimulation of GABAergic

neurons in the IPN was sufficient to elicit physical withdrawal signs in both nicotine-naive and chronic-nicotine-exposed mice (Zhao-Shea et al., 2013).

In agreement with the involvement of the MHb-IPN tract in nicotine withdrawal, we demonstrated that cholinergic MHb neurons display spontaneous tonic firing of 2–10 Hz generated by hyperpolarization-activated cyclic nucleotide-gated (HCN) pacemaker channels and that infusion of the HCN pacemaker antagonist ZD7288 in the habenula precipitates somatic and affective signs of withdrawal. This pacemaking activity was increased by nicotine via activation of α3β4-containing nAChRs and was not changed in mice treated with chronic nicotine. However the frequency of pacemaking activity in these neurons was further potentiated by exposure to nicotine in mice undergoing nicotine withdrawal. These findings demonstrated that the pacemaking mechanism of cholinergic MHb neurons modulates nicotine withdrawal (Gorlich et al., 2013).

1.1.2 Lateral habenula

1.1.2.1 Lateral habenula connectivity

The LHb displays a broader connectivity than the MHb (Fig. 2). It receives inputs mainly from the basal ganglia and the limbic forebrain. The major input from basal ganglia is the entopeduncular nucleus (EP, which is the non-primate equivalent of the globus pallidus internus). The second major input derives from the lateral preoptic area and lateral hypothalamus (Herkenham and Nauta, 1977). Furthermore, the LHb receives inputs from the diagonal band of Broca, the lateral septal nucleus, the nucleus accumbens, the medial frontal cortex (Greatrex and Phillipson, 1982); parts of the extended amygdala, including the bed nucleus of the stria terminalis (Herkenham and Nauta, 1977) and the suprachiasmatic nucleus (Buijs, 1978; Sofroniew and Weindl, 1978) (Fig. 2). In addition, it receives ascending projections from the median raphe and locus coeruleus (Gottesfeld, 1983; Herkenham and Nauta, 1977; Vertes et al., 1999), and from the interfascicular and paranigral nuclei of the VTA (Gruber et al., 2007; Phillipson and Pycock, 1982; Stamatakis et al., 2013).

LHb efferents enter the FR and compose the mantle portion of the bundle. Some axons terminate in the IPN (Goncalves et al., 2012; Kim and Chang, 2005); the rest split from the FR and turn to terminate in midbrain and hindbrain nuclei (Kim and

Chang, 2005). The LHb contains mainly glutamatergic neurons (Aizawa et al., 2012) in addition to some GABAergic and cholinergic cells (Herkenham and Nauta, 1979; Lecourtier and Kelly, 2007).

The LHb projects predominantly to the raphe nuclei, the substantia nigra, the VTA (Herkenham and Nauta, 1979) and the rostromedial tegmental nucleus (Goncalves et al., 2012; Jhou et al., 2009b; Kaufling et al., 2009) (Fig. 2).

Other efferent targets of the LHb include several thalamic nuclei (centromedial, mediodorsal, ventromedial, parafascicular nucleus), the nucleus incertus (Goto et al., 2001; Olucha-Bordonau et al., 2003), the superior colliculus, the dorsal tegmental region, the locus coeruleus, the lateral hypothalamic area, the lateral preoptic area, the substantia innominata, the ventrolateral septum (Herkenham and Nauta, 1979; Lecourtier and Kelly, 2007) and the periaqueductal gray (Li et al., 1993; Xie et al., 1998). Many of the LHb targets send afferents to the LHb, establishing feedback circuits.

1.1.2.2 Behavioral functions mediated by the lateral habenula

Recent studies have suggested that the LHb controls cognitive and motor behaviors based on the motivational values associated with the behaviors. LHb neurons encode negative reward prediction errors contrary to dopaminergic neurons (Matsumoto and Hikosaka, 2007). In response to aversive events (for example, unexpected punishments or omission of expected rewards), activation of LHb neurons precedes the inhibition of dopaminergic neurons, indicating a modulation of dopaminergic neurons by LHb neurons (Matsumoto and Hikosaka, 2007). These results are in accordance to previous studies showing that stimulation of LHb strongly inhibits dopamine neurons in the substantia nigra pars compacta (SNc) and the VTA (Christoph et al., 1986; Ji and Shepard, 2007; Lisoprawski et al., 1980). In contrast, pharmacological inhibition or lesions of the LHb increase dopamine release in the striatum (Lecourtier et al., 2008; Nishikawa et al., 1986).

Significant attention has been recently given to the rostromedial tegmental nucleus (RMTg, also referred to as the tail of the VTA) as the intermediary structure mediating the inhibition that LHb exerts onto midbrain dopaminergic neurons. In primates, the RMTg has been shown to mediate the negative reward signals from the LHb to dopamine neurons (Hong et al., 2011). Optogenetic activation of LHb glutamatergic

terminals in the RMTg of mice promotes active, passive and conditioned behavioral avoidance (Stamatakis and Stuber, 2012).

Moreover, functional magnetic resonance imaging (fMRI) studies performed in healthy human volunteers provided evidence that the habenula is activated in response to unexpected negative feedback or absence of expected positive feedback (Li et al., 2008; Noonan et al., 2011; Salas et al., 2010; Shepard et al., 2006; Ullsperger and von Cramon, 2003). Another fMRI study in humans further demonstrated a feed-forward connectivity between the habenula and the VTA/SN (Ide and Li, 2011).

Collectively, these data suggest that the LHb, in collaboration with dopaminergic nuclei, has a fundamental role in the motivational aspects of reinforcement learning and decision-making.

The LHb has also emerged recently as a key region in the pathophysiology of both depression and schizophrenia (reviewed in (Shumake and Gonzalez-Lima, 2003)). Serotonin neurons in the dorsal raphe, known to be involved in depression, are inhibited by stimulation of the habenula (Park, 1987; Reisine et al., 1982; Wang and Aghajanian, 1977). In agreement, increased LHb metabolism and reduced brain serotonin levels have been observed in several animal models of depression and can be diminished by antidepressant drugs (Caldecott-Hazard et al., 1988) or lesions of the LHb (Yang et al., 2008). Moreover, neuroimaging studies have identified heightened habenula activity in depressed patients (Morris et al., 1999). In fact, inactivation of the LHb by deep brain stimulation has been used in the treatment of major depressive illness (Sartorius and Henn, 2007).

In addition to its implications in depression, the LHb is thought to contribute to the pathology of schizophrenia. An increased frequency of habenular calcification has been observed in schizophrenic patients (Caputo et al., 1998; Sandyk, 1992). Interestingly, a human fMRI study showed altered activation of the habenula in schizophrenic patients (Shepard et al., 2006).

Other behavioral roles attributed to the LHb are sleep and pain regulation (reviewed in (Hikosaka, 2010)). A recent report showed that LHb activity is needed to maintain hippocampal theta oscillations (Aizawa et al., 2013), which is associated with REM sleep and spatial learning (Buzsaki, 2002) via the serotoninergic raphe (Aizawa et al.,

2013). The contribution of the habenula to pain modulation and analgesia seems to be mediated through its connections to the raphe and periaqueductal grey (PAG) (Shelton et al., 2012).

In addition to behaviors which involve the regulation of dopaminergic and serotonergic nuclei, LHb can influence sexual, maternal, feeding behaviors and circadian functions (reviewed in (Bianco and Wilson, 2009).

1.2 G protein-coupled receptors

G protein-coupled receptors (GPCRs) comprise one of the largest and most diverse protein families, encoding more than 800 genes in the human genome. GPCRs are involved in many physiological functions ranging from vision, smell, and taste to neurological, cardiovascular, endocrine, and reproductive functions. Thus, dysregulation of GPCRs is involved in the etiology of numerous diseases and disorders (Thompson et al., 2008). In fact, over 40% of prescription drugs target this type of receptor proteins (Bridges and Lindsley, 2008).

GPCRs transduce a wide variety of extracellular signals, including hormones, peptides, neuroamines, growth factors, lipids, ions, and sensory stimuli to the interior of the cell. They share a common seven-transmembrane (7TM) topology, an extracellular amino-terminus and an intracellular carboxyl-terminal domain. GPCRs can be classified into four classes based on sequence homology and functional similarity: Rhodopsin (class A), is the largest and functionally most important class and most current drug targets belong to this family (Rask-Andersen et al., 2011)); Secretin and Adhesion (class B), characterized by large N-terminal domain involved in ligand binding (Lagerstrom and Schioth, 2008); Glutamate (class C); and Frizzled/taste receptor 2 (TAS2) (Stevens et al., 2013).

1.2.1 Classical model of GPCR signaling

The canonical view of GPCRs signaling involves several steps (Fig. 3): the binding of the ligand to the GPCR promotes a conformational change in the transmembrane and intracellular domains of the receptor, which induces the coupling with the heterotrimeric G protein, composed of three subunits: the α-, β-, and γ-subunits. GPCRs act then as guanine nucleotide exchange factors (GEFs) for the α subunits of the G protein, promoting therefore the exchange of GDP for GTP. Subsequently, the

GTP-bound α subunit dissociates from the GPCR and from the βγ-complex, and the now active G-protein subunit can bind to its respective downstream effectors, including kinases, phosphatases, small GTPases, integral membrane proteins, and a multitude of additional targets (reviewed in (Luttrell, 2008)). Signaling is concluded by the hydrolysis of GTP either by the GTPase activity inherent of the Gα subunit or by the GTPase activity of proteins called Regulators of G protein Signaling (RGS proteins), which interact with the Gα subunit and stabilize the transition state for GTP hydrolysis (Ross and Wilkie, 2000).

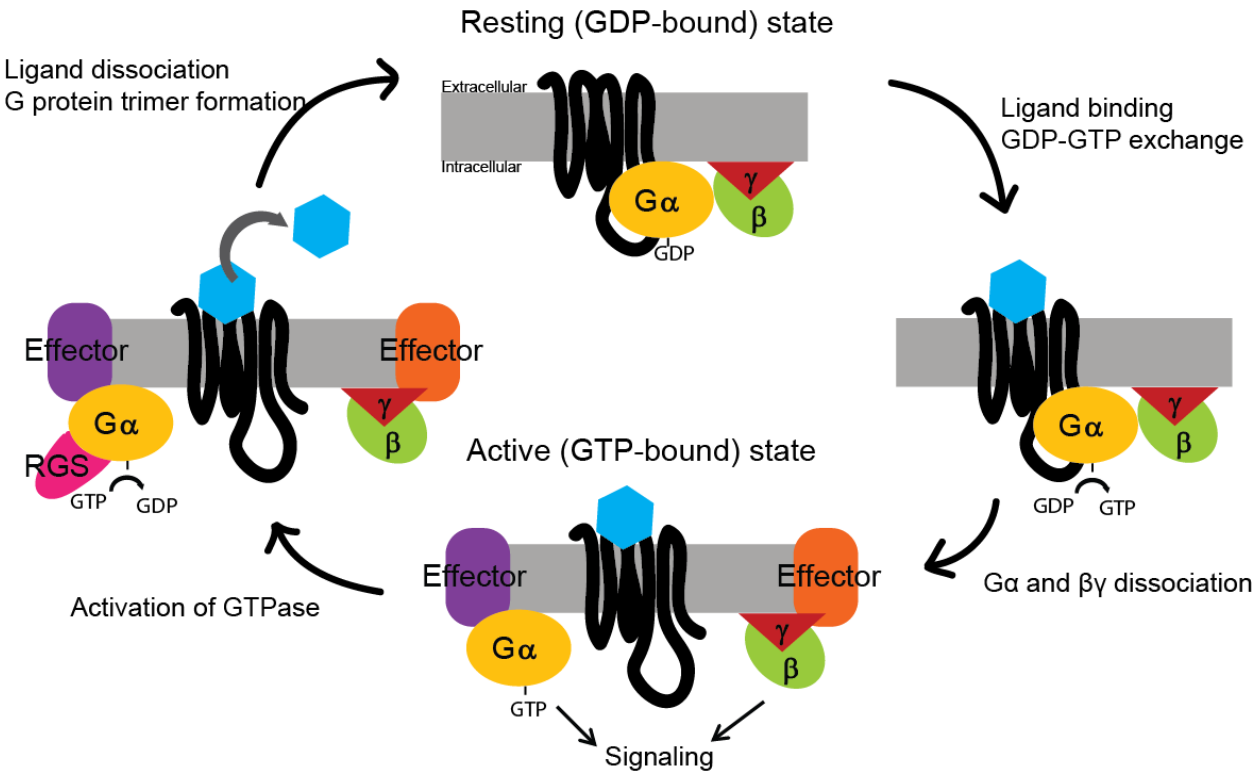

Figure 3. Representation of the classical model of GPCR signaling.

The heterotrimeric G protein dissociates into a GTP-bound Gα subunit and Gβγ heterodimer upon interaction with a ligand-bound receptor. Gα-GTP or Gβγ subunits activate then different signaling cascades. Signaling is terminated by the hydrolysis of GTP mainly by RGS proteins.

Signaling of GPCRs is terminated by phosphorylation of serine and threonine residues within the third intracellular loop and carboxyl-terminal tail of the activated receptors. Phosphorylation is catalyzed predominantly by GPCR kinases (GRKs) and promotes the translocation and binding of arrestins (most commonly β-arrestin 1 and β-arrestin 2). β-arrestins function as adaptors proteins that facilitate the targeting of receptors for clathrin-mediated endocytosis (Ferguson et al., 1996; Goodman et al., 1996). In summary, based on the classical model of GPCRs signaling, heterotrimeric

G proteins mediate signal transduction and β-arrestins mediate receptor desensitization and internalization.

The specific effectors modulated by a GPCR depend on the type of G-protein activated by the receptor. There are 18 Gα, 5 Gβ and 12 Gγ, allowing for a very large number of heterotrimeric complexes (Simon et al., 1991).

Gα subunits are subdivided into various classes, including Gαs (G stimulatory), Gαi (G inhibitory), Gαo (G other), Gαq/11, and Gα12/13. These subunits activate the following signaling pathways (Table 1):

- Gαs activates the cAMP-dependent pathway by direct stimulation of the membrane-associated enzyme adenylate cyclase.
- Gαi/o inhibits the adenylate cyclase and therefore the production of cAMP.
- Gαq activates the phospholipase Cβ, a membrane-bound enzyme that converts phosphatidylinositol-4,5-bisphosphate (PIP2) into diacylglycerol (DAG) and inositol-1,4,5-trisphosphate (IP3). IP3 is a soluble molecule that diffuses through the cytoplasm to the endoplasmic reticulum (ER). At the membrane of the ER, IP3 binds to the Ins3P receptor (Ins3PR). The binding of IP3 to InsP3R triggers the opening of the Ca^{2+} channel, and thus release of Ca^{2+} into the cytoplasm.
- Gα12/13 are involved in the Rho family GTPase signaling and modulation of cytoskeleton remodeling.

Besides the numerous effectors of Gα subunits, Gβ and Gγ can activate the phospholipases A2 and C, G-protein coupled inward rectifying potassium channels (GIRKs) and L-type calcium channels among others (reviewed in (McCudden et al., 2005)) (Table 1).

G-protein	G-protein subunit	Effector targets
Gα	$G\alpha_s$	Adenylate cyclase (+cAMP), Na^+ and Cl^- channels
	$G\alpha_{i/o}$	Adenylate cyclase (−cAMP), K^+ and Cl^- channels, phospholipases
	$G\alpha_{12/13}$	Rho proteins, Na^+/H^+ exchange
	$G\alpha_{q/11}$	Phospholipase Cβ (IP3: $+Ca^{2+}$)
Gβγ	Gβγ	Ion channels, GIRK, PI3K, phospholipases, adenylyl cyclase

Table 1. List of the primary downstream effectors activated or inhibited by each of the main G-protein subunits.

1.2.2 Non-canonical mechanisms of GPCR signaling

In addition to the classical model of GPCR signaling as a GEF factor for the Gα subunit, GPCRs can signal via G-protein independent mechanisms (Luttrell, 2008). GPCRs function as scaffolds for the recruitment of GPCR interacting proteins, which not only modulate GPCRs desensitization, endocytosis and subcellular localization; but also their function and signal transduction. There is now extensive evidence that β-arrestins act as alternative transducers of GPCR signals. β-arrestins have been shown to bind multiple mediators such as mitogen-activated protein kinases (MAPKs), SRC, nuclear factor-κB (NF-κB) and phosphoinositide 3-kinase (PI3K) (Fig. 4).

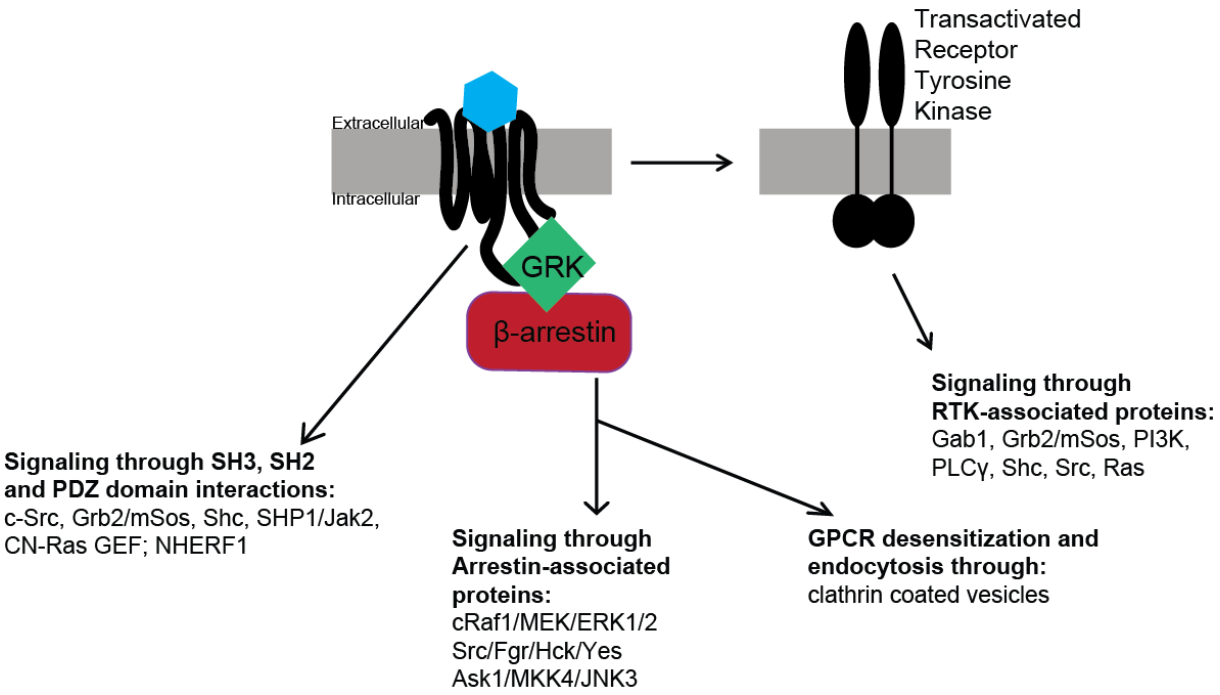

Figure 4. Non-canonical GPCR signaling mechanisms.

GPCRs mediate cell signaling by functioning as scaffolds for the recruitment of interacting proteins. Agonist activation of GPCRs promotes GRK-mediated phosphorylation and binding of β-arrestins, which mediate not only desensitization and internalization of GPCRs, but also the activation of signaling cascades. GPCRs can interact directly with SH2, SH3 or PDZ domain-containing adapters or enzymes and with 'transactivated' receptor tyrosine kinases, which activate tyrosine kinase signaling cascades and initiate Ras-dependent signaling. Adapted from (Luttrell, 2008).

In addition to β-arrestins, crosstalk between GPCRs and focal adhesions or 'transactivated' Receptor Tyrosine Kinase activates tyrosine kinase signaling cascades and initiates Ras-dependent signaling. Moreover, the intracellular domains of some GPCRs can bind directly to SH2, SH3 or PDZ domain-containing adapters or enzymes, including GEFs for small G proteins, nonreceptor tyrosine kinases, and

constituents of several of the MAP kinase pathways (reviewed in (Luttrell, 2008) and (Ritter and Hall, 2009)) (Fig. 4).

There are many additional GPCR interacting proteins, such as Shank/SSTRIP, PICK-1, MUPP1, Spinophillin, Homer proteins, AKAP 79/150 and 14-3-3 proteins, which bind other signaling molecules, and activate G-protein independent signaling cascades (reviewed in (Magalhaes et al., 2012).

1.2.3 Orphan G-protein-coupled receptors

Around hundred GPCRs are still “orphan receptors” meaning that their endogenous ligand has not yet been identified. Orphan GPCRs are usually given the name "GPR" followed by a number, for example GPR1. Fifty-seven class A receptors, twenty-eight class B and seven class C are still considered orphans (Davenport and Harmar, 2013). Given that GPCRs are the most important family of drug targets, it is not surprising that the pharmaceutical industry is making extensive efforts to identify functional ligands for orphan GPCRs.

The standard assays used to deorphanize GPCRs are radio-ligand binding, calcium flux, GTPγ binding, and modulation of cAMP levels. In the recent years, the reverse pharmacology strategy has been successfully used to identify the ligands of many orphan GPCRs (Howard et al., 2001), including peptides such as ghrelin, kisspeptin, orexin and hypocretin (Ozawa et al., 2010). However, deorphanization strategies have failed to identify specific ligands for around hundred orphan GPCRs. One of the limitations of the deorphanization process is that the assays used rely on monitoring changes at the second messenger level. Yet some orphan GPCRs require accessory proteins for their activity (Foord and Marshall, 1999); and therefore their ligands cannot be detected by classical strategies. There is a need for new screening assays, which take into account accessory proteins and other possible signaling mechanisms.

1.2.3.1 Ligand independent functions or constitutively active orphan receptors

Another limitation of the classical deorphanization process is the possibility that some orphan GPCRs form heterodimers with other GPCRs and function in a ligand-independent manner. Orphan GPCRs have been described to heterodimerize with GPCRs that have identified ligands, and by doing so, orphan GPCRs regulate receptor folding, maturation and transport of the non-orphan receptor to the cell

surface. Examples supporting this idea are the GABABR1/GABABR2 heterodimer (Galvez et al., 2001; Jones et al., 1998; Robbins et al., 2001), the Melatonin Receptor 1/GPR50 heterodimer (Levoye et al., 2006), and the umami and sweet taste receptors T1R1or2/T1R3 (Nelson et al., 2002; Nelson et al., 2001; Xu et al., 2004).
In the case of GABABR1 and GABABR2 heterodimer receptors, GABABR1 provides ligand-binding, while GABABR2 promotes efficient transport of GABABR1 to the cell surface and G protein coupling. Therefore GABABR2 is considered an orphan receptor in the heterodimer complex (Galvez et al., 2001; Jones et al., 1998; Robbins et al., 2001). In this context GPR156, which encodes a GABAB like receptor was proposed to function by heterodimerization with GABAB receptors. However its GABABR-like function remains to be elucidated since it could not get activated by GABA when expressed alone or with other GABAB receptor subunits (Calver et al., 2003).

In addition, other orphan GPCRs have been reported to have ligand-independent functions by being constitutively active. Constitutive active orphan receptors include the human orphan herpes virus-8-encoded receptor ORF74, which can cause Kaposi's sarcoma-like lesions due to its oncogenic potential (Rosenkilde et al., 2005; Sodhi et al., 2004); the human cytomegalovirus UL33 (Vischer et al., 2006; Waldhoer et al., 2002), Epstein-Barr virus-induced receptor 2 (Rosenkilde et al., 2006); and smoothened , which is involved in embryonic development (Riobo et al., 2006).

The fact that almost one hundred GPCRs remain orphan supports the idea that some might have ligand-independent functions. This possibility would require combinatorial complex strategies to develop novel screening assays.

1.3 Gpr151, also known as PGR7, GPCR-2037 or Galanin-receptor like 4

As mentioned earlier in the introduction, at the time I initiated the studies on Gpr151, the only information available on this receptor was its sequence and mRNA expression in the habenular nuclei by low resolution *in situ* hybridization (Berthold et al., 2003; Ignatov et al., 2004). The cloning and identification of Gpr151 was first described by Berthold et al., in 2003 (Berthold et al., 2003). Gpr151 belongs to the

family A type of GPCRs and shows highest homology with the galanin receptors 2 and 3. *In situ* hybridization in the rat brain showed that expression of Gpr151 mRNA was exclusively localized to the habenular complex, being more prominent in the MHb than in the LHb (Berthold et al., 2003). In 2004, Ignatov et al., localized Gpr151 to chromosome 5q32 in human and 18B3 in mouse (Ignatov et al., 2004). The human nucleotide sequence contained an open-reading frame of 1260 bp coding for a 419 amino-acid long protein, whereas the mouse nucleotide sequence contained an open-reading frame of 1257 bp coding for a 418 amino-acid protein. The GenBank accession number for human and mouse Gpr151 are AY351676 and AY351677, respectively (Ignatov et al., 2004).

Like all GPCR, Gpr151 contains seven transmembrane domains, an extracellular amino-terminus and an intracellular carboxyl-terminus (Fig. 5). The short amino-terminus contained no signal-peptide sequence, but two potential N-linked glycosylation sites. Phosphorylation sites for cAMP-dependent protein kinase A and protein kinase C were found in the intracellular loops and in the carboxyl-terminus. Two highly conserved cysteine residues were present in the second and third extracellular loops, which are responsible for protein folding and stability by disulfide-bridge formation (Fig. 5). Interestingly, both the human and mouse Gpr151 missed the well-conserved D–R–Y motif downstream of the third transmembrane domain, which is involved in the isomerization of class A GPCRs between inactive and active conformations (Flanagan, 2005). In the human Gpr151 this motif is replaced by F–M–Y and in the mouse by F–A–Y (Ignatov et al., 2004). Northern blot analysis from mouse and human tissue demonstrated expression of Gpr151 in the spinal cord and in the brain. *In situ* hybridization experiments revealed that Gpr151 was expressed at lower levels in the peripheral nervous system, specifically in neurons of sensory ganglia (Ignatov et al., 2004). During embryonic development, Gpr151 was expressed in the habenula, but also in the striatum, the locus coeruleus, and several hindbrain nuclei. Importantly, in adult mouse brain Gpr151 mRNA expression was shown to be restricted to the habenula (Ignatov et al., 2004).

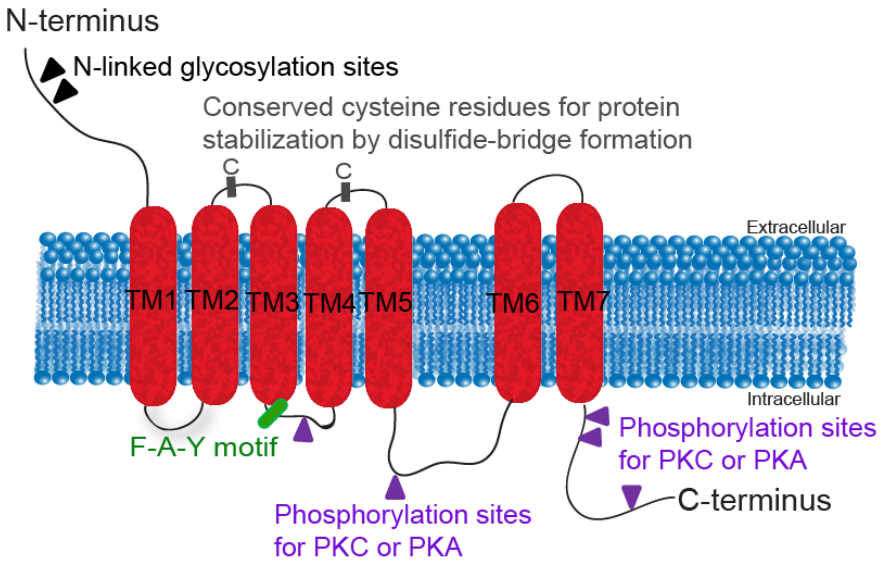

Figure 5. Schematic diagram of the mouse Gpr151 indicating sites or domains required for protein folding and activation.

Gpr151 contains seven transmembrane domains (TM1-7), an extracellular amino-terminus, an intracellular carboxyl-terminus, two potential N-linked glycosylation sites, five consensus phosphorylation sites for cAMP-dependent protein kinase A (PKA) and protein kinase C (PKC), two highly conserved cysteine residues which are responsible for protein folding and the F–A–Y motif, which replaces the well-conserved D–R–Y motif involved in the switch of class A GPCRs between inactive and active conformations (Flanagan, 2005).

1.4 TRAP analysis of cholinergic MHb neurons reveals enrichment of Gpr151

To begin to address the function of Gpr51 we wanted to determine whether Gpr151 was or not specific for a subpopulation in the habenula. As mentioned previously the MHb is subdivided in two functionally distinct ventral and dorsal parts (vMHb neurons are cholinergic, whereas neurons in the dMHb express substance P). For this purpose we analyzed the translational profile of all mRNAs from the cholinergic neurons within the mouse vMHb using the TRAP (translating ribosome affinity purification) methodology (Doyle et al., 2008; Gorlich et al., 2013). This methodology employs the EGFP-L10a ribosomal fusion protein to affinity purify the mRNAs that are being translated in the targeted cell population (Doyle et al., 2008).

As shown in Table 2, the TRAP samples obtained from habenular mouse extracts showed robust enrichment of all mRNAs known to be specifically expressed in cholinergic MHb neurons, including Chrna3, Chrnb4 and Pou4f1 (Aizawa et al., 2012; Quina et al., 2009). To identify genes that are highly specific to cholinergic MHb neurons, their transcriptional profile was compared to previously collected TRAP data from different cell types in the CNS, using the specificity index statistic (pSI <0.01)

(Doyle et al., 2008). These analyses resulted in the identification of the G protein-coupled receptor Gpr151 as highly and specifically enriched in this cell type (Gorlich et al., 2013).

	Gene Symbol	Gene Name	Specificity (pSI)	p-value	TRAP/ Total
Receptors	Chrna3	cholinergic receptor, nicotinic, alpha 3	2.72702E-06	7.41928E-06	15.0
	Chrnb4	cholinergic receptor, nicotinic, beta 4	2.72702E-06	2.85147E-05	13.7
	Gpr151	G protein-coupled receptor 151	2.72702E-06	0.000604251	6.3
	Gpr4	G protein-coupled receptor 4	2.72702E-06	5.08549E-05	3.9
	Htr5b	5-hydroxytryptamine (serotonin) receptor 5B	2.72702E-06	0.001201418	18.6
	Sstr2	somatostatin receptor 2	2.72702E-06	0.006961729	13.2
	Gfra1	glial cell line derived neurotrophic factor family receptor	1.09081E-05	4.16398E-05	41.9
	Gpr26	G protein-coupled receptor 26	0.002620671	0.000242272	33.2
	Gabbr1	GABA-B receptor 1	0.019991819	8.98934E-06	2.4
	Ror2	receptor tyrosine kinase-like orphan receptor 2	0.023328334	2.13098E-05	3.8
	GPR3	G-protein coupled receptor 3	0.052267521	0.032152315	2.5
	Epha8	Eph receptor A8	0.065173166	0.00099932	3.2
	Adrb1	adrenergic receptor, beta 1	0.075852195	0.05359426	1.6
Channels	Ano1	anoctamin 1, ca+ activated chloride channel (Tmem16)	2.72702E-06	3.33919E-06	6.9
	Cacnb3	ca+ channel, voltage-dependent, beta 3	8.18107E-06	0.000811727	7.5
	Kcnip1	Kv channel-interacting protein 1	8.18107E-06	0.000153449	8.2
	Kctd12b	K channel tetramerisation 12b	2.99973E-05	0.001887047	5.0
	Kctd8	K channel tetramerisation 8	3.54513E-05	2.76149E-05	6.1
	Kcnma1	K large cond. ca-activated channel M, a1 (BK)	0.000267248	0.0003421	3.0
	Trpm4	transient receptor potential channel, M, member 4	0.000610854	0.000266056	10.9
	Kcnd2	K voltage-gated channel, Shal-related family, member 2	0.019070085	2.25489E-05	2.4
	Kcnu1	K channel, subfamily U, member 1	0.0538042	5.59745E-05	8.5
DNA binding proteins	Irx2	Iroquois related homeobox 2 (Drosophila)	2.72702E-06	0.001252937	6.8
	Lhx9	LIM homeobox protein 9	2.72702E-06	0.008318666	1.0
	Nhlh2	nescient helix loop helix 2	2.72702E-06	6.23159E-05	3.6
	Pou4f1	POU domain, class 4, transcription factor 1	2.72702E-06	0.000140079	2.8
	Irx5	Iroquois related homeobox 5 (Drosophila)	2.99973E-05	0.002018597	6.6
	Pbx4	pre-B-cell leukemia transcription factor 4	0.000158167	0.000189643	31.0
Peptides/ Hormones	Nppa	natriuretic peptide A	2.72702E-06	4.90578E-05	13.7
	Tac2	tachykinin 2 (neurokinin B)	2.72702E-06	0.002540945	6.4

Table 2. Selected transcripts enriched in cholinergic MHb neurons.

Descriptions of columns are as follows: Gene Symbol and Description as assigned to the IDs by DAVID (Huang da et al., 2009); Specificity index (pSI), a measure of the uniqueness of the expression of this gene in the TRAP sample compared with all previously collected cell types (Doyle et al., 2008); p-value, FDR adjusted P value for TRAP vs. Total comparison, as calculated by Limma module of Bioconducter; TRAP/Total, ratio of expression between TRAP purified RNA from cholinergic MHb to total RNA from the dissection. Table adapted from (Gorlich et al., 2013).

1.5 Aims of this work

This project aims to identify the biological function of the orphan habenular receptor Gpr151. This work was conceived based on our finding that Gpr151 is highly enriched in cholinergic medial habenular neurons compared to other cell types in the CNS (Gorlich et al., 2013). As described in the following detailed aims, this work starts with the characterization of Gpr151 localization in the mouse and human brain, including Gpr151 ultrastructural localization in the IPN. This work extends to the analysis of the Gpr151 signaling pathway and Gpr151 putative ligands. And finally this project aims at identifying the functional contributions of Gpr151 to habenular-mediated behaviors, specifically related to nicotine dependence and withdrawal.

1.5.1 To determine the distribution of the Gpr151 protein in mouse and human brain.

Different commercial Gpr151 antibodies were tested for immunohistochemical analysis of mouse brain sections. Two of the antibodies tested were successfully used to determine the localization of Gpr151 expressing neurons and their projections in mouse brain. I next aimed to characterize the pattern of expression of Gpr151 by immunohistochemical analyses of post-mortem human brain sections containing the habenula, the fasciculus retroflexus and the interpeduncular nucleus.

1.5.2 To assess the subcellular ultrastructural localization of Gpr151 at habenular axonal terminals in the IPN.

To determine the subcellular localization of Gpr151 at presynaptic habenular terminals, I performed preembedding and postembedding immuno-electron microscopy of mouse coronal sections of the IPN (assisted by the Rockefeller Electron Microscopy core facility). To assess whether Gpr151 colocalizes with the synaptic vesicle transporters VAChT and VGlut1, we performed double immunogold labeling analysis. Finally I aimed at investigating whether deletion of Gpr151 affects the ultrastructure of the presynaptic terminals in the IPN. For this aim, I compared electron micrographs of wildtype and Gpr151 knockout (Gpr151-KO) mice.

1.5.3 To determine the signaling pathway activated by Gpr151.

The signaling pathway modulated by a GPCR depends on the type of G-protein that the receptor activates (Table 1). I aimed at identifying the G-protein that Gpr151 couples to and at analyzing whether Gpr151 activates the calcium or cAMP-dependent pathway. To accomplish this aim I performed second messenger assays with transfected human embryonic kidney (HEK293T) cells and ELISAs on mouse tissue extracts.

1.5.4 To identify putative ligands of Gpr151.

Three parallel lines of assays were carried out to search for Gpr151 ligands:

- I tested candidate peptide ligands that activate other galanin-like receptors or tachykinin-like receptors on Gpr151-transfected cells using second-messenger cell-based assays.
- Based on the hypothesis that the Gpr151 ligand could be released from habenular neurons upon their neuronal activation, I tested the supernatant of habenular neuronal cultures from mice expressing channelrhodopsin before and after blue light stimulation in Gpr151-transfected cells using second-messenger cell-based assays.
- I applied a bioinformatics docking simulation approach for *in silico* modeling of Gpr151 based on the use of multiple templates, and secondly for *in silico* screening a virtual chemical library.

1.5.5 To elucidate the contribution of Gpr151 to the function of the habenula using genetically modified mice.

I first aimed to knock down Gpr151 in the habenula of mice by injecting lentivirus containing shRNA directed against Gpr151. Given that the MHb is involved in nicotine-mediated behaviors (Fowler et al., 2011; Frahm et al., 2011; Glick et al., 2011; Salas et al., 2009), I assessed the consequences of Gpr151 knockdown in nicotine-related behaviors using behavioral assays of nicotine withdrawal and nicotine conditioned place preference.

I next aimed at assessing the behavioral consequences of Gpr151 gene deletion in Gpr151-KO mice concerning habenular and nicotine-related behaviors. I compared the behavioral results of Gpr151-KO mice and shRNA-injected mice. This comparison

was necessary to conclude whether Gpr151 is required either during development or only at adult stages for the control of nicotine related behaviors.

2. Materials and Methods

2.1 Preface

2.1.1 Animals

Mice were housed with ad libitum access to food and water in a room air conditioned at 22°C–23°C with a standard 12 hr light/dark cycle, with a maximum of five animals per cage. All experimental procedures have been carried out in accordance with ethical guidelines laid down by the local governing body.

Male CLBL/6 mice used for shRNA-injections were purchased from The Jackson Laboratory. Gpr151 knockout mice (Gpr151tm1Dgen) were obtained from Deltagen. They were backcrossed to C57BL/6 for eight generations. Male mice from 8-12 weeks were used for behavioral experiments. ChAT-ChR2-YFP BAC transgenic mice were obtained from The Jackson Laboratory (Strain name: B6.Cg-Tg(Chat-COP4*H134R/EYFP)6Gfng/J).

2.1.2 Chemicals

Table 3. List of chemicals used in this work

Name	Company
Agarose, ultra-pure	Invitrogen
Antibiotic-Antimycotic	Invitrogen
Ammonium chloride	Fisher Scientific
Ampicillin sodium salt	Sigma-Aldrich
B27-Supplement	Invitrogen (Gibco)
Betaisodona	Mundipharma
Bovine serum albumin (BSA)	Sigma-Aldrich
Bromphenolblue	Carl Roth GmbH & Co.
Calcium chloride dihydrate	Merck
Chloroform	Fisher Scientific
Citric acid, pH 6	Genemed Biotechnologies
Collagenase Type I	Sigma-Aldrich
3,3′-Diaminobenzidine tablets SigmaFast	Sigma-Aldrich
Dimethyl sulfoxide (DMSO)	Merck
dNTP-Mix	Sigma-Aldrich Chemie
EDTA disodium-dihydrate	Fisher Scientific
Ethanol	Decon Labs
Ethidium bromide	Carl Roth GmbH & Co.
FBS (fetal bovine serum)	Invitrogen (Gibco)
FuGene Transfection Reagent	Promega
D-(+)-glucose	Sigma-Aldrich
D-MEM	Invitrogen (Gibco)
DNAse I	Sigma-Aldrich
Glacial acetic acid	Fisher Scientific
GlutaMAX™	Invitrogen (Gibco)

Name	Company
Glutaraldehyde	Sigma-Aldrich
Glycine	Fisher Scientific
Glycerol	Fisher Scientific
HBSS (10x)	Invitrogen (Gibco)
HEPES	Sigma-Aldrich
Hexamethylenetetramine	Sigma-Aldrich
Hydrogen peroxide solution 30 % (w/w) in H2O	Sigma-Aldrich
Immu-Mount™	Thermo Scientific
Isopropanol	Fisher Scientific
Ketamin 10 %	WDT eG, Garbsen, Germany and Fort Dodge, Iowa, USA
Lipofectamine™ 2000	Invitrogen
ß-mercaptoethanol	Sigma-Aldrich
Mecamylamine hydrochloride	Sigma-Aldrich
Methanol	Fisher Scientific
$MgCl_2$ (50 mM)	Invitrogen
Mineral oil	Sigma-Aldrich
Neurobasal medium	Invitrogen (Gibco)
Nicotine-tartrate	Sigma-Aldrich
O.C.T.™ Tissue Tek	Sakura Finetek
Oligonucleotides	BioTeZ Berlin Buch GmbH, Berlin, Germany
Opti-MEM®	Invitrogen (Gibco)
Osmium tetroxide	Sigma-Aldrich
Paraformaldehyde	Electron Microscopy Sciences
PBS (10x)	Invitrogen (Gibco)
PCR Rxn buffer (10x)	Invitrogen
Penicillin/streptomycin	Invitrogen (Gibco)
Poly-D/L-ornithine hydrobromide	Sigma-Aldrich
Poly-L-lysine 0.01 %	Sigma-Aldrich
Potassium ferrocyanide	Sigma-Aldrich
Protease inhibitor tablets complete mini	Roche
Regephitel®	Alcon Pharma
Xylazine hydrochloride	Sigma-Aldrich
Saccharin	Sigma-Aldrich
Saponin	Sigma-Aldrich
Silver nitrate	Sigma-Aldrich
Sodium acetate anhydrous	Sigma-Aldrich
Sodium borohydride	Sigma-Aldrich
Sodium cacodylate trihydrate	Electron Microscopy Sciences
Sodium chloride	Fisher Scientific
Sodium hydrogen sulfate	Sigma-Aldrich
Sodium hydroxide	Sigma-Aldrich
Sodium tetraborate	Sigma-Aldrich
Sodium thiosulfate pentahydrate	Sigma-Aldrich
Sucrose	Sigma-Aldrich
TEA	Sigma-Aldrich
Tricaine	Sigma-Aldrich
TRIS	Fisher Scientific
Triton X-100	Sigma-Aldrich

Name	Company
Trypsin-EDTA (0.25 %)	Invitrogen (Gibco)
Trypsin inhibitor Type I-S (soybean)	Sigma-Aldrich
Tween 20	Sigma-Aldrich
Xylene cyanol	Fisher Scientific
Uranyl acetate	Sigma-Aldrich
Yeast extract	Carl Roth GmbH & Co.

2.1.3 Buffers and solutions

All buffers and solutions described below were prepared using either double-distilled water or MQ water produced with a Barnstead E-pure or Millipore water purification system. Nicotine tartrate salt solutions for nicotine drinking experiments were prepared with tap water.

2.1.3.1 General buffers and solutions

Table 4. Composition of buffers and solutions

Name	Composition
1 kb DNA ladder	1 kb plus DNA ladder (Invitrogen), 10 mM Tris-HCl, 50 mM NaCl, 1x DNA loading buffer
4% PFA	4% paraformaldehyde in 1 x PBS
6x loading dye	0.2 % Xylene cyanol, 0.2 % Bromphenolblue, 30 % Glycerol
50x TAE	242 g/l Tris base, 5.71 % (v/v) Glacial acetic acid, 0.05 M EDTA, pH 8.0
Blocking solution for immunostaining without permeabilization	1 x PBS with 10 % goat serum
Blocking solution for immunostaining with permeabilization	1 x PBS with 10 % goat serum and 0.3 % Triton X-100
Cryosection buffer	0.1 M phosphate buffer with 25% glycerol and 25 % ethylene glycol, pH 7.4
Mouse Habenular culture dissection buffer	1x HBSS with 25 mM Glucose and 15 mM HEPES
LB agar	LB-medium + 15 % (w/v) agarose
NP40 Lysis buffer (Western Blot)	50 mM Tris pH 7.4, 250 mM NaCl, 5 mM EDTA, 50 mM NaF, 1mM Na_3VO_4, 1% Nonidet P40 (NP40), 0.02% NaN_3, 1mM PMSF, 1x protease inhibitor cocktail.
PBS (10x)	80 g/l NaCl, 2 g/l KH_2PO_4, 2 g/l KCl, 21.6 g/l $Na_2HPO_4 \bullet 7H_2O$
Saline	0.9 % NaCl in MQ
TBS (10x)	0.5 M Tris/HCl pH 7.9, 1.5 M NaCl, 0.2 g/l KCl
TBS-T	TBS + 0.05 % Tween-20
TE buffer	10 mM Tris pH 8.0, 1 mM EDTA

2.1.3.2 Culture media

Table 5. Culture media used in this work

Name	Composition
LB medium	10 % Tryptone, 5 % Yeast extract, 10 % NaCl, adjusted to pH 7.0
Mammalian cell culture medium	10 % FBS in D-MEM with GlutaMAX™
Mouse habenular culture start medium	Neurobasal medium with 1x B27-supplement,1x Antibiotic/Antimycotic, GlutaMAX (0.5mM), glutamate (0.01 mM), 1% FBS
Mouse habenular culture medium	Neurobasal medium with 1x B27-supplement,1x Antibiotic/Antimycotic, GlutaMAX (0.5mM)

2.1.3.3 Solutions for behavioral experiments

Table 6. Solutions used for chronic nicotine treatment experiments

Name	Composition
Nicotine drinking solution	500µg/l of nicotine tartrate salt and 0.2% of saccharin in tap water
Saccharin drinking solution	0.2% of saccharin in tap water

2.1.4 Molecular biology reagents

2.1.4.1 Bacteria strains

Table 7. Bacteria strains used in this work

Name	Genotype
E.coli TOP10	F-*mcr*A Δ(*mrr-hsd*RMS-*mcr*BC) φ80*lac*ZΔM15 Δ*lac*X74 *rec*A1 *ara*D139 Δ(*ara*leu) 7697 *gal*U *gal*K *rps*L (StrR) *end*A1 *nup*G
E.coli DH5α	F-φ80*lac*ZΔM15Δ(*lac*ZYA-*arg*F)U169 *rec*A1 *end*A1 *hsd*R17(rk^-, mk^+) *pho*A *sup*E44*thi*-1 *gyr*A96 *rel*A1 *ton*A
E.coli Hb101	F- *sup*E44, *hsd*S20(r_B^-,m_B^-), *rec*A13, *ara*-14, *pro*A2, *lac*Y1, *gal*K2, *rps*L20, *xyl*-5, *mtl*-1, *leu*B6, *thi*-1

2.1.4.2 Cell lines

Table 8. Cell lines used in this work

Name	Source	Affiliation/Address
HEK 293TN	System Biosciences (SBI)	Mountain View, CA, USA

2.1.4.3 Plasmids

Table 9. Plasmids used in this work

Name	Source
pCS2+	Addgene Inc.
pFUGW	Addgene Inc.
pCMV-HA	Clontech Laboratories

Name	Source
pSicoR-GFP	Addgene Inc.
Lentiviral packaging plasmids pLP1, pLP2, pLP-VSV-G	ViraPower™ Lentiviral expression system; Invitrogen GmbH (Gibco)

2.1.4.4 Primers

Table 10. Primers used in this work

Name	Sequence 5‘- 3‘	Purpose
Gpr151-BglII-F	CATAGATCTCCATGGGAAAGGCAATGCTGAGAG	pCMV-HA-Gpr151cloning
Gpr151-XhoI-R	CATCTCGAGTTAATTGCAGCCCTCTGTCTCTTG	pCMV-HA-Gpr151cloning
Gpr151-AgeI-F	CATACCGGTGCCACCATGTACCCATACGATG	pFU-HA-Gpr151 cloning
Gpr151-BsrGI-R	CATTGTACATTAATTGCAGCCCTCTGTCTC	pFU-HA-Gpr151 cloning
Gfp-F	GCA CGA CTT CTT CAA GTC CGC CAT GCC	EGFP genotyping
Gfp-R	GCG GAT CTT GAA GTT CAC CTT GAT GCC	EGFP genotyping
Gpr151-F	CGT GGG AAA CCT GTG TGT GAT TGG	Gpr151-KO genotyping
Gpr151-wt-R	AGT CAG AGG ACT TGC AGA TGA ACC	Gpr151-KO genotyping
Gpr151-KO-R	GGG TGG GAT TAG ATA AAT GCC TGC TCT	Gpr151-KO genotyping

2.1.4.5 Oligonucleotides used for shRNA cloning

Table 11. Oligonucleotides used for shRNA knockdown of Gpr151

Name	Sequence 5‘- 3‘	Purpose
shRNA1-F	TGCCAAGAGCTTGACATTTGTTTTCAAGAGAAACAAATGTCAAGCTCTTGGCTTTTTTC	pSicoR-shRNA1
shRNA1-R	TCGAGAAAAAAGCCAAGAGCTTGACATTTGTTTCTCTTGAAAACAAATGTCAAGCTCTTGGCA	pSicoR-shRNA1
shRNA2-F	TGTCACGCAGGTGTGGAAATGTTTCAAGAGAACATTTCCACACCTGCGTGACTTTTTTC	pSicoR-shRNA2
shRNA2-R	TCGAGAAAAAAGTCACGCAGGTGTGGAAATGTTCTCTTGAAACATTTCCACACCTGCGTGAA	pSicoR-shRNA2
shRNA3-F	TGGCGAGCTTATGACCAATGTATTCAAGAGATACATTGGTCATAAGCTCGCCTTTTTTC	pSicoR-shRNA3
shRNA3-R	TCGAGAAAAAAGGCGAGCTTATGACCAATGTATCTCTTGAATACATTGGTCATAAGCTCGCCA	pSicoR-shRNA3
shRNA4-F	TGAGGCACCTGCTGGAAACACATTCAAGAGATGTGTTTCCAGCAGGTGCCTCTTTTTTC	pSicoR-shRNA4
shRNA4-R	TCGAGAAAAAAGAGGCACCTGCTGGAAACACATCTCTTGAATGTGTTTCCAGCAGGTGCCTCA	pSicoR-shRNA4
shRNA5-F	TAACATGCATCCTAGACACAGATTCAAGAGATCTGTGTCTAGGATGCATGTTTTTTTTC	pSicoR-shRNA5
shRNA5-R	TCGAGAAAAAAAACATGCATCCTAGACACAGATCTCTTGAATCTGTGTCTAGGATGCATGTTA	pSicoR-shRNA5
shRNA-control	TGGATACCGTCGCATAGTAAGTTTCAAGAGAACTTACTATGCGACGGTATCCTTTTTTC	pSico-shRNA-nc
shRNA-control	TCGAGAAAAAAGGATACCGTCGCATAGTAAGTTCTCTTGAAACTTACTATGCGACGGTATCCA	pSico-shRNA-nc

2.1.4.6 Enzymes

Table 12. Enzymes used in this work

Name	Source
DNAse (Type I)	Sigma-Aldrich
Restriction enzymes	New England Biolabs
T4 DNA ligase	New England Biolabs
T4 DNA ligase (LigaFast Rapid Ligation System)	Promega
Trypsin from bovine pancreas	Sigma-Aldrich

2.1.4.7 Kits

Table 13. List of the kits used in this work

Name	Supplier
cAMP ELISA kit	NewEast Biosciences
EndoFree® plasmid maxi kit	Qiagen
Eponate 12 embedding kit with DMP-30	Ted Pella
Fluo-4 Direct™ Calcium Assay	Invitrogen
GloSensor™ cAMP Assay	Promega
mMessenger mMachine® SP6 kit	Applied Biosystems (Ambion)
QIAfilter™ plasmid maxi kit	Qiagen
QIAprep® spin miniprep kit	Qiagen
QIAquick® gel extraction kit	Qiagen
RNeasy mini kit	Qiagen
QuikChange Site-Directed Mutagenesis Kit	Stratagene
QuikChange Site-Directed Mutagenesis Kit XL	Stratagene
SuperSignal Pico Chemiluminescent Substrate	Thermo Scientific
Vectastain Elite ABC	Vector Labs

2.1.4.8 Antibodies

Table 14. Antibodies used in this work (IS: immunostaining, iEM: immuno electron microscopy, WB: Western Blot).

Name	Purpose	Supplier
Anti-GFP, polyclonal, rabbit	IS	Invitrogen
Anti-Gpr151, polyclonal, rabbit	IS, iEM	Sigma-Aldrich
Anti-Gpr151, polyclonal, goat	IS	Santa Cruz
Anti-Chat, polyclonal, goat	IS	Chemicon
Anti-Substance P, monoclonal, rat	IS	Santa Cruz
Anti-VGlut1, polyclonal, guinea pig	IS, iEM	Synaptic Systems
Anti-TH, monoclonal, mouse	IS	Sigma-Aldrich
Anti-Tph, polyclonal, sheep	IS	Millipore
Anti-βGal, polyclonal, chicken	IS	Abcam
Anti-Neurofilament H, monoclonal, mouse	IS	Calbiochem
Alexa Fluor® conjugated or Cy2, Cy3 and Cy5 donkey secondary antibodies	IS	Jackson ImmunoResearch
Anti-HA, monoclonal, mouse	WB	Sigma-Aldrich
Biotin-conjugated secondary antibodies	iEM	Vector Labs
Secondary antibodies IgG conjugated to gold particles	iEM	Jackson ImmunoResearch

2.1.4.9 Peptides used for cell-based second messenger assays

Table 15. Peptides tested in cell-based second messenger assays

Name	Supplier
Galanin	Tocris
Galanin associated peptide	Sigma-Aldrich
GR159897 (NK2 antagonist)	Tocris
GR 64349 (NK2 agonist)	Tocris
Neurokinin B	Tocris
MEN 10376 (NK2 antagonist)	Tocris
Substance P	Tocris

2.1.5 Equipment and software

Table 16. Equipment used in this work

Molecular biology:

MJ Research PTC-200Thermo Cycler	MJ Research
FlexCycler	Analytik Jena
PerfectBlue mini-/midigel system	Peqlab Biotechnologie
Gel Jet Imager	Intas Science Imaging Instruments
BioPhotometer	Eppendorf
J6-MI centrifuge	Beckmann Coulter
Heareus Megafuge 400	DJB Labcare Ltd, Birminghamshire, UK
Microcentrifuge 5415D	Eppendorf AG, Hamburg, Germany
Immobilon polyvinylidene fluoride membranes (PVDF)	Millipore
CL-X Posure™ film	Thermo Scientific

Microscopy:

Confocal microscope: Zeiss LSM700	Zeiss
Inverted microscope: Axiovert.A1	Zeiss
Imaging software: Zen	Zeiss
Transmission Electron Microscopy: JEOL JEM-100CX	Jeol

Cell culture:

Incubator CB 150	Binder
Beckman Optima L-90K ultracentrifuge + SW32 Ti rotor	Beckman Coulter
Heraeus Multifuge 1S-R	Thermo Fisher Scientific Inc.
BD FACSCalibur™ • 488nm argon laser, 635 nm diode laser • FL1 – Green emission (filter: 530/30) • FL2 – Red/Orange emission (filter: 585/42) • FL3 – Red emission (filter: 650 LP) • FL4 – Far Red emission (filter: APC – 661 nm) • software: CellQuest Pro	BD Biosciences
Neubauer counting chamber	Paul Marienfeld
Tissue culture plates 12 well Tissue culture plates 24 well	Corning
Tissue culture flasks 75 cm^2/150 cm^2	Corning
Cellstar serological pipettes 5/10/25ml	Greiner Bio-One International
MultiGuard™ Barrier Tips 2/20/200/1000µl	Molecular Bioproducts
Stericup vacuum filtration units, 150ml	Millipore
Ultraclear centrifuge tubes 25x89 mm/16x102 mm	Beckman Coulter
Superfrost glass slides	Fisher Scientific
Glass coverslips, 13mm	Karl Hecht KG
GloMax Multiplate Reader	Promega

Stereotactic injections:

Benchmark digital stereotaxic instrument with fine drive and Cunningham mouse and neonatal rat adaptor	Leica Microsystems
MO-10 oil hydraulic micromanipulator	Narashige Scientific Laboratory
Micromotor drill	Leica Microsystems
PCR micropipets 1-5 µl	Drummond scientific company, Broomall, PA, USA
Microelectrode puller FP-830	Narashige Scientific Laboratory
Sterican® needles	Braun Melsungen AG
Reglo digital tubing pump	Ismatec Laboratoriumstechnik

Sectioning:

Vibratome VT1000 S	Leica Microsystems
Sliding microtome SM2000R	Leica Microsystems
Reichert-Jung Ultracut E Ultramicrotome	Reichert

Behavioral analysis:

Fusion Open field Software: Fusion	Accuscan
Light Dark boxes Software: Fusion	Accuscan
Elevated Plus Maze Software: EthoVision XT	Noldus Information Technology
Startle Response System Software: Startle	SR Lab

2.1.6 Statistical analyses

Statistical analyses were performed using GraphPad Prism software. One way ANOVA, Repeated Measures ANOVA or Student's t-test were used. Data is presented as mean ± S.E.M. P values < 0.05 were considered statistically significant (* ≤ 0.05, ** ≤ 0.01, *** ≤ 0.001).

2.2 Molecular Biology protocols

2.2.1 Vector construction

All vectors were made using standard cloning procedures. pCMV-HA-Gpr151 was generated by PCR amplification of Gpr151 with primers carrying overhanging ends and inserted into the pCMV-HA backbone using BglII and XhoI sites. HA-Gpr151 was subcloned into the lentiviral vector pFUGW between AgeI and BsrGI cutting sites after PCR amplification with overhanging primers to introduce the desired restriction enzyme sites. shRNAs were generated by annealing the oligonucleotides at 95 °C for 10 min. Oligonucleotides were then cloned into the HpaI and XhoI sites of pSicoR-GFP backbone. Sequences and vector maps of the generated constructs were created with Vector NTI 10.3 (Invitrogen) and are attached in the appendix (p.118).

2.2.2 Oligonucleotides design

Primers were designed using Vector NTI 10.3 (Invitrogen); in accordance to the following standard guidelines: the melting temperature of a primer pair needs to be similar (~60-75 °C), the GC content does not exceed 40-60 % and secondary structures like hairpins and cross-pairing are not allowed. Primers used for cloning were flanked by restriction sites used for subsequent insertion of the amplified sequences into vector backbones. Primers were ordered from Biotez Berlin-Buch GmbH (Berlin, Germany) or GeneLink (New York, USA). They were purified by gel filtration. Sequences are shown in Table 10.

Oligonucleotides used for shRNA cloning were designed to contain a sense strand of 21-nucleotide sequences matching the target sequence, followed by a short spacer (TTCAAGAGA), the reverse complement of the sense strand, and five thymidines as an RNA polymerase III transcriptional stop signal. They also contained different 5'-overhangs that anneal to the sticky ends of the shRNA plasmid digested, in this case with HpaI and XhoI restriction enzymes. Oligonucleotides were 5’ phosphorylated and purified by HPLC. Sequences are shown in Table 11.

2.2.3 Amplification of DNA fragments by PCR

PCR (polymerase chain reaction) was performed for different purposes: to analyze sequences in extracted plasmid DNA (analytical PCR) or from bacterial colonies after transformation (analytical colony PCR); to generate DNA fragments for subcloning of sequences (preparative PCR); and for the genotyping of mice.

The composition of the reaction mix is shown in Table 17. For colony PCR, the DNA template was substituted by part of a bacterial colony, picked with a sterile plastic pipette and transferred to the PCR tube. The PCR thermocycler program was modified from the standard program (Table 18) depending on the primer’s melting temperature and fragment lengths. PCR products were analyzed on 1-1.5 % agarose gels.

Table 17. Standard PCR mix for one reaction

Amount	Substance
5 µl	10 x PCR buffer
3 µl	$MgCl_2$ (50 mM)
2 µl	dNTP mix (80 mM)
1 µl	DNA template (50 ng)
1 µl	Primer forward (50 µM)
1 µl	Primer reverse (50 µM)
0.1 µl	Taq-Polymerase
37 µl	MQ
50 µl	

Table 18. Standard PCR program

Temperature	Time	Cycles	Function
94 °C	3 min	1x	denaturation step, Taq activation
94 °C	30 s	25 x	denaturation step
x °C*	30 s		annealing step
72 °C	x min**		extension step
72 °C	5-10 min	1x	final extension step
15 °C	storage	1x	

* depending on the primer melting temperatures (50-65 °C)

** depending on the fragment length (e.g. ~1 min for 1 kb)

2.2.4 Agarose gel electrophoresis

DNA samples were run on a 1-2 % agarose gel prepared in 1x TAE buffer with 0.001 % ethidiumbromide. Approximately 200-500 ng of DNA (analytic gels) or 1-4 µg of DNA (preparative gels) was mixed with 6x DNA loading dye before running. The 1 kb plus DNA ladder (Invitrogen) was used as DNA size marker. Electrophoresis was performed at 80-100 volts for 80 min and gels were subsequently analysed under UV light in a Gel Imager.

2.2.5 DNA purification from agarose gels

Selected DNA fragments were cut out of the agarose gel under UV light using a scalpel and processed with the QIAquick® Gel Extraction Kit (Qiagen) according to the manufacturer's recommendations. DNA was eluted from the purification column with 30 µl MQ water.

2.2.6 Restriction digest and subcloning

DNA (0.5-4 µg) was enzymatically digested with 10 U of specific restriction endonucleases (New England Biolabs). Samples were incubated for 1.5–2 h for test digestions or o/n for digestions to subclone sequences at the temperature required for the respective restriction enzyme. Ligations were performed as sticky end ligations with 3-6 fold molar ratios of inserts to vectors. Ligations were carried out in a total volume of 10 µl containing 2 µl of T4 DNA ligase (New England Biolabs) and 1x ligation buffer at 16 °C o/n or at RT for >4 h.

2.2.7 Transformation

Heat-shock transformation was applied to self-made chemically competent *E.coli*. Cells were thawed on ice, 100µl were mixed with 10 µl of the ligation preparation and incubated on ice for 10-20 min. The mix was then heat shocked at 42 °C for 60 s and immediately placed on ice for 2 min. Afterwards, 500 µl LB medium was added and the cells were incubated at 37 °C for 1-2 h with shaking at 200 rpm. Finally, cells were streaked on agar plates containing the appropriate antibiotic (ampicillin 100 µg/ml or kanamycin 50 µg/ml) and incubated in a 37 °C incubator o/n.

2.2.8 Glycerol stock preparation

For long-term storage of bacteria, glycerol stocks were prepared by mixing 0.7 ml bacteria overnight culture with 0.7 ml of 40 % glycerol. Samples were then frozen in liquid nitrogen and stored at -80 °C. To resuscitate the culture for a subsequent plasmid preparation, a small bud of the frozen glycerol stock was immersed in the 5 ml LB medium with 5µl of 100mg/ml ampicillin using a pipette tip. Cells were cultured at 37°C o/n and used for plasmid extraction or inoculation of the large-scale DNA extraction culture.

2.2.9 Plasmid DNA extraction

Plasmid DNA extraction was carried out using the QIAprep® spin miniprep kit (Qiagen), the QIAfilter™ plasmid maxi kit (Qiagen) or the QIAfilter™ EndoFree plasmid maxi kit (Qiagen) for plasmids for lentivirus production. All steps were performed according to the manufacturer's instructions. DNA samples were stored at -20 °C.

2.2.10 Sequencing

DNA sequencing was carried out by Invitek Gesellschaft für Biotechnik & Biodesign mbH, Berlin or by Genewiz, NJ, USA. For double-stranded plasmid-DNA, 10 µl of DNA (0.1 µg/µl) and 10 µl of sequencing primers (10µM) were sent to sequence. Results obtained as text file (.seq) and chromatogram files (.ab1) were analyzed with Vector NTI 10.3 (Invitrogen) and Chromas 1.45 (Griffith University).

2.3 Cell culture protocols

2.3.1 Cell culture of HEK293T cells

Adherent human embryonic kidney cells stably expressing the SV40 large T-antigen (HEK293T) cells were cultured in Dulbecco's modified Eagle medium (DMEM + GlutaMAX™), supplemented with 10% Fetal Bovine Serum (FBS) (Invitrogen). Cells were grown at 37 °C and 5% CO_2 in the humidified Binder CB150 incubator. Cells were passaged every 3-4 days (min. 80-90% confluence).

2.3.2 Preparation of cryostocks of HEK293T for long term storage

For long term storage, freezing stocks of HEK293T were prepared. Low-passage cells cultured in 150 cm^2 cell culture flasks were trypsinized and pelleted by centrifugation at 1200 rpm for 3 min. The cell pellet of one flask was resuspended in 3 ml ice-cold cell culture freezing medium, consisting of DMEM + GlutaMAX™ and 10 % FBS with 10 % DMSO. Cells were then aliquoted into 2 ml cryotubes (1ml each) and cooled at the rate of -1 °C/min in a Cryo 1°C freezing container (Nalgene, Thermo Fisher Scientific). The following day, cells were transferred to a liquid nitrogen tank for long-term storage.

2.3.3 Thawing of HEK293T cryostocks for culturing

Cryostocks of HEK293T were thawed in a 37 °C water bath, transferred to the 15 ml Falcon tube and supplemented with 9 ml pre-warmed medium DMEM + GlutaMAX™ with 10 % FBS. Cells were then centrifuged at 1000 rpm for 2 min to discard the supernatant. The cells were finally resuspended in 30 ml culture medium in the 150 cm^3 cell culture flask and cultured at 37 °C and 5% CO_2.

2.3.4 Lentivirus production

Recombinant lentiviral vectors were prepared using transient transfection in HEK293T cells. $5x10^6$ HEK293T cells were plated on 24x 10cm dishes pre-coated with poly-l-lysine (0.0005 % in 1 x PBS). The following day, the lentiviral transfer vector plus the packaging vectors pLP1, pLP2 and the envelope vector pLP-VSV-G (Invitrogen) were co-transfected with PEI transfection. The transfection mix was prepared as follows (for one dish): 12 µg transfer plasmid, 6.5 µg pLP1, 3.5 µg pLP2, and 3.5 µg pCMV-VSV-G were added to 800 µl OptiMEM® (Invitrogen) and incubated at RT for 5 min. In the meantime, 51 µl PEI solution (1 mg/ml) was added to 800 µl OptiMEM® (Invitrogen) in a separate tube. Both solutions were mixed and incubated at RT for 30 min. The medium of the cells was changed to 5 ml OptiMEM® (Invitrogen) per dish. Finally, 3 ml transfection mix was added dropwise to each dish. The medium was replaced 16 hours after transfection with OptiMEM® (Invitrogen) without serum. The virus-containing medium was harvested 40-45 h after medium change, cleared by centrifugation at 3000 rpm for 10 min at 4°C and filtered through 0.45 µm Stericup® vacuum filtration units (Millipore).

2.3.5 Lentivirus concentration

Ultracentrifugation of harvested lentivirus was carried out to increase final titers ~100-400 fold. The centrifugation was performed in a Beckman Optima L-90K ultracentrifuge using a SW32 Ti rotor at 50,000g for 3 h with a purification layer of 1-3 ml 20% sucrose (w/v) in 1x Optimem added to the bottom of the tubes. Subsequently, the virus was resuspended in 50-100 µl of 1xPBS by slowly shaking on ice for 1h. To remove possibly remaining virus aggregates, the solution was centrifuged at 10,000 rpm for 10-20 s and the supernatant was transferred to a fresh tube. The virus solution was aliquoted in amounts of 5-20 µl and stored at -80°C.

2.3.6 Lentivirus titration

The titer of concentrated lentiviral stocks was determined by transducing HEK293T cells with limiting virus dilutions (1/200, 1/400, 1/800, 1/1600, 1/3200, 1/7200 and 1/14400). 50 µl of each viral dilution was added to 1x 10^5 HEK293T cells per well of a 24-well plate immediately after seeding the cells. Cells were incubated at 37°C with 5% CO_2 for 72h. Afterwards, cells were trypsinized, transferred to 1.5ml tubes, pelleted by centrifugation (1000 rpm, 2 min) and resuspended in 500 µl 1 x PBS. GFP positive cells were finally quantified by fluorescent-activated cell sorting (FACS)

analysis and the transducing units per ml, representing the number of infectious lentiviral particles, were calculated according to the following formula:

$$TU/\mu l = (P \times N / 100 \times V) \times 1/DF$$

P: % GFP^+ cells, N: number of cells at time of transduction (1 x 10^5), V: volume of dilution added to each well (50 µl) and DF: dilution factor. Only dilutions yielding 1-20 % of GFP-positive cells in a linear range were considered for titer calculations, as below 1 % FACS analysis may not be accurate and above 20 % the chance for multiple infections increases. On average, titers of non-concentrated lentivirus productions were in the range of 5x 10^6 transducing units (TU)/ml and concentrated virus titers were 5x 10^8–2x10^9 TU/ml.

2.3.7 FACS analysis

HEK293T cells were analyzed on a FACSCalibur™ system equipped with a 488 nm Argon laser and a 635 nm diode laser according to the instructions of the manufacturer. HEK293T cells were trypsinized, washed once and fixed with 4 % PFA for 10 min. After adjusting the settings with a control sample, EGFP fluorescence was detected (FL1 filter: 530/30) and the percentage of EGFP positive cells as well as the mean fluorescence intensity (MFI) were measured.

2.3.8 Protein extraction of transfected HEK293T cells

Briefly, 1-2 days after transfection, cell cultures dishes were placed on ice and cells were washed with ice-cold PBS. Afterwards, 1 ml of ice-cold NP40 lysis buffer was added per 10cm dish. Cells were scraped with a cold plastic cell scraper and transferred to a pre-cooled microfuge tube. Tubes were placed on a rotator for 30 min at 4 °C. The lysate was centrifuged for 10 min at 14000 rpm. Supernatant was transferred to a pre-cooled microfuge tube and kept at -80 °C until SDS-PAGE was performed.

2.3.9 SDS-PAGE and Western blotting

Protein samples were analyzed by discontinuous SDS-PAGE (sodium dodecyl sulfate-polyacrylamide gel electrophoresis) by separation in a polyacrylamide gel according to their molecular weight using the Xcell SureLock™ mini-cell system (Invitrogen). Samples were added with NuPAGE® LDS sample buffer (4 x) and reducing agent (10 x) and heated at 95 °C for 4 min. Proteins were separated according to their molecular weight on 4–12 % gradient polyacrylamide gels at 150 V

for 90 min. 1 x NuPAGE® MES SDS running buffer was used. The gel was removed from the chamber and used for Western blotting. Before use, Immobilon polyvinylidene fluoride (PVDF) membranes (Millipore) were soaked in methanol for 1 min and washed in water for 5 min. The membrane was then incubated for 5 min in 1 x NuPAGE® transfer buffer together with the gel as well as blotting and filter papers. The blotting sandwich was built according to the manual. The transfer was performed in semi-wet conditions with 1x NuPAGE® transfer buffer for 90 min at 100 V in the Xcell SureLock™ mini-cell system (Invitrogen). Subsequently, the membrane was washed in 1 x TBS, blocked in 5 % Bovine Serum Albumin (BSA) in TBS-T for 1-2 hours at RT. The membrane was then incubated in 1/500 anti-HA (mouse, monoclonal) in blocking solution at 4 °C o/n. The following day, the membrane was washed 4 x 10 min with TBS-T and then incubated with a goat anti-mouse-HRP (horse radish peroxidase) secondary antibody (1/10000 in blocking solution) for 1.5 h. Following three washing steps, the signal was detected using the ECL plus western blotting detection system (GE Healthcare). 1 ml of solution A was mixed with 25 µl solution B and incubated on the membrane for 30 s. The membrane was then wrapped in transparent film, placed into a cassette and exposed to a CL-X Posure™ film (Thermo Scientific) for 1-30 min to detect the chemiluminescence. The films were developed in a film processor apparatus (Fuji).

2.3.10 Mouse habenular primary cultures

Cultures of dissociated mouse habenular neurons were prepared from E15 (embryonic day 15) mouse embryos. Pregnant females were anesthetized and sacrificed by cervical dislocation. Embryos were then removed from the uterus and placed in ice-cold dissection buffer. Subsequently, brains of mouse embryos were dissected and transferred to fresh dissection buffer kept on ice. First the hemispheres were isolated by cutting dorsal to ventral between midbrain and cortex. Afterwards, the meninges were removed and both habenulae were cut out. The right and left habenula were sliced in smaller pieces and triturated in 2 ml culture medium by passing them 10-15 times through the 1 ml and 200 µl pipette tips. The number of dissociated neurons was determined by counting them in the Neubauer hematocytometer (0.1 cm^3 in each square), calculating the mean and multiplying it with dilution factor and 10^4 to obtain cell number per ml. The cells were seeded in 1 ml of habenular culture start medium with a density of 2.5 x 10^5 cells per well on 13

mm glass coverslips, pre-coated overnight with poly-D-/L-ornithine in MQ (50 µg/well). The culture plate was incubated at 37 °C and 5 % CO_2 and one third of the medium (300 µl) was replaced with habenular culture medium twice a week, starting at the fifth day in vitro (DIV 5).

2.4 Cell-Based Second Messenger Assays

2.4.1 Assay to measure cAMP levels

The GloSensor™ cAMP Assay was used to measure levels of cAMP on HEK293T cells. This assay employs a genetically modified form of firefly luciferase that contains a cAMP-binding protein domain. Binding of cAMP induces a conformational change that leads to an increase of light output. The procedure was carried out according to the instructions of the manufacturer. Briefly, HEK293T cells were resuspended at a density of 1.5 x 10^5 cells/ml in growth medium prewarmed to 37ºC and a 100µl was added (15,000 HEK293T cells) to the individual wells of a tissue culture treated, 96-well plate. The following day, cells were transfected with pGloSensor™-22F cAMP plasmid, Gpr151 and pFU-PC using the FuGENE® Transfection Reagent. 24 hours after transfection, medium was removed and a 100µl of equilibration medium, which contained 2% v/v dilution of the GloSensor™ cAMP Reagent stock, was added to each well. Cells were then incubated for 2 hours at room temperature. The luminescence signal was measured using the GloMax Multiplate reader (Promega). When a steady-state basal signal was obtained, different compounds at different concentration were added to the wells and luminescence levels were recorded for 20-40 min. Forskolin (10 µM) was used as a positive internal control to maximally increase cAMP levels.

2.4.2 Assay to measure calcium levels

Fluo-4 Direct™ Calcium Assay was used to measure calcium levels in Gpr151-transfected HEK293T cells. This assay involves a fluorescent calcium indicator. When calcium binds to it, fluorescence increases. Consequently, changes on calcium levels can be detected by measuring fluorescence. The procedure was carried out according to the instructions of the manufacturer. Briefly, HEK293T cells were resuspended at a density of 1.5 x 10^5 cells/ml in growth medium pre-warmed to 37ºC and a 100µl was added (15,000 HEK293T cells) to the individual wells of a tissue

culture treated, 96-well plate. The following day, cells were transfected with Gpr151 and pFU-PC as a control, using the FuGENE® Transfection Reagent. 24 hours after transfection, 100 µL of the 2X Fluo-4 Direct™ calcium reagent, containing 5mM of probenecid to inhibit anion transporters that contribute to high background signal, was added per well. Plates were incubated at 37°C for 60 minutes and fluorescence was then measured using the GloMax Multiplate reader (Promega), setting the excitation wavelength at 494 nm and emission at 516 nm.

2.5 cAMP ELISA

Habenula and interpeduncular nuclei were dissected from wildtype or Gpr151-KO mice. Tissues were homogenized with a motorized tissue grinder (Fisherbrand), lysed with 0.1 mM HCl for 5 min, and centrifuged (14,000 × g) at 4 °C for 10 min. The concentration of cAMP in the supernatant obtained from mouse extracts was measured with the Monoclonal Anti-cAMP Antibody Based Direct cAMP ELISA Kit, Non-acetylated Version (NewEast Biosciences Inc); following the manufacturer's instructions. Briefly, 100 µl of the cAMP standards (250, 50, 10, 2, 0.4 and 0.08 pmol/mL) were prepared in 0.1M HCl from the 5,000 pmol/mL cAMP standard solution. Afterwards 100 µl of standards and 100 µl of the samples were pipetted into the appropriate wells of a goat-anti-mouse IgG coated 96-well plate. Subsequently, 50 µl of conjugate (horse radish peroxidase conjugated with cAMP) and 50 µl of antibody (mouse monoclonal antibody to cAMP) were loaded into each well containing mouse tissue extracts, except the Blank wells. Plate was incubated at room temperature for 2 hours on a plate shaker at 300 rpm. Next, each well was washed 3 times by adding 400 µl of wash solution. After the final wash, the washing buffer was aspirated and the plate was tap on a lint free paper towel to remove any remaining washing buffer. 200 µl of substrate solution was added to every well and the plate was incubated at room temperature for 30 minutes without shaking. Finally, 50 µl of stop solution was pipetted to every well and the plate was immediately read on a microplate reader at 450 nm. The measured optical density was used to calculate the concentration of cAMP in the samples based on the curve from the cAMP standards.

2.6 Mouse brain stereotactic injections

Mice, 8-9 weeks old, were anesthesized with ketamine/xylazine (130 mg/kg and 10 mg/kg, respectively), and placed in a Benchmark stereotaxic frame with a Cunningham mouse adaptor (Leica). The eyes were covered with Regephitel® ointment to prevent desiccation. Four holes were drilled on the skull with a micromotor drill with a 0.35 mm diameter bit. The coordinates used to target the medial habenula were the following: anterior-posterior (from Bregma): -1.4 and -1.75; lateral +/-0.33; dorso-ventral (from the skull) -2.72 and -2.70. Glass PCR micropipets (Drummond) that had been pulled with a microelectrode puller (Narashige) to create a narrow, fine tip of ~10-12 mm length were used for the injections. The cannula was filled from the backside with lentivirus, followed by mineral oil. A metal plunger was inserted into the upper part of the cannula and placed in the stereotaxic apparatus. 0.5-1 µl of virus was injected into the mouse medial habenula using a MO-10 oil hydraulic micromanipulator (Narashige) with a flow rate of ~0.1 µl/min. The cannula was left in place for 5 min, allowing the virus solution to disperse in the tissue, before it was slowly retracted. The incision was closed with the tissue adhesive Vetbond (3M). After surgery, mice were warmed up by the infrared lamp and left for recovery for 2h. Mice were kept under S2 conditions for a week.

2.7 Behavioral analysis

For all behavioral analysis, mice were transported from their housing room to the behavioral room and allowed to habituate for 60 min prior to the testing. All behavioral studies were conducted blind to the genotype of the tested mice.

2.7.1 Conditioned Place Preference

Nicotine conditioned place preference (CPP) was performed using three-chamber CPP boxes from Med Associates. Two conditioning chambers with retractable doors were separated by a smaller, grey neutral chamber with a grey Plexiglas floor. One conditioning chamber had black walls and wire mesh floor and the other had white walls and a metal grid floor. Movement of each animal was detected by photocell beam breaks and time spent in each chamber was recorded with Med-PC IV software.

On day 1 (pre-conditioning test), mice were placed in the center chamber and allowed to explore the three chambers for 15 min to determine baseline preference for each of the chambers. Mice that showed greater than 70% preference for any chamber were excluded from further testing. Two conditioning sessions per day were performed on days 2, 3, and 4. During the morning session (beginning at approximately 09:00 h), mice were confined to one conditioning chamber for 30 min following a saline injection. During the afternoon session (beginning at approximately 14:00 h), mice were confined to the opposite conditioning chamber for 30-min following a nicotine injection (0.05, 0.15, 0.25, 0.35 mg/Kg free base, intraperitoneal). On day 5, the post-conditioning test was conducted. Mice were placed in the center chamber and allowed free access to all three chambers for 15 min. Time spent in each chamber was recorded. Animals were counterbalanced for the drug-paired chamber based on the genotype and baseline preference. The pre- and post-conditioning tests were performed at an intermediate time between the morning and afternoon conditioning sessions (at approximately 11:00 h). Data were collected as time spent in each chamber (sec) during the pre- and post-conditioning test. Preference score was expressed as the difference between the time spent during the post-conditioning test and the preconditioning test in the drug-paired or saline-paired compartment.

2.7.2 Elevated Plus maze

Elevated Plus Maze was used to assess anxiety-like behavior. The apparatus consisted of a central platform (5 × 5 cm), two opposed open arms (25 × 5 cm) and two opposed closed arms with 15-cm-high black walls. The edges of the open arms were raised 0.25 cm to decrease the chance of a mouse falling. Mice were placed on the central platform and the time and activity were recorded for 10 min via a camera positioned above the apparatus. Time spent in each arm and the distance traveled was recorded automatically using EthoVision XT Tracking Software.

2.7.3 Open field and light/dark test

To measure exploratory locomotor activity and anxiety, open field boxes were used (Accuscan & Omnitech Electronics). Mice were placed in the center of the field and activity was recorded for 30 min by the Fusion Software.

To measure anxiety, a dark enclosure with a doorway was placed on one side of the open field boxes. Mice were place in the dark chamber and allowed to move freely

between both chambers for 10 min. Horizontal activity and time spent in each chamber were recorded.

2.7.4 Prepulse Inhibibition

Startle reflexes were measured in four identical startle response SR-LAB apparatus (San Diego Instruments). Each system contained a Plexiglas cylinder, 5.5 cm in diameter and 13 cm long, mounted on a Plexiglas platform located in a ventilated, sound-attenuated chamber. Startle responses were transduced by piezoelectric accelerometers mounted under each platform. Output signals were digitized and the average startle response and maximum amplitude of the startle response were recorded as startle units. The startle session began with a 5 min acclimation period in the presence of a 65-dB background white noise, followed by presentation of five 120 dB pulse trials to ensure a stable baseline and reduce variability. Afterwards mice were presented with four startle stimulus of different intensities (80, 90, 100, 110, 120 dB). A total of 20 trials in a pseudo-randomized manner with an average inter-trial-interval of 15 sec (range: 6-21 sec) were presented. Amplitude of startle was measured within a 100 msec window following the stimuli.

Prepulse Inhibition was examined using prepulses of 3, 6 or 12 dB (20ms) above background. Testing consisted of twelve 120 dB pulses (40 ms duration) alone and ten pulses preceded (100 ms) by each prepulse (20 ms duration). One last block of five 120 db pulses was presented to ensure again a stable baseline. Percent PPI was calculated using the following formula: {100x (startle alone – startle with prepulse/startle alone)}. PPI was reported as percent inhibition of the average startle response.

2.7.5 Nicotine treatment

To induce nicotine dependence, we used a previously described protocol (Gorlich et al., 2013; Grabus et al., 2005; Sparks and Pauly, 1999). Mice were given nicotine in the drinking water for 28 days. The water contained 2% saccharin to mask the bitter taste of nicotine, which was increased from 65 mg/L to 163 mg/L nicotine free base during the first week, and maintained at 163 mg/L nicotine free base during the following weeks. Based on the volume intake, mice consumed 26.2 $mg \cdot kg^{-1} \cdot day^{-1}$ of nicotine free base (Gorlich et al., 2013). In C57BL/6J mice, this dose correlates to plasma cotinine (the major metabolite of nicotine) levels of 43 ng/mL (Sparks and Pauly, 1999). This concentration is comparable with nicotine plasma levels measured

in the afternoon in smokers (10-50 ng/mL of cotinine, or 60–310 nM of nicotine) (Matta et al., 2007). Control mice were given 2% saccharin.

2.7.6 Nicotine Withdrawal Assessment.

Nicotine withdrawal was precipitated by an intraperitoneal injection of mecamylamine (2 mg/kg) on the morning of day 29. Mice were evaluated 5 min after injection. They were first tested for 10 min on the light/dark test for anxiety-like behavior. Mice were then observed for somatic signs of withdrawal for 20 min. The following somatic signs were counted, with each event receiving a score of one point: scratching, jumping, shaking, head nodding, retropulsion, genitals licking and paw tremors.

2.8 Immunohistochemistry

2.8.1 Perfusion of mice

Mice were anesthetized by an intraperitoneal injection of a mixture of ketamine and xylazine (260 mg/kg and 20 mg/kg, respectively). The intracardiac perfusion was carried out by opening the thoracic cage along its length to the level of sternum and by inserting a 27 gauge injection needle into the left ventricle of the heart, followed by a small incision in the right ventricle. Mice were perfused with 5 ml ice-cold 1 x PBS, followed by 15 ml 4 % PFA in 1x PBS with a flow rate of 1.3 ml/min. Afterwards brains were dissected, post-fixed o/n in 4 % PFA in 1xPBS and transferred to 30 % sucrose in 1x PBS the following morning.

2.8.2 Cryosections of perfused mouse brains

40 µm thick brain sections were prepared using a SM2000R sliding microtome (Leica Microsystems). Brains were fixed at the microtome stage on a layer of O.C.T.™ Tissue Tek (Sakura) by freezing the stage with dry ice. The sections were transferred immediately after cutting to a plate containing cryoprotectant buffer (0.1 M phosphate buffer with 25% glycerol and 25 % ethylene glycol, pH 7.4) and stored at -20 °C until further analysis.

2.8.3 Immunohistochemistry of mouse sections

For free-floating immunohistochemistry, selected brain sections were washed twice with 1xPBS and blocked in 1xPBS containing 10 % normal donkey serum (NDS) and 0.3 % Triton X-100 for 1h. Sections were then incubated overnight at 4 °C with primary antibodies diluted in 1xPBS containing 1% NDS and 0.1% Triton X-100.

Subsequently, sections were washed with 1xPBS and incubated for 2 h at room temperature with secondary antibodies (1:500; Jackson ImmunoResearch). Sections were then washed twice for 15 min in 1 x PBS, counterstained with the nuclear stain DAPI and mounted on object slides with ImmuMount™ (Thermo Scientific).
The antigen retrieval protocol was used for ChAT immunostaining. Selected sections were mounted on slides and incubated in 0.01 M citric acid, pH 6, for 15 min at 95 °C before blocking and primary incubation.
Confocal fluorescent images were acquired with a Zeiss LSM700 confocal microscope and processed with Adobe Photoshop CS6.

2.8.4 Immunohistochemistry of human samples

Human tissue was obtained from the NICHD Brain and Tissue Bank for Developmental Disorders at the University of Maryland, Baltimore, MD. Samples of about 2 cm wide x 5 cm long x 1 cm deep containing the habenula, the fasciculus retroflexus or the interpeduncular nucleus were obtained from four adult human brains, ranging between 22–52 years of age. After receiving the samples, they were cryoprotected for 4 days in sucrose, the first two days in 15% sucrose and the two following days in 30% sucrose. 50 µM sections were sectioned on a SM2000R sliding microtome. Sections were washed for one hour in 1xPBS containing 0.2%TX100 and then blocked for 2 hours in 1xPBS containing 0.5%TX100 and 4%NDS. Subsequently, sections were incubated overnight at 4 °C with primary antibodies diluted in blocking buffer. The following morning, sections were washed with 1xPBS containing 0.2%TX100 and incubated for 2 h at room temperature with secondary antibodies (1:250; Jackson ImmunoResearch). Sections were mounted on slides; and examined and photographed with a Zeiss LSM700 confocal microscope.

2.9 Electron microscopy

2.9.1 Perfusion of mice

Adult mice were anesthetized with an intraperitoneal injection of a mixture of ketamine and xylazine (260 mg/kg and 20 mg/kg, respectively) and perfused through the heart with 0.9% NaCl for 1 min followed by fixative containing 4% PFA in 0.1M sodium cacodylate buffer (pH 7.4) for 10 min. After perfusion the brains were removed from the skull. 4% PFA in 0.1M sodium cacodylate buffer was injected into the cortex using a 27 gauge injection needle for 2 min. Afterwards brains were kept

overnight at 4°C in 4% PFA in 0.1M sodium cacodylate buffer. The following day, brains were sectioned on a VT1000S vibratome (Leica) at 50 µm thickness. Sections were stored at -20°C in cryoprotectant buffer containing 0.13M sucrose in 0.1M cacodylate Buffer until used.

2.9.2 Pre-embedding immunocytochemistry

Brain vibratome sections were washed for 10 min on 0.1M sodium cacodylate buffer pH 7.4. Sections were incubated in 0.5% H_2O_2 to quench endogenous peroxidase activity prior to treatment with 0.1% sodium borohydride. Sections were then incubated in blocking solution (5% BSA, 0.1% saponin in 0.1M sodium cacodylate) for 2 hours at room temperature. Sections were transferred to serial dilutions of rabbit, anti-Gpr151 (Sigma SAB4500417) antibody (1:6000, 1:9000, 1:12,000) diluted in blocking solution and left to incubate overnight at 4°C. After visualization under light microscopy, 1:9000 was selected as the optimal dilution.

Sections were incubated in biotin, anti-rabbit (Vector Labs) diluted in blocking solution to 1:1000 for two hours at room temperature. Subsequently the sections were washed and incubated in avidin-biotin-peroxidase complex (Vectastain Elite ABC) for 60 min. The labeling was visualized using DAB (SigmaFast). Sections were then postfixed overnight in 2.5% glutaraldehyde at 4°C and subsequently underwent silver enhancement and gold toning. Sections were rinsed in 2% sodium acetate for 10 min. In the meantime, silver developer was prepared (3% Methenamine, 5% silver nitrate, and 1% sodium tetraborate). Sections were incubated in the developer for 20 min in a 60 °C oven. To stop the reaction, sections were rinsed in 2% sodium acetate for 10 min. Afterwards, stabilization of the silver intensification was obtained by incubation in 3% sodium thiosulfate for 5 min. Gold toning was carried out by incubation in 0.1% gold chloride for 5 min. Sections were then rinsed in 2% sodium acetate for 10 min, stabilized with 3% sodium thiosulfate for 5 min, rinsed again in 2% sodium acetate for 10 min and finally rinsed in sodium cacodylate for 10 min.

The interpeduncular nucleus was removed from the section with a feather blade and treated with 1% osmium tetroxide in 0.1M cacodylate buffer in the presence of potassium ferrocyanide for 1 hour on ice. Sections were then counterstained with 1% uranyl acetate for 30 min and dehydrated in a graded series of ethanol followed by incubation in acetone for 10 min. Finally the tissue was infiltrated overnight at room temperature using Eponate 12™ Embedding Kit, with DMP-30 (Ted Pella) and

embedded between two sheets of Aclar® film (Ted Pella). Samples were polymerized for 48h at 60°C. A series of 60nm ultrathin sections were cut with a diamond knife (Diatome) on a Reichert-Jung Ultracut E Ultramicrotome, collected on carbon film 200 mesh nickel grids (Electron Microscopy Sciences) and imaged on a JEOL JEM-100CX at 80kV using an AMT bottom mount camera.

As the control experiment, sections were treated alongside following the same procedure while omitting the primarily antibody and incubating with blocking solution instead.

2.9.3 High pressure freezing and freeze substitution

Isolated IPN from 50 µm vibratome sections were applied to a high pressure freezer (Leica EM PACT2) in cryoprotectant (30% BSA). The sample reached -170°C within 300 ms at ~2000 bar. They were transferred to a freeze substitution unit (Leica EM AFS2 Automatic Freeze Substitution System) filled with liquid nitrogen and processed in substitution media, containing 1% Uranyl Acetate, 95% Acetone and 5% water at -85°C. The sample was then washed in acetone and embedded in Lowicryl HM20 at -45°C. Ultrathin sections (90nm) were cut and processed for post-embedding immunolabeling.

2.9.4 Post-embedding immunocytochemistry

Post-embedding immunocytochemistry was carried out on 90 nm ultrathin sections mounted on carbon film 200 mesh nickel grids (Electron Microscopy Sciences). Sections were rinsed on drops of 1xPBS and incubated in blocking solution containing 3% BSA, 0.1% saponin, and 15 mM ammonium chloride in 1xPBS for 1h. Sections were placed on drops of primary antibody (anti-Gpr151, Sigma #SAB4500417, 1:200, 1:400, 1:800; anti-VGlut1, Synaptic Systems #135304, 1:200; 1:400) diluted in blocking solution containing 3% BSA, 0.1% saponin in 1xPBS overnight at 4°C. Sections were rinsed in blocking solution and incubated in secondary antibody (anti-rabbit IgG conjugated to 12 nm gold particles and anti-guinea pig IgG conjugated to 6 nm gold particles (Jackson ImmunoResearch) diluted 1/20 in 1XPBS containing 0.5% BSA. Finally sections were washed twice in PBS and twice in ultrapure water and imaged on a JEOL JEM-100CX at 80kV using an AMT bottom mount camera.

2.10 Comparative modeling and molecular docking

Gpr151 modeling and the *in silico* screening of a compound library was performed with the Molecular Operating Environment 2011.10 (MOE) software. Gpr151 sequence was downloaded from NCBI (Reference Sequence: NP_853521.1). Gpr151 model was built based on multiple templates from crystallographic structures of class A GPCRs. The alignment was carried out by the Align program of MOE with default parameters and the comparative model building was produced with the MOE Homology Model program. 1U19.pdb was set as primary template. Ten independent models were built and refined, and then the highest scoring model was submitted to an additional round of energy minimization. To make sure that the stereochemical quality of the final model was acceptable, its structure was evaluated through the MOE Protein Geometry module. To calculate possible active sites in the Gpr151 model, we used the MOE Site Finder module, which employs a geometric approach to calculate possible binding sites in a receptor starting from its 3D atomic coordinates. Afterwards, we carried out the *in silico* screening with the Dock program contained in the MOE Simulation module. We downloaded the The Asinex Platinum Collection (http://www.asinex.com/) which is a lead-like structural library containing 113.962 in-house synthesized compounds. The library was imported through the MOE Conformation Import module and a single low-energy conformation for each compound was produced. The selected protocol for the molecular docking was Triangle Matcher, in which the poses are generated by superposing triplets of ligand atoms and triplets of receptor site points. Before scoring all the generated poses, duplicate complexes were removed. The remaining poses were scored according to the London dG scoring, which estimates the free energy of binding of the ligand from a given pose.

3. Results

3.1 Gpr151 is localized at the axonal projections of habenular neurons in the mouse brain.

Although the localization of Gpr151 mRNA in the habenular neurons was well documented (Aizawa et al., 2012), expression of the protein was still unknown. *In situ* hybridization of Gpr151 in mouse and rat brain revealed strong and restricted expression to the habenula (Aizawa et al., 2012; Berthold et al., 2003; Ignatov et al., 2004). In the medial habenula, Gpr151 mRNA was found in the ventrolateral (cholinergic part), in agreement with our translational TRAP data (Table 2). Gpr151 mRNA was also observed in the lateral habenula, especially in the superior part of the medial division and in the parvocellular part of the lateral division (Aizawa et al., 2012). To determine the protein localization of Gpr151 we performed immunohistochemical analysis of mouse brain sections using two antibodies raised against the intracellular domain of Gpr151. As shown in figures 6-10, Gpr151 immunoreactivity is very specific and robust and importantly, the protein is not localized in the cell bodies, where Gpr151 mRNA is labeled by *in situ* hybridization, but in the axonal projections of habenular neurons.

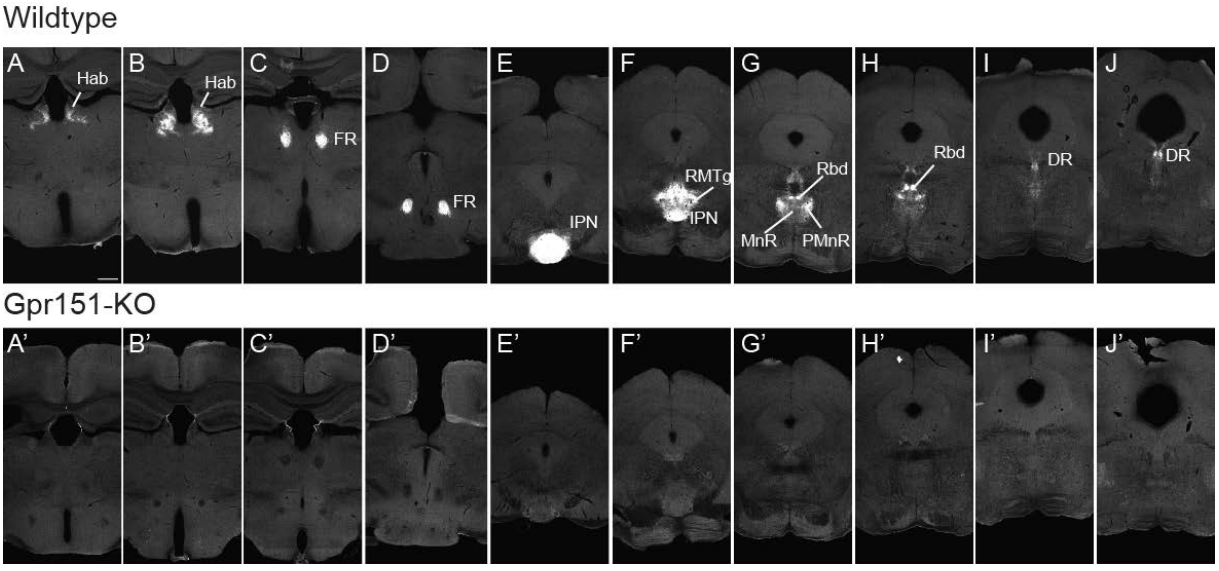

Figure 6. Gpr151 is localized at the axonal projections of habenular neurons.

Immunohistochemical analysis of coronal sections of wildtype mice (upper row) shows the restricted expression of Gpr151 in the habenula (Hab) (A-B), the fasciculus retroflexus (FR) (C-D), interpeduncular nucleus (IPN) (E), median raphe (MnR) and paramedian raphe (PMnR) (F-G), rhabdoid nucleus (Rbd) (F-H) and dorsal raphe (DR) (I-J). Gpr151 immunoreactivity is completely absent on Gpr151 KO mice (lower row). Scale 500 µm.

The axonal projections of MHb and LHb neurons bundle together to form the FR, which displayed strong Gpr151 immunoreactivity (Fig. 6B-D). The axonal projections from MHb terminate in the IPN, which displays the strongest Gpr151 immunoreactivity (Fig. 6E). In addition a subpopulation of lateral habenular (LHb) axonal projections are positive for Gpr151. These LHb axons labeled by Gpr151 project to the rostromedial tegmental nucleus (Fig. 6F), rhabdoid nucleus (Fig. 6F-H), median raphe (Fig. 6F-G), paramedian raphe (Fig. 6F-G) and dorsal raphe (Fig. 6I-J). To validate the specificity of the antibody, we analyzed Gpr151-KO mice. Homozygous Gpr151-KO mice did not express the Gpr151 protein by immunofluorescence (Fig. 6A'-J'), indicating successful recombination of the targeted allele in Gpr151-KO mice and confirming the specificity of the Gpr151 immunostaining.

We next examined in detail the expression of Gpr151 in the habenula. MHb has been subdivided in the vMHb and the dMHb depending on molecular markers and connectivity. Neurons in the dMHb express the neuropeptide Tachykinin 1 (substance P: SP) (Contestabile et al., 1987; Cuello et al., 1978) and project to the rostral and lateral subnuclei of the IPN (Contestabile et al., 1987). Neurons in the vMHb express the ACh synthesizing enzyme choline acetyltransferase (ChAT) (Aizawa et al., 2012) and project to the central and intermediate subnuclei of IPN (Contestabile et al., 1987).

In the MHb, Gpr151 was detected in the cholinergic part of MHb (vMHb), but not in the Substance P-ergic part (dMHb) (Fig. 7). Strong expression was detected in habenular projections forming the FR and at the habenular commissure (hbc) (Fig. 7).

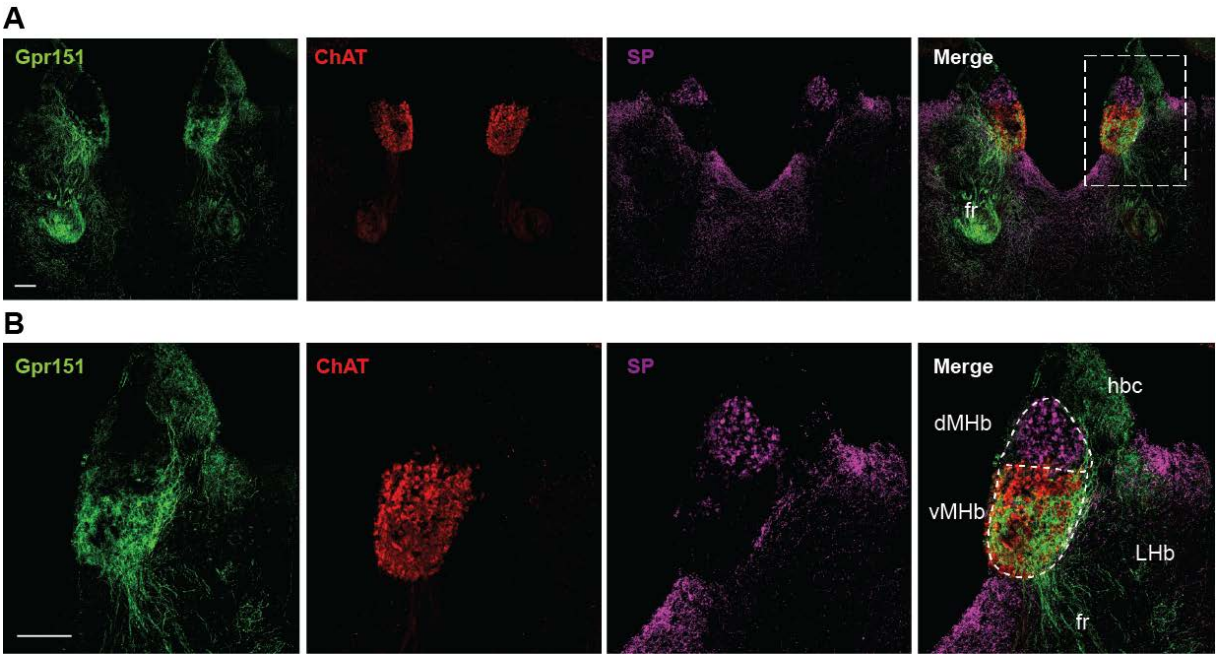

Figure 7. Gpr151 expression in the medial habenula.

(A) Coronal sections of mouse habenula showing Gpr151 colocalization with ChAT in the ventral part of MHb, but not with Substance P in the dorsal part. (B) Higher magnification of the boxed area in A. Scale bar: 100µm. ChAT, acetylcholine transferase; SP, Substance P; dMHb, dorsal medial habenula; vMHb, ventral medial habenula; LHb, lateral habenula; hbc, habenular commissure; fr, fasciculus retroflexus.

In addition a subpopulation of lateral habenular (LHb) neurons was positive for Gpr151. To study the localization of Gpr151 within subnuclei of the LHb, we used the mouse habenula subdivision definition proposed by Wagner and colleagues (Wagner et al., 2014). LHb includes the medial division, which is further subdivided into superior part (LHbMS), parvocellular part (LHbMPc), central part (LHbMC), magnocellular part (LHbMMg); and the lateral division, which is further subdivided into parvocellular part (LHbLPc), magnocellular part (LHbLMc), oval part (LHbLO), basal part (LHbLB), and marginal part (LHbLMg) (Fig. 8). Given that Neurofilament H (NF-H) has been used as a marker to delineate the LHb subnuclei of rat and mouse brain sections (Geisler et al., 2003; Wagner et al., 2014), we performed colabeling of Gpr151 and NF-H. As observed in figure 8, LHbMPc and LHbMC are completely devoid of NF-H immunoreactivity. In contrast, Gpr151 immunoreactivity is strongly expressed in these subnuclei.

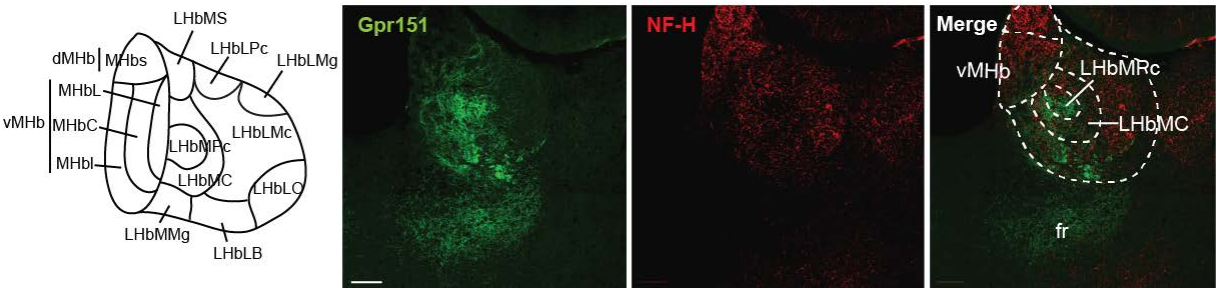

Figure 8. Gpr151 expression in the lateral habenula.

Schematic diagram showing the subdivision of the habenula according to (Wagner et al., 2014). Gpr151 is expressed in the LHb subdivisions (LHbMPc and LHbMC) devoid of NF immunostaining. Scale bar: 100µm. NF, neurofilament H; dMHb, dorsal medial habenula; vMHb, ventral medial habenula; MHbC, central part of MHb; MHbI, inferior part of MHb; MHbL, lateral part of MHb; MHbS, superior part of MHb; LHbMC, central part of the medial division of LHb; LHbMMg, marginal part of the medial division of LHb; LHbMPc, parvocellular part of the medial division of LHb; LHbMS, superior part of the medial division of LHb; LHbLMc, magnocellular part of the lateral division of LHb; LHbLO, oval part of the lateral division of LHb; LHbLPc, parvocellular part of the lateral division of LHb; LHbLMg, marginal part of the lateral division of LHb; LHbLB, basal part of the lateral division of LHb.

We next analyzed the projections of MHb and LHb neurons positive for Gpr151. As shown in coronal mouse sections of figure 6 and in sagittal sections of figure 10, Gpr151 habenular neurons project to the IPN, the rostromedial tegmental nucleus (RMTg), the median raphe (MnR), the paramedian raphe (PMnR) and the dorsal raphe (DR), the rhabdoid nucleus (Rbd) and the dorsal tegmental nucleus (DTg).

In the IPN, Gpr151 showed a stronger expression in the rostral subnucleus (IPR) and a weaker expression in the central subnucleus (IPC). Colocalization of Gpr151 and ChAT (Fig. 9A) and Gpr151 and VGlut1 (Fig. 9B) was observed in the rostral subnucleus and in the dorsal part of the central subnucleus. These results demonstrate that Gpr151 neurons from MHb projecting to the IPN are cholinergic and glutamatergic.

To study whether LHb neurons expressing Gpr151 project to the ventral tegmental nucleus (VTA), we performed colabeling of Gpr151 with tyrosine hydroxilase (TH). No colocalization was observed (Fig. 9B), indicating that Gpr151 LHb neurons do not project to VTA.

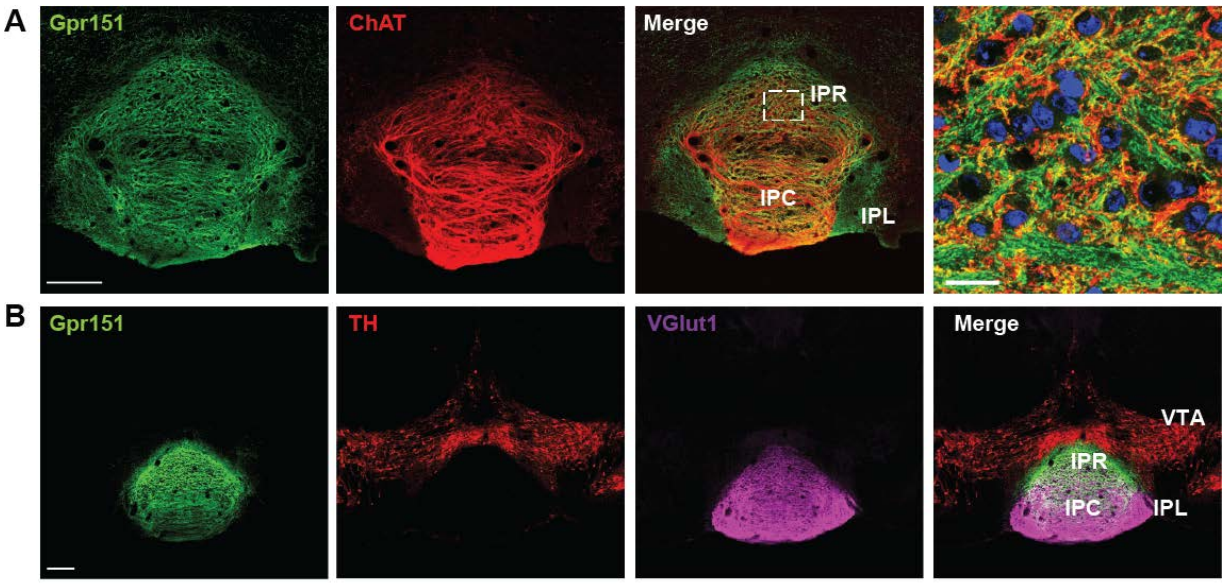

Figure 9. Gpr151 habenular neurons project to the IPN.

(A) Gpr151 and ChAT colocalize in IPR and IPC. Scale bar: 100 µm. Right panel: Higher magnification of the boxed area in the merged panel showing colocalization of Gpr151 and ChAT. Scale bar: 20 µm. (B) Colocalization of Gpr151 and VGlut1 is observed in the IPR and the dorsal part of IPC. Colocalization of Gpr151 and TH is not observed in the VTA. Scale bar: 100µm. ChAT, acetylcholine transferase; TH, Tyrosine Hydroxilase; VGlut1, Vesicular glutamate transporter 1; IPR, rostral; IPC, central; IPL, lateral subnucleus of the interpeduncular nucleus; VTA, ventral tegmental area.

In addition we observed that there are two main Gpr151 projections which continue caudally from the IPN: one passes dorsally to the superior cerebellar peduncle and terminates in the dorsal raphe, where serotoninergic neurons labeled with the serotoninergic marker tryptophan hydroxylase (TpH) are observed (Fig. 10B); the other main projection passes through the rhabdoid nucleus ventrally to the superior cerebellar peduncle and terminates in the central part of the dorsal tegmental nucleus (Fig. 10). These two efferent tracts from the LHb clearly delineated by Gpr151 have not been previously visualized, thus Gpr151 may serve as a specific marker of a functional distinct subpopulation.

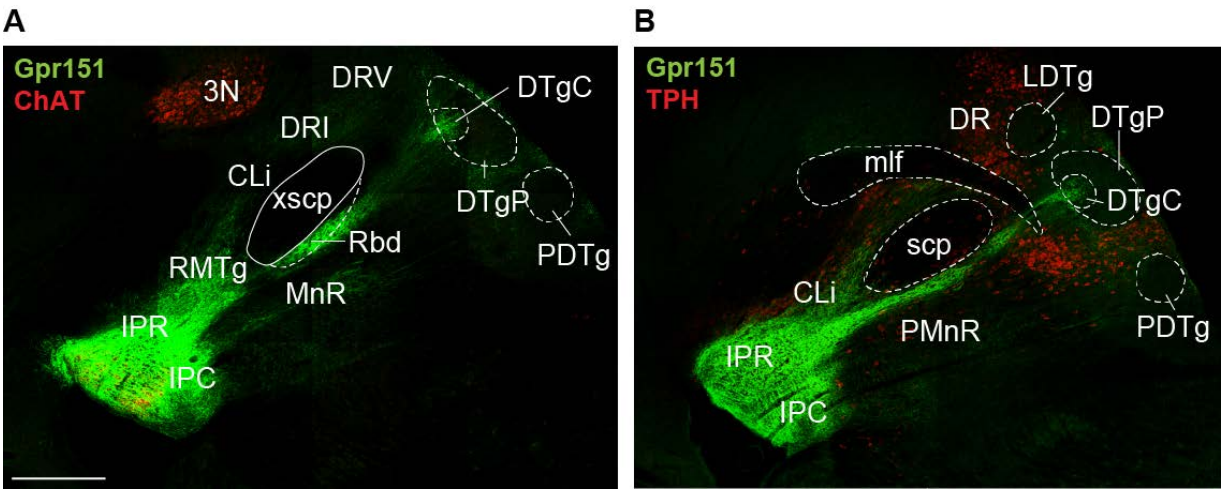

Figure 10. Gpr151 habenular neurons project to the IPN, tegmental nuclei and raphe nuclei

(A-B) Sagittal sections of mouse midbrain and pons showing Gpr151 expression in habenular neurons projecting to the IPN, the RMTg, the Rbd, the dorsal tegmental nucleus and the raphe nuclei. (A) ChAT immunostaining labels the oculomotor nucleus. (B) TpH immunostaing labels the serotoninergic neurons in the raphe. Scale bar: 500µm. ChAT, acetylcholine transferase; TpH, tryptophan hydroxylase; CLi; caudal linear nucleus of the raphe; DR, dorsal raphe; DRI, dorsal raphe interfascicular; DRV, dorsal raphe ventral part; DTgC, dorsal tegmental nucleus central; DTgP, dorsal tegmental nucleus pericent; IPR, interpeduncular nucleus rostral ; IPC, interpeduncular nucleus central; LDTg, laterodorsal tegmental nucleus; mlf, medial longitudinal fasciculus; MnR, median raphe; PDTg, posterodorsal tegmental nucleus; PMnR, paramedian raphe; Rbd, rhabdoid nucleus; RMTg, rostromedial tegmental nucleus; scp, superior cerebellar peduncle; xscp, decussation superior cerebellar peduncle.

In the mesopontine tegmentum, Gpr151 expression was observed in the median (MnR) and paramedian (PMnR) raphe, in the rhabdoid nucleus (Rbd) and in the rostromedial tegmental nucleus (RMTg) (Fig. 11B). Moreover, colabeling of Gpr151 and tryptophan hydroxylase (TPH) indicated that Gpr151 is expressed in the habenular projections terminating in the interfascicular nucleus of the dorsal raphe (DRI), and in the dorsal part (DRD) and ventrolateral part (DRVL) of the dorsal raphe, suggesting that Gpr151 positive neurons of the habenula make synaptic contacts with the serotonergic neurons of the raphe (Fig. 11C).

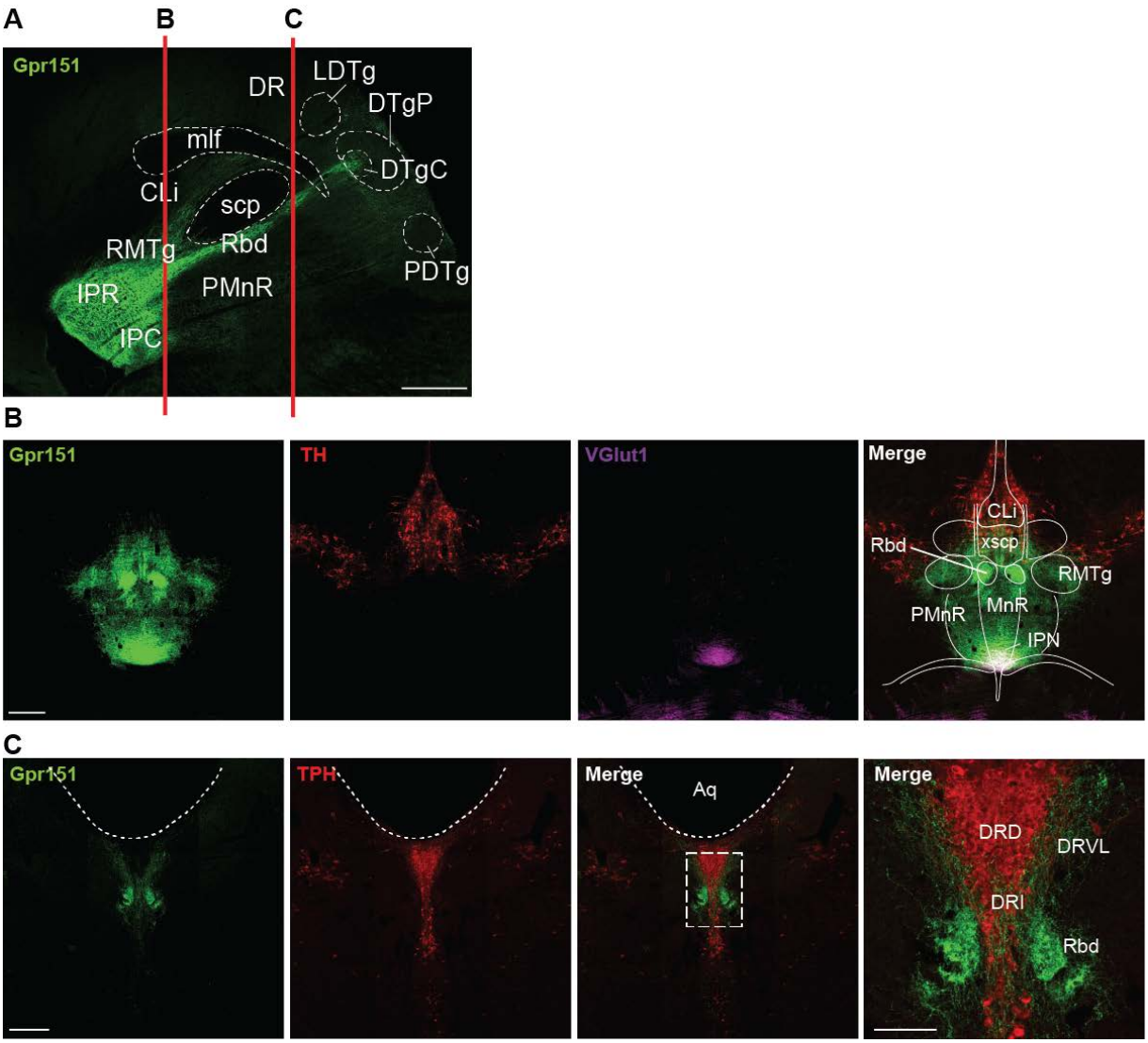

Figure 11. Gpr151 habenular neurons project to the RMTg, raphe and rhabdoid nucleus.

(A) Sagittal section of the mouse midbrain and pons showing the plane of section in subsequent views. (B) Gpr151 and VGlut1 colocalization in the posterior part of the IPN. Gpr151 expression is detected in MnR, PMnR, Rbd and RMTg. Scale bar: 200 µm. (C) Gpr151 habenular neurons project to the Rbd, DRI, DRD and DRVL. Colabeling of Gpr151 and TpH suggests that Gpr151 neurons might make synaptic contacts with serotonergic neurons in DRI. Scale bar: 200 µm. Right panel: Higher magnification of the boxed area in the merged panel. Scale bar: 100 µm. TH, Tyrosine hydroxylase; VGlut1, vesicular glutamate transporter 1; TPH, Tryptophan hydroxylase; Aq, aqueduct; CLi; caudal linear nucleus of the raphe; DR, dorsal raphe; DRD, dorsal part of dorsal raphe nucleus; DRI, interfascicular dosal raphe; DRVL, dorsal raphe ventrolateral; DTgC, dorsal tegmental nucleus central; DTgP, dorsal tegmental nucleus pericent; IPN, interpeduncular nucleus; LDTg, laterodorsal tegmental nucleus; mlf, medial longitudinal fasciculus; MnR, median raphe; PDTg, posterodorsal tegmental nucleus; PMnR, paramedian raphe; Rbd, rhabdoid nucleus; RMTg, rostromedial tegmental nucleus; xscp, decussation superior cerebellar peduncle.

Next, we took advantage of the Gpr151-KO mouse line to visualize the cell body of Gpr151 expressing neurons. In the Gpr151-KO mouse line, a bacterial lacZ gene was inserted into the Gpr151 gene locus such that the endogenous gene promoter drives expression of beta-galactosidase. After staining Gpr151-KO coronal sections with an

antibody against beta-galactosidase, we detected Gpr151 expressing neurons not only in the habenula, but also in the anteromedial, anteroventral and paraventricular thalamic nucleus (Fig. 12A).

In agreement with Aizawa et al. (Aizawa et al., 2012), Gpr151 expressing neurons were abundantly found in the central and lateral part of the MHb. In the LHb, Gpr151 neurons were mainly observed in the superior part of the medial division and in the parvocellular part of the lateral division (Fig. 12B-C).

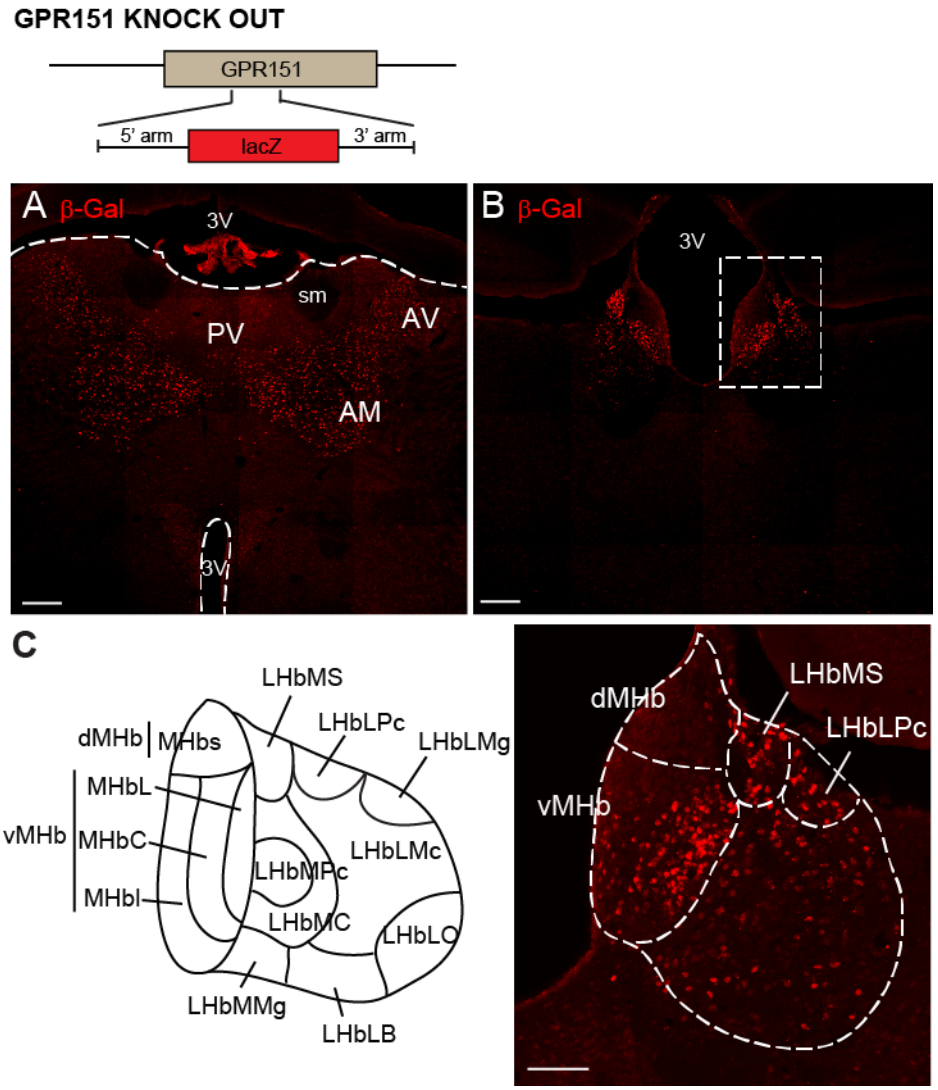

Figure 12. Gpr151 expressing neurons are labeled with β-galactosidase in the thalamus and habenula in Gpr151-KO mouse coronal sections.

Diagram showing Gpr151-KO construct. A bacterial lacZ gene was inserted into the Gpr151 gene such that the endogenous gene promoter drives expression of β-galactosidase. (A-B) β-galactosidase staining was observed in the anteromedial, anteroventral and paraventricular thalamic nucleus and in the habenula. Scale bar: 200 µm. (C) Schematic diagram showing the subdivision of the habenula according to (Wagner et al., 2014). Higher magnification of the boxed area in B shows β-galactosidase expression in the MHbC and MHbL and in the LHb, predominantly in LHbMS and LHbLPc. Scale bar: 100µm. AV, anteroventral thalamic nucleus; AM, anteromedial thalamic nucleus;

PV, paraventricular thalamic nucleus; 3V, third ventricle; sm, stria medullaris; dMHb, dorsal medial habenula; vMHb, ventral medial habenula; LHb, lateral habenula; hbc, habenular commissure; MHbC, central part of MHb; MHbI, inferior part of MHb; MHbL, lateral part of MHb; MHbS, superior part of MHb; LHbMC, central part of the medial division of LHb; LHbMMg, marginal part of the medial division of LHb; LHbMPc, parvocellular part of the medial division of LHb; LHbMS, superior part of the medial division of LHb; LHbLMc, magnocellular part of the lateral division of LHb; LHbLO, oval part of the lateral division of LHb; LHbLPc, parvocellular part of the lateral division of LHb; LHbLMg, marginal part of the lateral division of LHb; LHbLB, basal part of the lateral division of LHb.

3.2 Gpr151 is expressed in the human brain with the same specific axonal compartimentalization as in mice

We analyzed Gpr151 expression by immunohistochemical staining of post-mortem adult human brain samples provided by the NICHD Brain and Tissue Bank. As shown in figure 13, human Gpr151 expression pattern matches the one observed in mice. Gpr151 expression is exclusively localized in the habenula nucleus (Fig. 13A), fasciculus retroflexus (FR) and IPN (Fig. 13B).

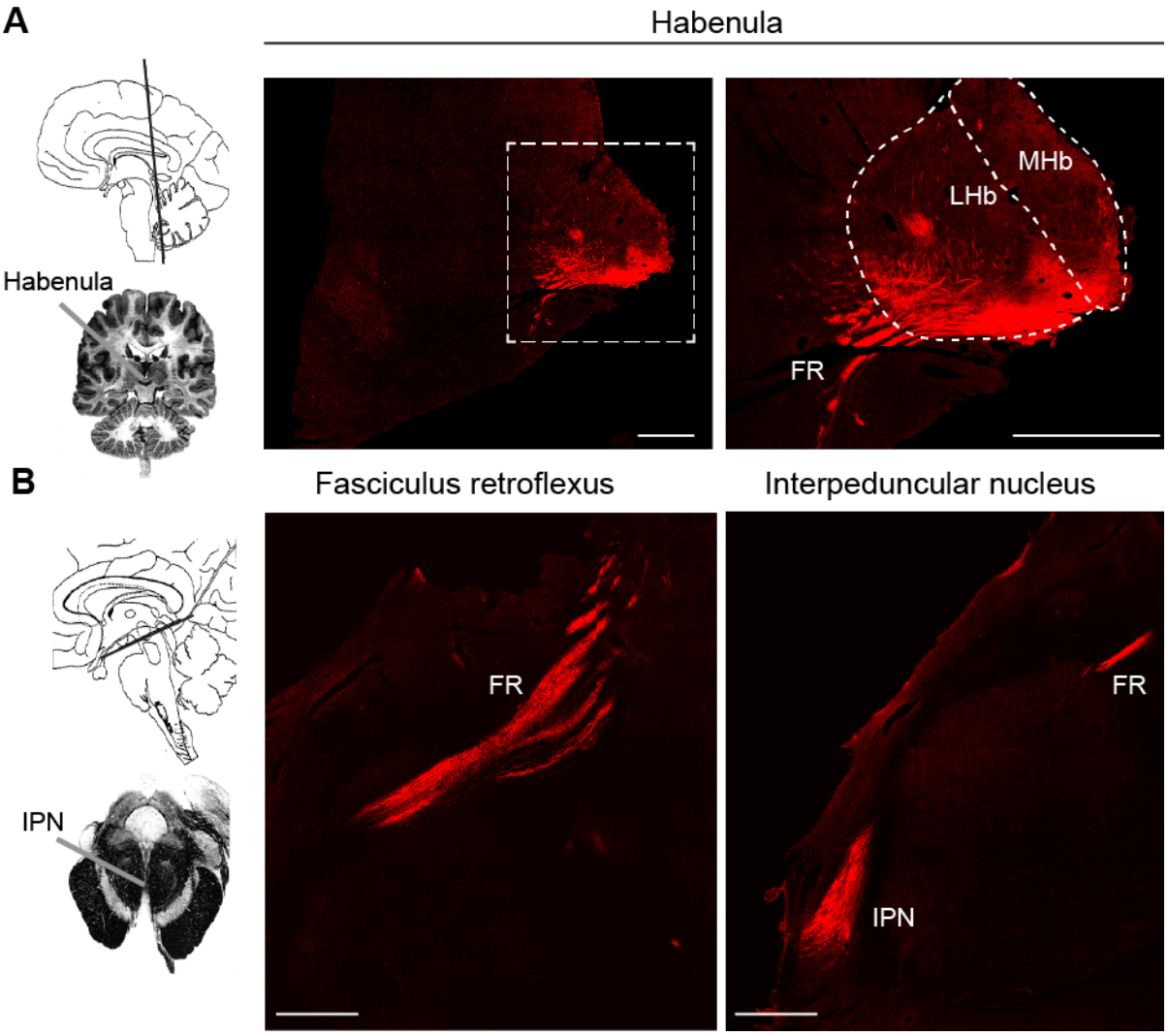

Figure 13. Gpr151 is expressed in the human MHb-IPN pathway.

(A) Diagram of a midsagittal and coronal section through the human brain at the level of habenula. Gpr151 expression is localized in the habenula and beginning of the FR. Right panel is a higher magnification of the left panel. Scale bar: 2 mm. (B) Schematic drawing of a sagittal and horizontal section at the level of the IPN. Gpr151 is expressed at the FR (left panel) and IPN (right panel). Scale bar: 1mm.

The extraordinary bright and restricted expression of Gpr151 uniquely in this axonal tract is remarkable, confirming the importance of the proposed studies to human health. We observed the same restricted pattern of expression of Gpr151 in 3 control donors and one heavy smoker, albeit the immunofluorescence signal appeared stronger in the smoker. Of course, data indicating that the expression of this receptor is altered as a consequence of addiction in humans would be highly significant. However a quantitative analysis of Grp151 immunohistochemistry in post-mortem human sections was out of the scope of this thesis.

3.3 Ultrastructural sub-localization of Gpr151 in the interpeduncular nucleus.

To assess the ultrastructural localization of Gpr151 within habenular terminals, we performed immuno-electron microscopy (iEM) of coronal sections of the IPN of wildtype mice. For iEM, the immunocytochemical labeling can be performed either prior to the embedding of the sample in the resin (preembedding iEM) or after sections are embedded in the resin (postembedding iEM). Pre-embedding iEM provides the opportunity to examine immune immunocomplexes under light microscopy, thus giving the advantage of localizing the immunocomplex in heterogeneous structures, such as the brain. It also tends to give a robust signal, compared to post-embedding iEM and better tissue quality (Heimer et al., 2006). For these reasons, we first performed preembedding peroxidase iEM labelling on coronal sections of the IPN.

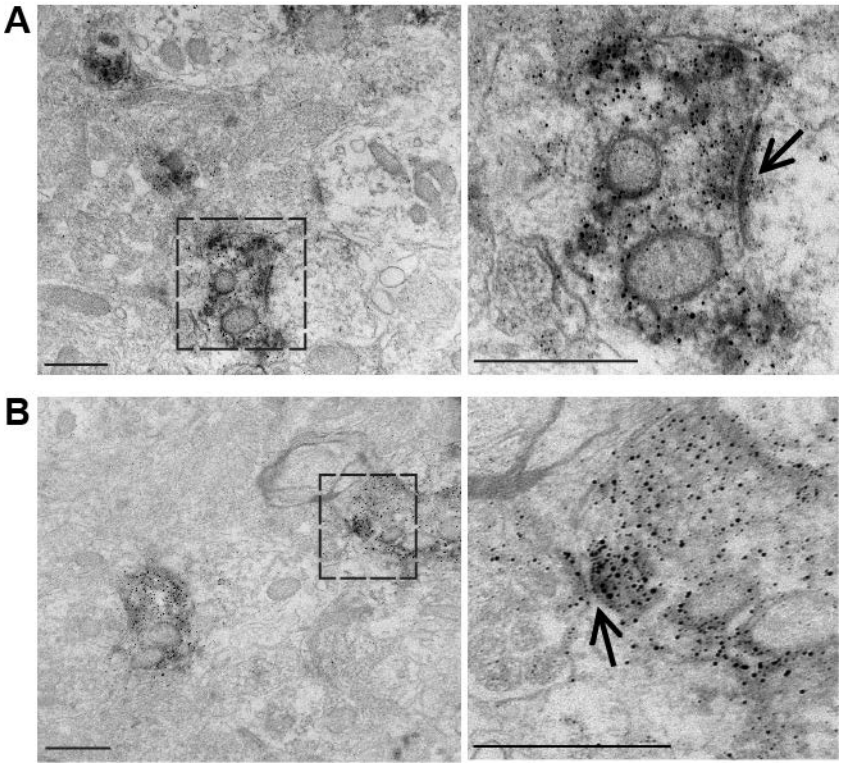

Figure 14. Gpr151 is localized at habenular terminals in the IPN.

(A-B) ImmunoEM with DAB stain and silver enhancement of IPN sections shows Gpr151 labeling in some presynaptic terminals. *En-passant* boutons (arrow in A) and crest synapse (arrow in B) and are both positive for Gpr151.Scale 500 nm.

As shown in figure 14, Gpr151 labeling can be observed in habenular terminals. Gpr151 was localized at the presynaptic boutons in both synaptic specializations of

habenular axons: S synapses (arrow, Fig. 14A) and crest synapses (arrow, Fig. 14B). S synapses are composed of *en passant* boutons forming asymmetrical contacts with small dendritic processes. Crest synapses are composed of two parallel boutons of habenular axons contacting an attenuated dendritic process (Hamill and Lenn, 1984; Kawaja et al., 1989; Lenn, 1976). Interestingly Gpr151 labeling was localized over the presynaptic active zone (Fig. 14A-B). In addition immunoreactivity was observed within the extrasynaptic plasma membrane; inside the terminal, in association with large transport vesicles or cisternae; and in the mitochondrial membrane. However as the peroxidase reaction product is known to diffuse away from the location of the antigen (Courtoy et al., 1983; Novikoff, 1980), this signal may be an artifact of the immunoperoxidase technique.

To overcome this problem and determine more accurately the localization of Gpr151 at habenular terminals, we next performed post-embedding iEM. Immunogold particles labelling Gpr151 were found to localize at the plasma membrane of presynaptic boutons (arrows, Fig. 15A), suggesting that Gpr151 could be modulating synaptic transmission and/or plasticity. Surprisingly, some immunoreactivity was also observed in close association with synaptic vesicles (arrowheads, Fig. 15A).

Given that different types of vesicles can be found at the terminals, including synaptic vesicles, transport vesicles and endocytic vesicles (Ahmari et al., 2000; Sudhof, 2004), we next performed double labeling with Gpr151 and vesicular glutamate transporter 1 (VGlut1) antibodies to ensure that the vesicles associated with Gpr151 were indeed synaptic vesicles filled with neurotransmitter. Gpr151 was labeled with 12 nm gold particles, whereas VGlut1 was labeled with 6 nm gold particles. Gpr151 and VGlut1 immunogold particles were found close to each other in association with synaptic vesicles (SV) (left panel, Fig. 15B), suggesting that Gpr151 might be translocated from SVs to the plasma membrane of the active zone upon depolarization of the neuron and neurotransmitter release.

As shown on the right panel of figure 15B, Gpr151 and VGlut1 were also found in close proximity to each other along the microtubules in a longitudinal section of an habenular axon. This result indicates the following: first, Gpr151 is not localized at the axonal plasma membrane, but inside the axons in contact with the microtubules. Second, Gpr151 and VGlut1 are transported in close association along the microtubules to the terminals.

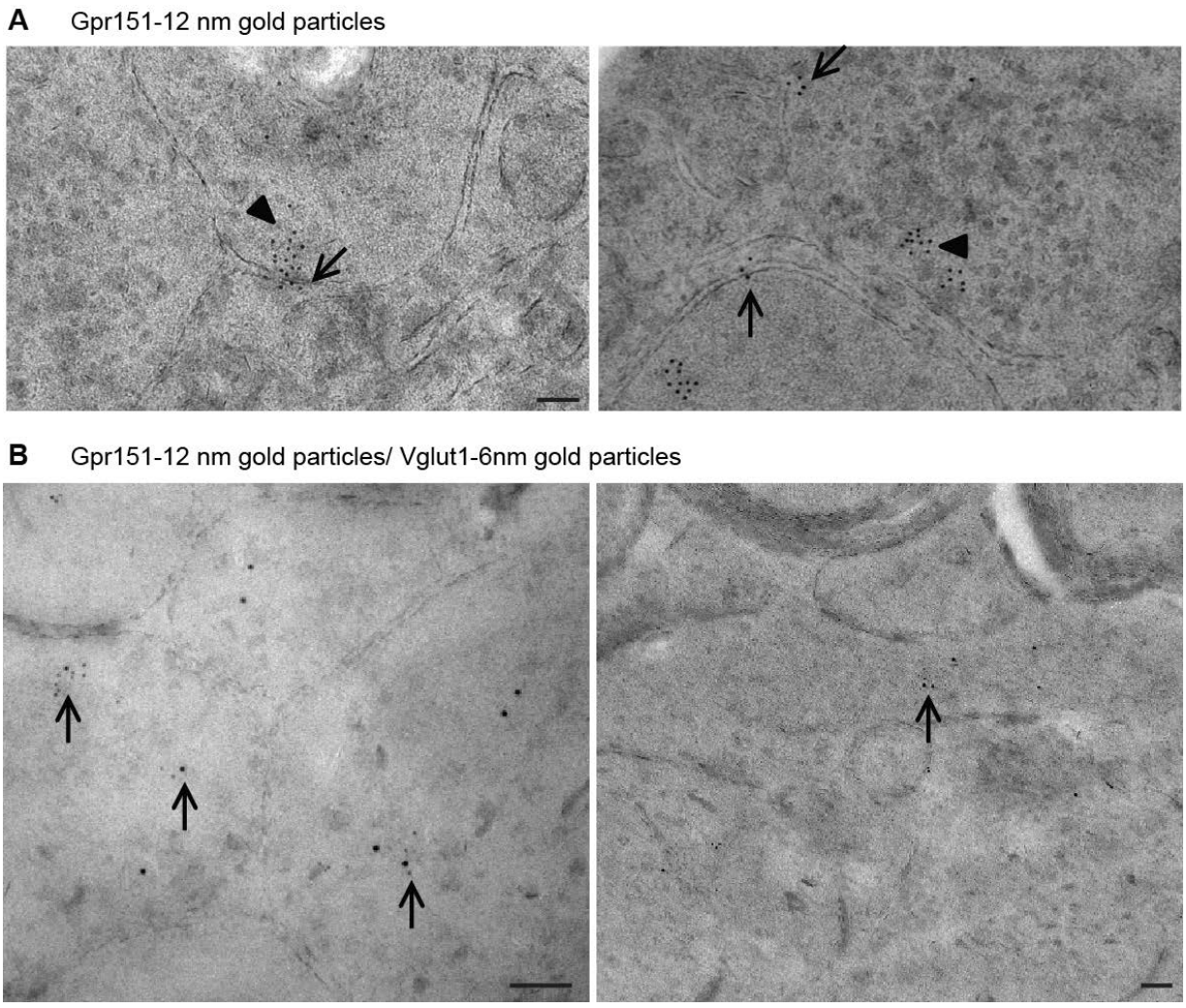

Figure 15. Distribution of Gpr151 immunogold particles in habenular terminals in the IPN.

(A) Two examples of Gpr151 immunogold labeling at the terminals. On the left panel, Gpr151 is localized at the membrane of the active zone (arrow) and in association with synaptic vesicles (arrowhead). On the right panel, Gpr151 is found at the extrasynaptic membrane (arrows) and also in association with synaptic vesicles (arrowhead). (B) Two examples of Gpr151 and VGlut1 co-labeling. On the left panel, Gpr151 and VGlut1 are found in close proximity associated with synaptic vesicles (arrows). On the right panel, Gpr151 and VGlut1 are localized very close to each other along the microtubules of a longitudinal axon (arrow). Scale 100nm.

In summary, data acquired from pre-embedding and post-embedding iEM indicate that Gpr151 is found to be associated with:

- The plasma membrane at the habenular terminals in the IPN. Some labeling was observed at the active zone and peri-active zone region, indicating that Gpr151 may modulate synaptic transmission. In addition, Gpr151 labeling was observed at the extrasynaptic plasma membrane.

- Transport vesicles or cisternae inside the terminals and along the microtubules.

- Synaptic vesicles, some of them glutamatergic. These results suggest that Gpr151 could be translocated from SVs to the plasma membrane when, upon neuronal depolarization, SVs fuse to the plasma membrane and release their content to the synaptic cleft.

3.3.1 Ultrastructure of the IPN is not altered in Gpr151-KO mice

In addition we investigated whether deletion of Gpr151 affects the ultrastructure of the presynaptic terminals in the IPN. To address this aim, electron micrographs of wildtype mice were compared to Gpr151-KO mice. We found no visible differences in the number of terminals that establish synaptic contacts with dendritic spines (Fig. 16A). We next examined the size of the presynaptic terminals and the organization of synaptic vesicles; and as shown in figure 16B, no major differences were observed. The fact that Gpr151 absence does not alter the synaptic morphology is important as it indicates that Gpr151 may change synaptic activity but not synaptic scaffolding, thus allowing us to test the contribution of Gpr151 to behavioral changes observed in basal conditions or upon activating this neuronal tract, for instance with nicotine.

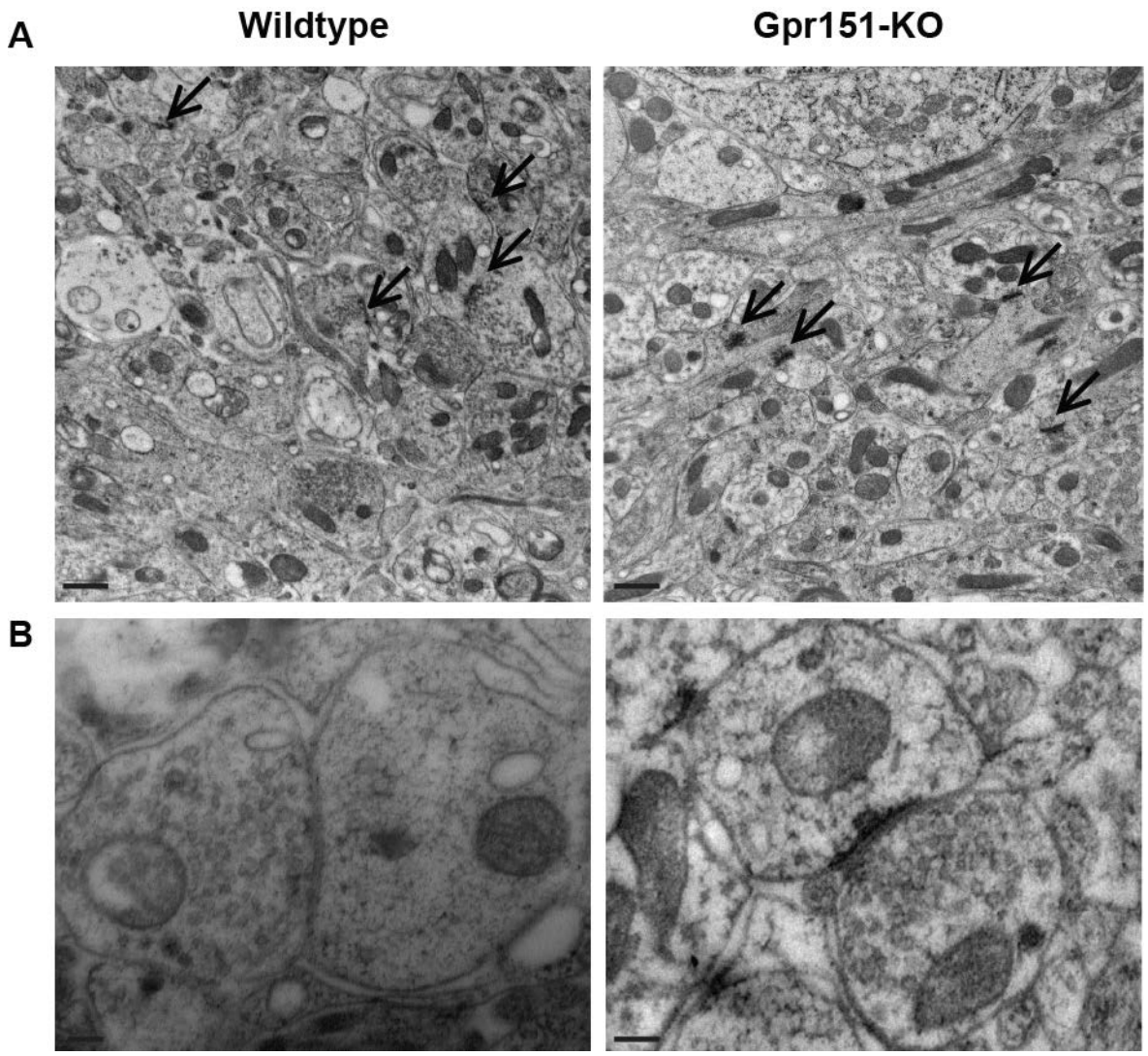

Figure 16. Ultrastructure of the IPN is not altered in Gpr151-KO mice.

(A) Representative low-magnification electron micrographs of synaptic neuropil in the IPN of wildtype and Gpr151-KO mice. The number of synaptic contacts (arrows) is not changed. Scale bar: 500 nm. (B) Electron micrographs illustrate organization of synaptic vesicles within an habenular axon terminal from a wildtype and Gpr151-KO mouse. The size and organization of synaptic vesicles is not affected by Gpr151 deletion. Scale bar: 100 nm.

3.4 Analysis of the Gpr151 signaling pathway

We next sought to identify the Gpr151 signaling pathway. All members of the GPCR family bind to heterotrimeric G proteins at the plasma membrane. Stimulation by an agonist leads to dissociation of G-protein subunits α,β,γ. G-protein families regulate different intracellular second messenger pathways based on the type of G-protein subunit involved (Fig. 17A) (Table. 1).

Given that cAMP levels have been shown to modulate neurotransmitter release in axonal terminals of MHb neurons (Hu et al., 2012) and that many proteins activated by cAMP are highly expressed in MHb neurons (Görlich et al., 2013), we measured the levels of cAMP by ELISA in wildtype and Gpr151-KO mice. As shown in figure 17B, cAMP concentration was significantly increased in the IPN of Gpr151-KO mice compared to wildtype mice. Reciprocally, downregulation of Gpr151 by injection of LV-shRNA showed a 36% increase of cAMP levels. These data suggest that Gpr151 couples to a Gαi/o protein, which inhibits adenylyl cyclase activity and therefore leads to a decrease of intracellular cAMP levels.

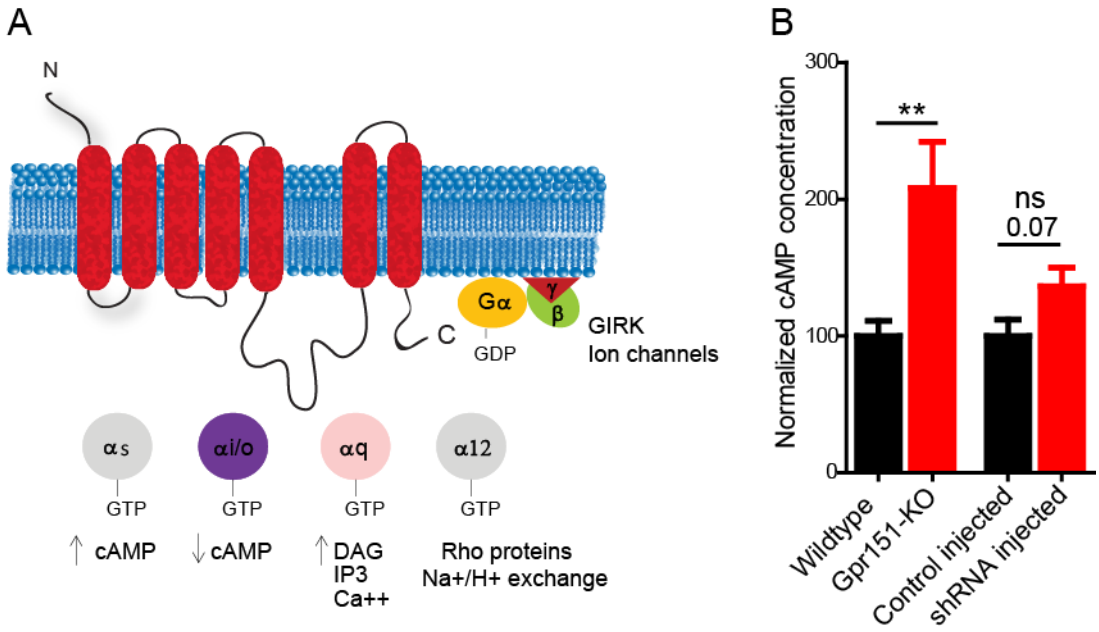

Figure 17. Gpr151 is likely to couple to Gαi/o.

(A) Schematic representation of a GPCR, the trimeric G protein and the main G-protein-mediated signaling pathways, mediated by four sub-classes of Gα-proteins (Gαs, Gαi/o, Gαq/11, and Gα12/13) and Gβγ. (B) Normalized cAMP levels in the IPN of Gpr151-KO mice (n=6-8 per group). Data are expressed as mean ± SEM (*p<0.05; **p<0.01; within groups t-test) (ns, not significant).

To confirm the result of Gpr151 coupling to Gαi/o, we next set up two different assays to measure cAMP and calcium levels in HEK293T cells.

First we used the GloSensor™ cAMP Assay, which involves a genetically modified form of the firefly luciferase containing a cAMP-binding protein domain. Binding of cAMP to this domain induces a conformational change, which in turn leads to luciferase activity. HEK293T cells were transfected with the Gpr151-HA plasmid and the luciferase plasmid. In this assay although the ligand is not present, we can test whether dimerization of Gpr151 might have an activity in cAMP signaling. Indeed autoactivation of GPCRs when overexpressed in cells or in transgenic mice has been reported (Bond et al., 1995; Rosenkilde et al., 2006; Vischer et al., 2006).

Cells were transfected with luciferase and equal or double amounts of Gpr151 (1x and 2x). As a control, cells were transfected only with luciferase (negative control) or with luciferase plus equal amounts of a transmembrane receptor, the PDGF-receptor fused to mCherry (named as pFU-PC) (Auer et al., 2010). The following day, we measured luminescence levels, which are proportional to cAMP levels, for 20 min at a basal situation. As shown on the left panel of figure 18A, there were no significant differences between Gpr151 and control transfected cells. We then applied 10 µM forskolin to cells activating the enzyme adenylyl cyclase, and therefore, increasing the intracellular levels of cAMP. Consequently, luminescence levels were increased in all conditions (Fig. 18A, right panel). Again we did not detect any differences between the Gpr151 and control transfected cells. Indeed we saw that doubling the amount of Gpr151 reduced the levels of luciferase activity. Surprisingly, the pFU-PC control showed also reduced luciferase activity. We believe that reduced luciferase activity could have resulted from lower expression levels of luciferase plasmid. In conclusion, these results show that overexpression of Gpr151 does not modulate the cAMP signaling pathway.

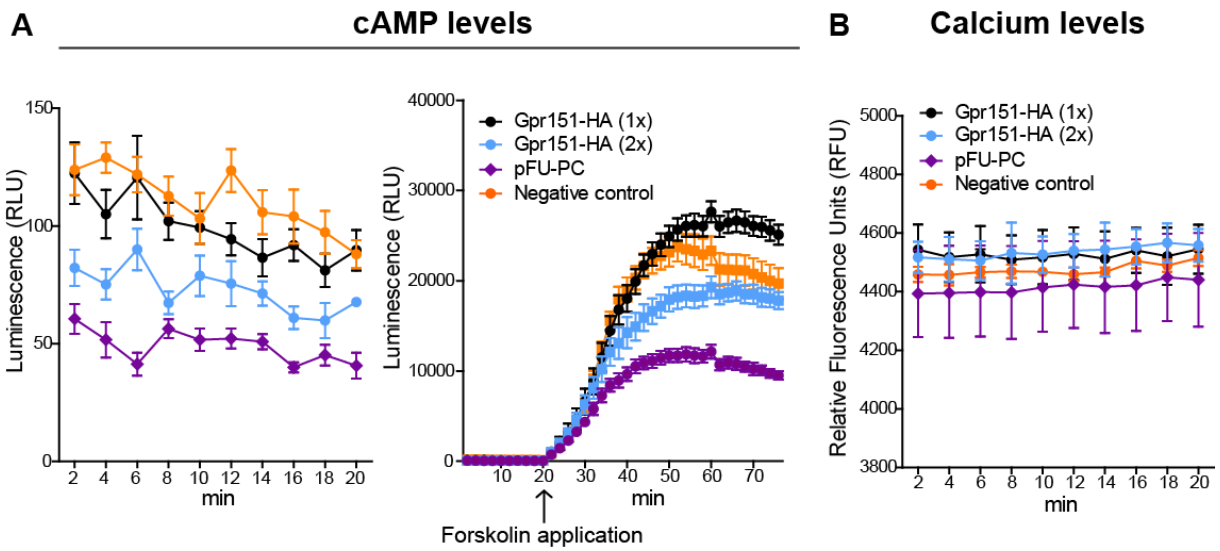

Figure 18. Gpr151 overexpression does not activate cAMP or calcium signaling.

(A) Luminescence levels, which are indicative of cAMP levels, were measured on HEK293T cells transfected either with Gpr151 or pFU-PC as a control plus the luciferase plasmid. Gpr151 expression did not modulate cAMP levels compared to control cells. (B) Relative Fluorescence Units, indicative of calcium levels, were measured on HEK293T cells transfected either with Gpr151 or pFU-PC as a control. Increasing Gpr151 concentration did not change calcium levels. Data are expressed as mean ± S.E.M.

We next tested whether Gpr151 overexpression activates calcium signaling. For this purpose, we used the Fluo-4 Direct™ assay, which involves a fluorescent calcium indicator. Fluorescence calcium indicators are widely used to measure agonist-activated and antagonist-inhibited calcium signaling through GPCRs. Cells were transfected with Gpr151 (1x and 2x concentration) and pFU-PC (1x) as a control. Levels of calcium measured by relative fluorescent units showed no statistical difference between Gpr151 transfected cells and control. Moreover calcium levels were not changed by increasing amounts of Gpr151, suggesting that overexpression of Gpr151 does not activate calcium signaling (Fig. 18B).

In summary, results from the cAMP ELISA experiments using IPN samples of wildtype and Gpr151-KO mice indicates that Gpr151 possibly couples to the Gαi subunit and therefore, its activation leads to a decrease of cAMP intracellular levels. In contrast, the cell-based cAMP assay was not conclusive. Moreover, results from the calcium assay indicated that Gpr151 does not significantly modulate calcium signaling. However, we should consider that we are testing whether overexpression of Gpr151 modulates the cAMP or calcium signaling just by autoactivation. It is likely therefore that overexpression of Gpr151 in transfected cells does not result in a robust autoactivation of the receptor.

3.5 Approaches used to identify Gpr151 ligands

Three parallel lines of assays were used to test and search for putative Gpr151 ligands and intracellular binding partners:

1) Cell-based assays to test the activity of galanin, galanin-like peptides and tachykinin-like peptides.

2) Use of habenular primary cultures as a source of the putative ligand.

3) Bioinformatics approach to simulate *in silico* docking of Gpr151 with a lead-like structural library of synthetic compounds.

3.5.1 Cell-based assays to test the activity of galanin, galanin-like peptides and tachykinin-like peptides

Gpr151 shows the highest homology with the galanin receptors 2 and 3. For this reason we hypothesized that the ligand for Gpr151 is probably a peptide related to galanin. To test this possibility we assayed the activity of the galanin peptide and the galanin-message-associated peptide (GMAP), a second peptide which derives from the same preprogalanin precursor that has unknown receptor activity. We measured cAMP and calcium levels on HEK cells expressing Gpr151. We applied galanin at different concentrations to HEK293T cells transfected with Gpr151 and measured cAMP levels using the Glo-Sensor cAMP assay. As shown in figure 19A, application of galanin (1 µM) did not produced significant differences in the levels of cAMP between Gpr151 expressing and control cells. Moreover, there were no differences upon application of galanin at 10, 5, 0.5, 0.1, 0.01 µM (data not shown). We also measured calcium-induced fluorescence after application of galanin (5 µM, 1µM and 0.5 µM) on HEK293T cells transfected with Gpr151. Galanin did not induce a significant change between Gpr151 and control expressing cells (Fig. 19B). These results indicated that galanin does not activate the cAMP or calcium signaling pathway on cells expressing Gpr151.

In addition application of the related peptide GMAP (data not shown) did not induce a significant change on cAMP or calcium levels between Gpr151 and control expressing cells.

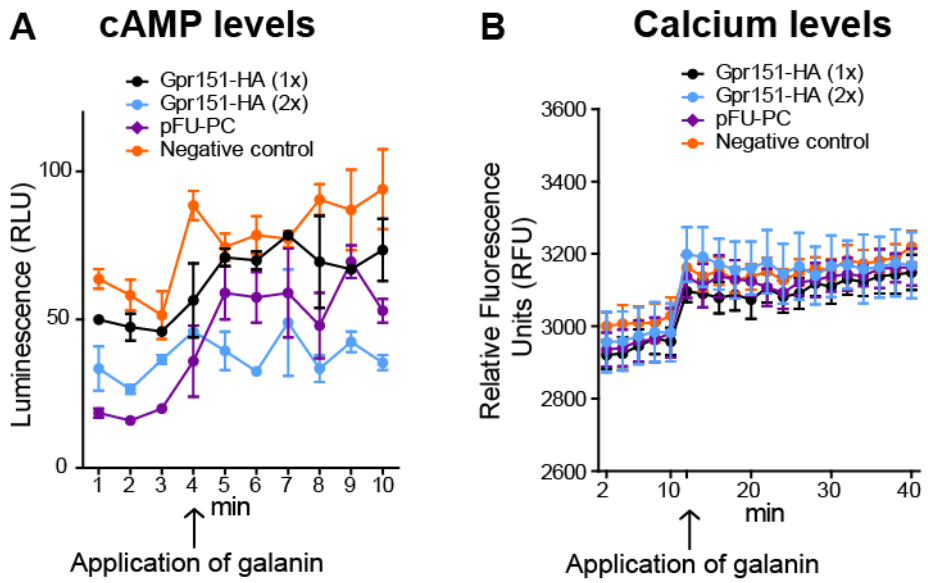

Figure 19. Galanin does not activate cAMP or calcium signaling on HEK293 cells expressing Gpr151.

(A) Luminescence levels, which are indicative of cAMP levels, were measured on HEK293T cells transfected with Gpr151 plus the luciferase plasmid or pFU-PC as a control. Application of galanin did not change cAMP levels compared to control cells. (B) Relative Fluorescence Units, indicative of calcium levels, were measured on HEK293T cells transfected either with Gpr151 or pFU-PC as a control. Application of galanin did not change calcium levels differently in Gpr151 expressing cells compared to control cells. Data are expressed as mean ± S.E.M.

Galanin has been shown to activate Gpr151 with an EC50 value of 2 µM in transfected CHO cells (Ignatov et al., 2004). Ignatov et al., used stably transfected CHO cells with apoaequorin as calcium sensor and with Gα16 as promiscuous G-protein subunit (Ignatov et al., 2004; Stables et al., 1997). Therefore we could explain this discrepancy by the potential lack of the G-protein subunit and/or other adaptor proteins necessary for Gpr151 signaling in our assays, which might not have been limiting in the apoaequorin heretologous assay.

We also found that Gpr151 shows homology to the tachykinin receptors neurokinin 2 (NK-2) and NK-3 receptors. We performed a BLAST search in the NCBI database for *mus musculus* proteins homologous to Gpr151 (NP_853521.1) which indicated that in addition to Galanin-receptor 2 and 3, Gpr151 shows between 60 and 80% homology to NK-2 and NK-3 receptors. For this reason, we tested the activity of various agonists and antagonists of NK2 and NK3 receptors, including Substance P, Neurokinin B, GR64349, GR159897 and MEN10376. Gpr151 transfected cells failed to show an increase of cAMP (Fig. 20A) or calcium levels (Fig. 20B) higher to the one observed in the control upon application of any of the peptides mentioned, indicating that these peptides do not modulate Gpr151 activity in these cell-based assays.

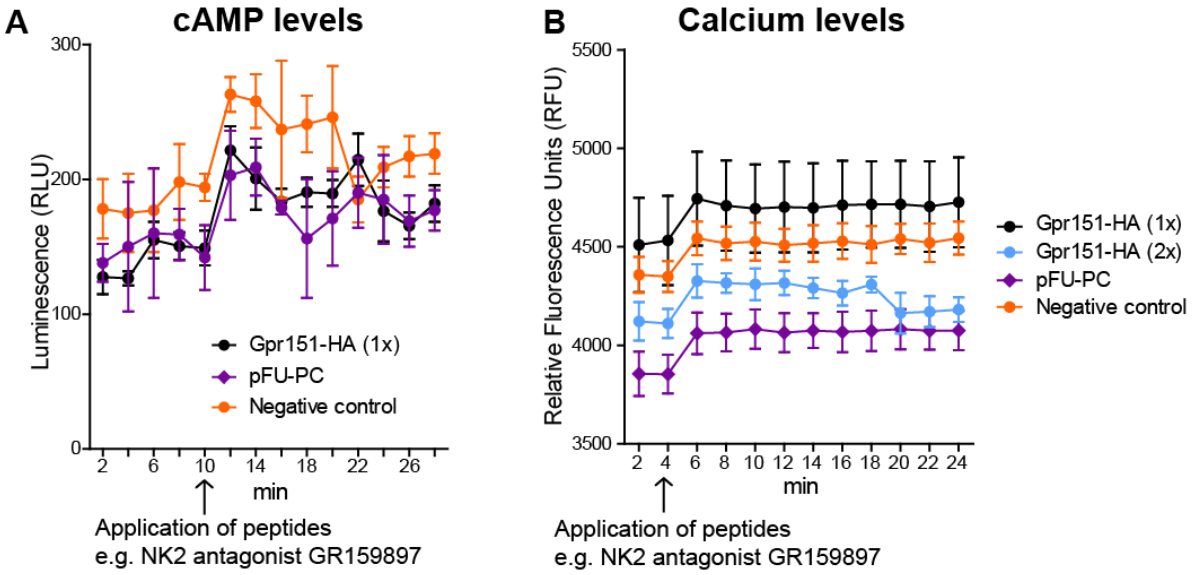

Figure 20. Different galanin-like and tachykinin-like peptides do not activate cAMP or calcium signaling on HEK293 cells expressing Gpr151.

(A) Luminescence levels, which are indicative of cAMP levels, were measured on HEK293T cells transfected with Gpr151 plus the luciferase plasmid. Application of the NK2 antagonist GR159897 did not change cAMP levels compared to control cells expressing pFU-PC or non-transfected cells. (B) Relative Fluorescence Units, indicative of calcium levels, were measured on HEK293T cells transfected either with Gpr151 or pFU-PC as a control. Application of the NK2 antaginst GR159897 did not change calcium levels differently in Gpr151 expressing cells compared to control cells. Data are expressed as mean ± S.E.M.

3.5.2 Use of habenular primary cultures as a source of the ligand

Data obtained from the nicotine-related behavioral studies revealed that Gpr151-KO mice displayed increased sensitivity to nicotine-conditioned reward and increased physical and affective nicotine withdrawal signs (see 3.6 section, Fig. 24 and 27). These results together with Gpr151 localization at the membrane of the synaptic vesicles (Fig. 15), suggest that Gpr151 might be acting as an inhibitory regulator in the control of these behaviors. For this reason, we hypothesized that Gpr151 may act as an autoreceptor. Hence the ligand might be synthesized by Gpr151 expressing neurons and would be released upon stimulation of these neurons. The ligand would then bind to Gpr151 at the presynaptic site and inhibit or reduce neurotransmitter release as a feedback mechanism.

To test this hypothesis, we acquired CHAT-ChR2-YFP BAC (ChAT-ChR2) transgenic mice expressing an improved channelrhodopsin-2/EYFP fusion protein directed to cholinergic neuronal populations (Zhao et al., 2011). A recent study has shown that ChAT positive neurons co-release glutamate and ACh upon different intensity of blue

light stimulation in transgenic ChAT-Channelrhodopsin mice (Ren et al., 2011). Brief photostimulation of cholinergic MHb terminals produces fast glutamatergic excitatory postsynaptic potentials in IPN neurons whereas tetanic stimulation generates slow cholinergic responses (Ren et al., 2011).

We prepared primary cultures of habenular neurons of ChAT-ChR2 embryos (Fig. 21A) or wildtype embryos (Fig. 21B). On day in vitro 10, we stimulated the neurons with blue light pulses of 5 ms, with a 5 seconds interval, during 2 minutes. Blue light stimulation of ChAT-ChR2 neurons leads to their activation and hypothetically, to the release of Gpr151 ligand. We then collected the supernatant and applied it immediately to HEK293T cells expressing Gpr151 (1x and 2x), luciferase and pFU-PC (1x and 2x) as a control. Luminescence levels were measured as an indication of cAMP levels. Application of both supernatants, from ChAT-ChR2 and control habenular primary cultures, induced an increase of cAMP levels in all conditions, but this increase was independent of Gpr151 expression (Fig. 21C). Moreover, there were no differences in cAMP levels after application of supernatant from ChAT-ChR2 stimulated neurons compared to control neurons (Fig. 21C).

The lack of cAMP activity observed can be explained by the following reasons: 1) Gpr151 ligand might be produced upon a longer chronic stimulation; 2) Gpr151 is not being produced by the cholinergic habenular neurons; 3) Gpr151 ligand is not concentrated enough in the supernatant to be able to activate the cAMP signaling pathway on HEK cells expressing Gpr151; 4) the G-protein subunit and/or other adaptor proteins necessary for Gpr151 signaling are not expressed in HEK cells transfected only with Gpr151 and therefore, cAMP levels remained unaffected upon the application of the supernatant of habenular primary cultures.

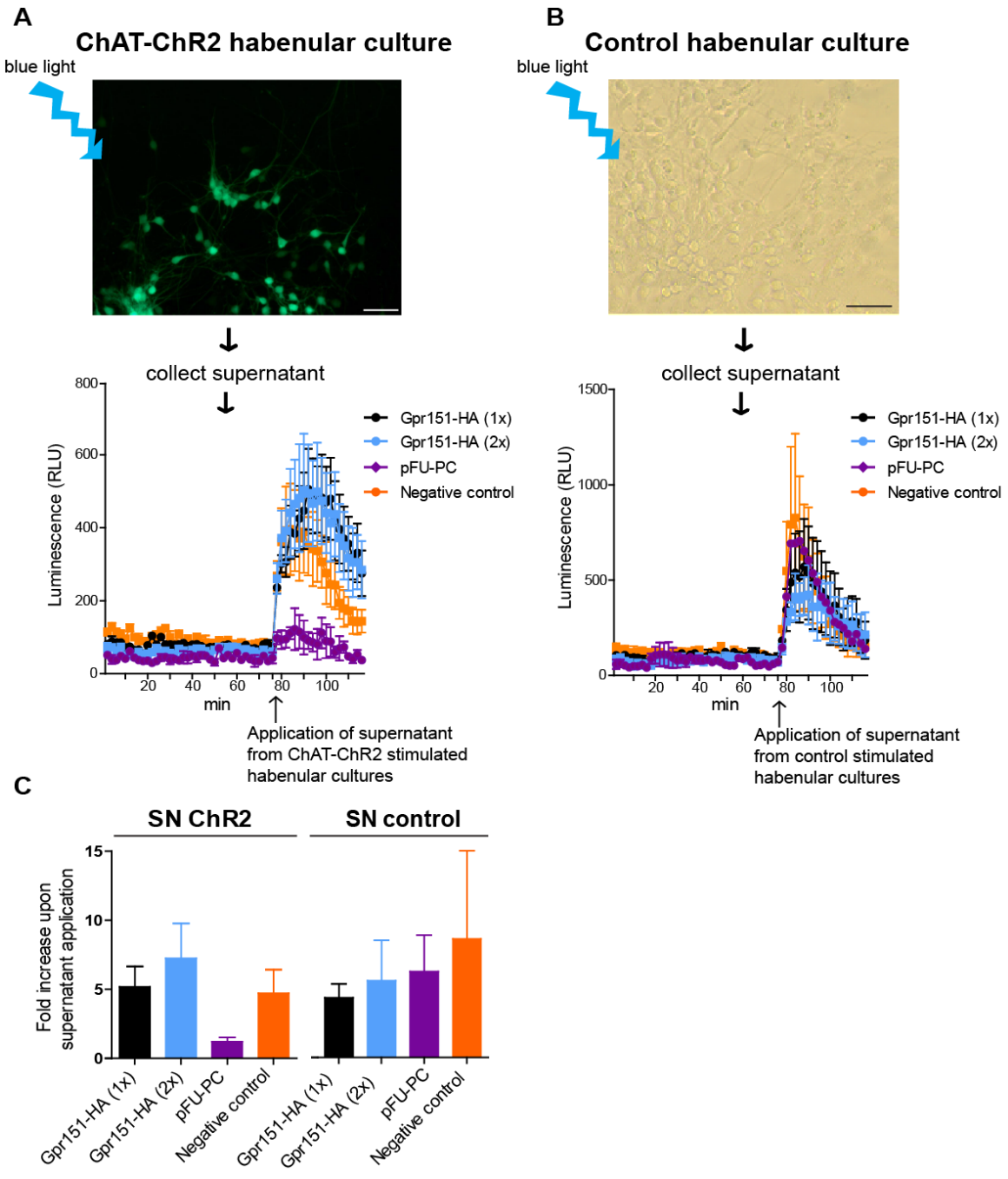

Figure 21. Application of the supernatant of light-stimulated habenular cultures does not result on activation of cAMP signaling on HEK293T cells expressing Gpr151.

(A) Top: ChAT-ChR2 habenular culture at DIV5. ChAT-ChR2 neurons were stimulated at DIV10 with blue light for 2 minutes and the supernatant was immediately applied to HEK293T cells. Bottom: Luminescence levels, which are indicative of cAMP levels, were measured on HEK293T cells transfected with either Gpr151 or pFU-PC as a control plus the luciferase plasmid. Application of the supernatant did not change cAMP levels in Gpr151 expressing cells compared to control cells. (B) Top: Wildtype habenular culture at DIV5. The same procedure than for (A) was performed with wildtype neurons. Bottom: Luminescence levels, which are indicative of cAMP levels, were measured on HEK293T cells transfected with either Gpr151 or pFU-PC as a control plus the luciferase plasmid. (C) Fold increase of luminescence levels upon application of the supernatant is not different between conditions. (SN, supernatant). Scale bar: 20µm. Data are expressed as mean ± S.E.M.

3.5.3 Bioinformatics approach to simulate *in silico* docking of Gpr151 with a lead-like structural library of synthetic compounds

In silico homology modeling of GPCRs followed by high throughput screening of chemical databases and experimental validation has led to the identification of pharmacological compounds acting as antagonists or inverse agonists (Jaakola and Ijzerman, 2010). Our goal was to identify potential Gpr151 ligands using the following strategy: 1) the *in silico* modeling of Gpr151 based on the use of multiple templates; 2) the *in silico* screening of virtual chemical libraries. For this purpose, we used the Molecular Operating Environment (MOE) software, which has been used successfully in the identification of synthetic binding ligands for GPCRs (Eberini et al., 2011) and glycoproteins (Tomar et al., 2010). Gpr151 sequence was downloaded from NCBI (Reference Sequence: NP_853521.1) and the Gpr151 model was built based on multiple templates from crystallographic structures of class A GPCRs. The active site was calculated using the site finder tool of MOE. The suggested active site comprising Ile42, Ile43, Pro44, Ser45, Leu46, Leu47, Ala49, Val50, Tyr103, Lys116 was chosen for the *in silico* screening (Fig. 22A). Most of the amino acids in the suggested active site are hydrophobic and they are located on the extracellular part of the transmembrane domain 1, 2 and 3. We then carried out the screening of compounds with the Dock Program against The Asinex Platinum Collection (http:// www.asinex.com/) which is a lead-like structural library containing 113.962 in-house synthesized compounds. The binding of the ligand to the Gpr151 model was scored according to the London dG scoring, which estimates the free energy of binding of the ligand from a given pose. The three ligands with the lowest energy scores (more favorable poses) are shown in figure 22B. Unfortunately the score of the tested compounds was not low enough to qualify them as putative ligands of Gpr151.

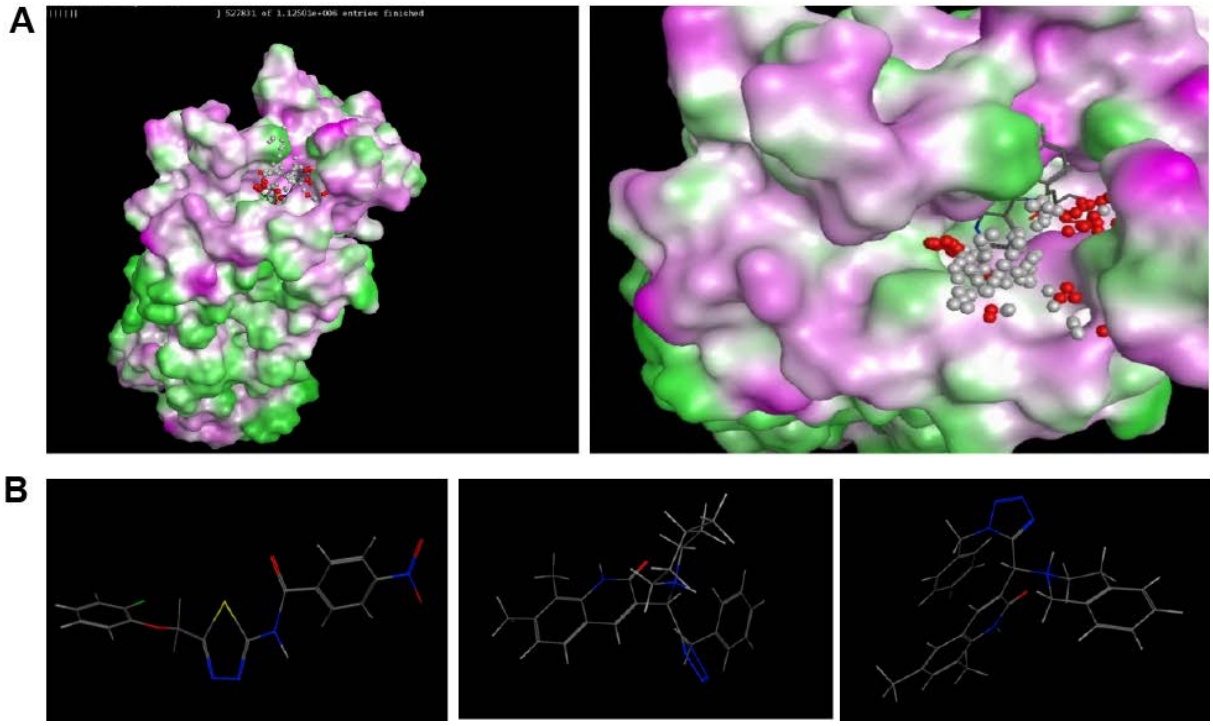

Figure 22. Docking of Gpr151 model against Asinex Platinum database using Molecular Operating Environment software.

(A) Gpr151 model showing a compound being docked within the binding pocket. Green regions are hydrophobic, purple are hydrophilic. (B) Chemical structures of the three top-scoring ligands from left to right: (1) N-[5-(2-Fluoro-phenoxymethyl)-[1,3,4]thiadiazol-2-yl]-4-nitro-benzamide. (2) 3-[(1-Benzyl-1H-tetrazol-5-yl)-(4-methyl-piperidin-1-yl)-methyl]-7,8-dimethyl-1H-quinolin-2-one. (3) 3-[(1-Benzyl-1H-tetrazol-5-yl)-(3,4-dihydro-1H-isoquinolin-2-yl)-methyl]-6,8-dimethyl-1H-quinolin-2-one.

3.6 Contribution of Gpr151 to habenular-related behaviors

3.6.1 Gpr151 knockout mice showed normal locomotor activity, no anxiety-like behaviors and regular sensorimotor gating

To address the function of Gpr151, we examined Gpr151 knockout (Gpr151-KO) mice using a series of behavioral assays. Homozygous mutant mice showed no significant differences in weight and size when compared with age- and gender-matched wildtype (WT) control mice. As shown previously in figure 6, Gpr151-homozygous KO mice do not express Gpr151 as revealed by undetectable immunoreactive signal in brain sections.

Classic lesion studies in rodents have suggested a role of the habenular nuclei in modulating exploratory behavior, locomotor activity and anxiety (Kobayashi et al., 2013; Lee and Huang, 1988; Murphy et al., 1996; Yamaguchi et al., 2013). We therefore analyzed whether Gpr151-KO mice showed impaired locomotion by testing these mice in the open field. No significant differences in total locomotor activity were observed in Gpr151-KO when compared to WT mice (Fig. 23A). We next measured anxiety-like behavior in the elevated plus maze and found no differences in the time spent in the open and closed arms between WT and Gpr151-KO mice (Fig. 23B).

Dysfunctions of the habenula have also been implicated in various psychiatric disorders including depression and schizophrenia (Caputo et al., 1998; Lecourtier et al., 2004; Ranft et al., 2010; Sandyk, 1992; Shepard et al., 2006). To study whether deletion of Gpr151 would confer schizophrenia-like behavior, we measured prepulse inhibition (PPI) of the startle response in WT and Gpr151-KO mice. PPI refers to the ability of a weak pre-stimulus to transiently inhibit the response to a following startling stimulus. It represents a common measure of sensorimotor gating, which is found to be deficient in schizophrenic patients (Braff and Geyer, 1990; Geyer et al., 2001). In both WT and Gpr151-KO mice, PPI was successfully detected at three different prepulse intensities (3, 6 and 12 dB above background), and it increased with higher prepulse intensities ($F_{prepulse\ intensity}(2,54) = 20.19$; $p<0.0001$; two-way ANOVA). There were no differences in percent PPI between WT and Gpr151-KO mice ($F_{genotype}(1,54) = 3.26$; $p=0.07$; two-way ANOVA, n=8-12) (Fig. 23C), indicating that sensorimotor gating is not impaired by Gpr151 deletion.

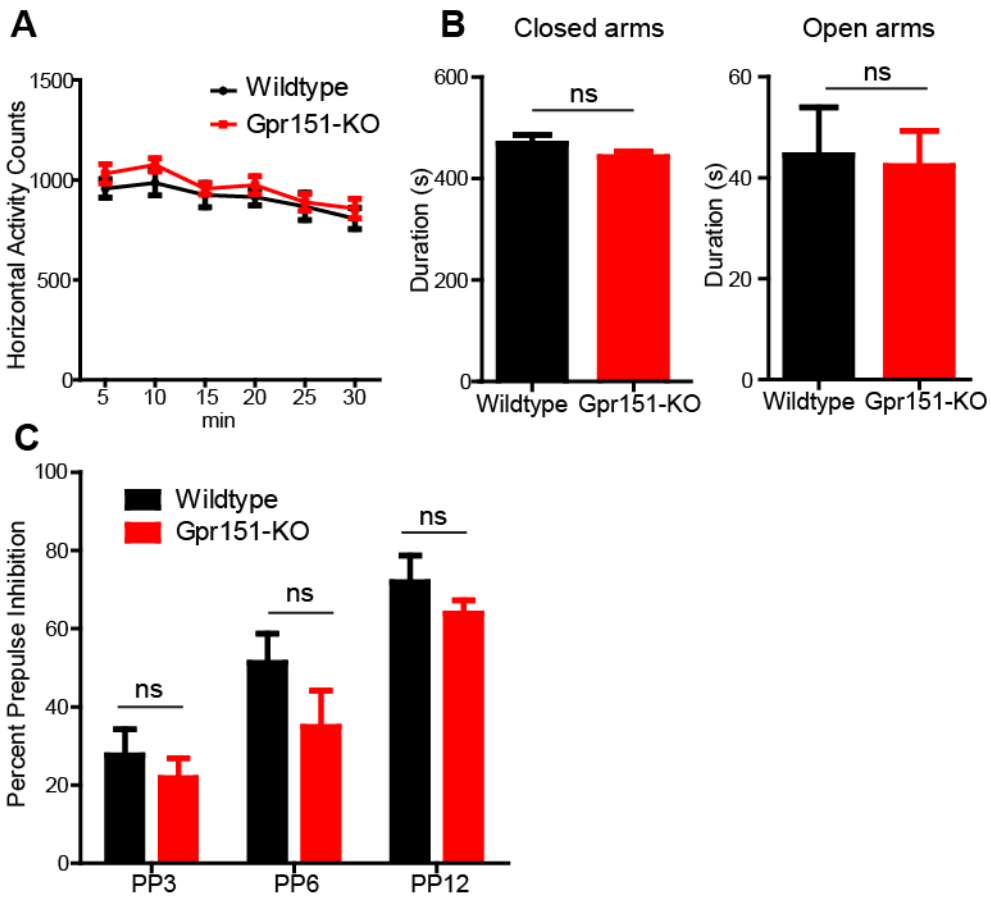

Figure 23. Gpr151-KO mice showed normal locomotor activity, anxiety-like behavior and prepulse inhibition.

(A) Number of total activity counts in the open field test. Beam breaks (locomotion) are recorded in 5 min bins for 30 min. There were no significant differences between WT and Gpr151-KO mice (Fgenotype (1,18)=1.27; p=0.27; Repeated measures two-way ANOVA; n=8-12). (B) Time spent in the closed and open arms in the elevated plus maze is not significantly different in Gpr151-KO mice compared to WT (unpaired t-test, n=8-12). (C) Gpr151-KO mice exhibited normal percent prepulse inhibition of the acoustic startle response across prepulse (PP) intensities (3, 6, 12 dB above background) (Fgenotype (1,54) = 3.26; p=0.07; two-way ANOVA, n=8-12). Data are expressed as mean ± S.E.M. (ns, not significant).

3.6.2 Gpr151 modulates nicotine reward and nicotine withdrawal

Given that habenular cholinergic neurons regulate aversion to nicotine and nicotine withdrawal (Fowler et al., 2011; Frahm et al., 2011; Salas et al., 2009), we tested the hypothesis that Gpr151 could contribute to the control of these behaviors. To assess nicotine reward we used the conditioned place preference (CPP) model with paired injections of either saline or nicotine at increasing doses of nicotine. Nicotine follows an inverted U-shaped dose-response curve due to a lack of rewarding effects at low doses and the emergence of aversive effects at high doses (De Biasi and Dani, 2011; Picciotto, 2003). Gpr151 deletion induced a leftward shift of the nicotine dose–response curve (Fig. 24A-B). WT mice showed significant preference for the nicotine-

paired chamber at 0.25 mg/Kg nicotine ($p<0.001$) and 0.35 mg/kg nicotine ($p<0.01$; two-way ANOVA; Bonferroni post-hoc test) (Fig. 24A); whereas Gpr151-KO mice showed nicotine preference at a lower dose, at 0.15 mg/Kg nicotine ($p<0.01$; two-way ANOVA; Bonferroni post-hoc test) (Fig. 24B). These results reveal that elimination of Gpr151 increases the sensitivity to reinforcement responses induced by nicotine.

We next analyzed physical (somatic signs) and affective (anxiety-related) nicotine withdrawal signs using a precipitated nicotine withdrawal model (Grabus et al., 2005; Sparks and Pauly, 1999). After 28 days of nicotine treatment in the drinking water, mice were intraperitoneally injected with 2 mg/Kg of the nAChRs antagonist mecamylamine and immediately placed into the light-dark box to measure anxiety-like behavior. Nicotine-withdrawn Gpr151-KO mice spent significantly more time in the dark chamber compared to saccharin-treated Gpr151-KO and nicotine-withdrawn WT mice ($F(3,33)=3.15;p=0.03$; one-way ANOVA; Newman-Keuls post-hoc test) (Fig. 24C); demonstrating that deletion of Gpr151 induces an anxiety-like response in mice undergoing nicotine withdrawal.

Somatic signs of withdrawal, including scratching, jumping, body and paw tremors, genital licking, head nodding and retropulsion were counted for 20 minutes immediately after the light-dark test. As expected, withdrawn control mice and withdrawn Gpr151-KO mice both displayed significantly more somatic signs compared to saccharin-treated control and Gpr151-KO mice respectively ($F(3,33)=6.34;p=0.001$; one-way ANOVA; Newman-Keuls post hoc test) (Fig. 24D). Post hoc analysis revealed that the number of total somatic signs was significantly increased in nicotine-withdrawn Gpr151-KO mice when compared to nicotine-withdrawn WT mice, suggesting that Gpr151 expression in habenula terminals attenuates physical signs of nicotine withdrawal.

In summary, Gpr151-KO mice displayed increased sensitivity to nicotine-conditioned reward and increased physical and affective nicotine withdrawal signs. These results reveal the Gpr151 receptor acts as a key component of the MHb/IPN pathway controlling nicotine-mediated behaviors.

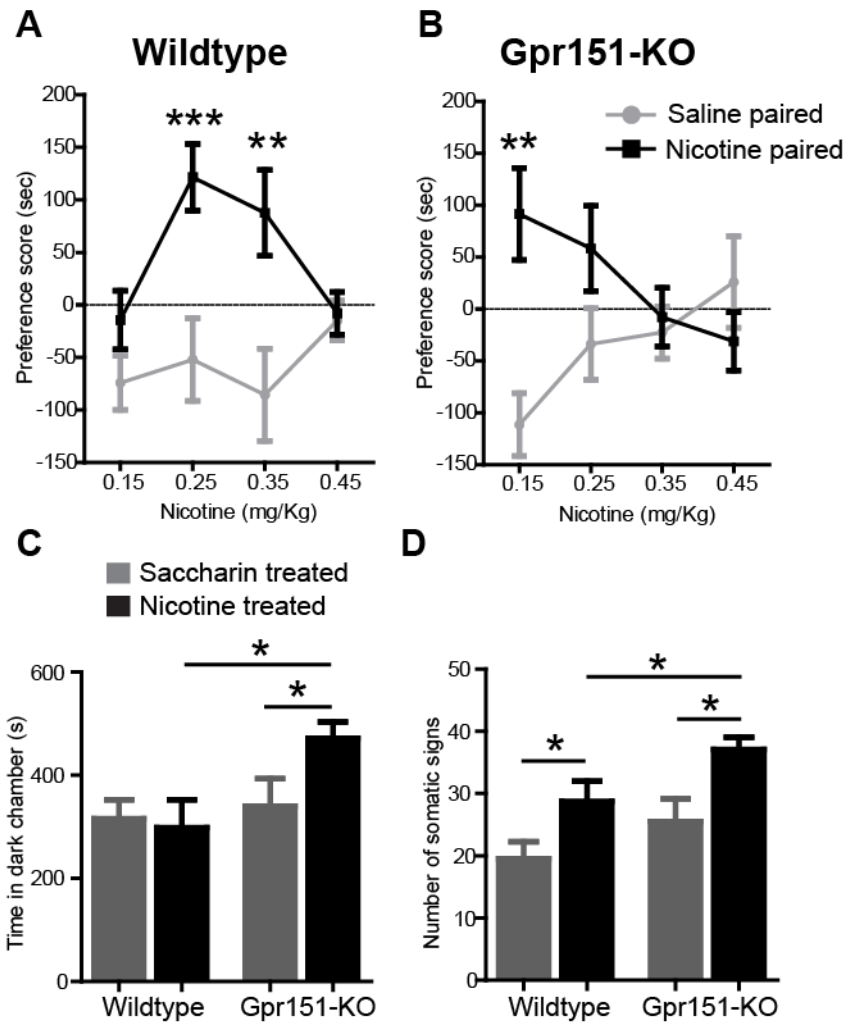

Figure 24. Increased sensitivity to nicotine and withdrawal manifestations in Gpr151-KO mice.

(A-B) Nicotine conditioned place preference at different nicotine concentrations. Gpr151-KO mice are more sensitive to nicotine compared to control mice as observed by the shift to the left in the nicotine dose-response curve. (A) WT mice showed nicotine CPP at 0.25 and 0.35 mg/kg nicotine (two-way ANOVA; **p<0.01, ***p<0.001, Bonferroni post-hoc test). (B) Gpr151-KO mice showed nicotine CPP at 0.15 mg/nicotine (two-way ANOVA;**p<0.01, Bonferroni post-hoc test). (C) Nicotine-withdrawn Gpr151-KO showed an increased anxiety-like behavior measured by the time spent time in the dark chamber (one-way ANOVA;*p<0.05, Newman-Keuls post-hoc test). (D) Total number of somatic signs of withdrawal. Nicotine withdrawn mice display a significant increase in total somatic signs compared to saccharin-treated counterparts. Nicotine withdrawn Gpr151-KO showed a significant increase of somatic signs compared to nicotine withdrawn WT mice (one-way ANOVA;*p<0.05, Newman-Keuls post-hoc test). Each point represents the mean ± S.E.M of 7-11 mice per group.

3.6.3 Downregulation of Gpr151 in the medial habenula increases sensitivity to nicotine

We next wanted to investigate whether Gpr151 presence/absence in adult mice is required to maintain control of nicotine sensitivity rather than the possibility that Gpr151 developmentally establishes a higher/lower nicotine sensitivity. To address this, we sought to knock-down Gpr151 in the habenula of adult mice and test whether

this manipulation would recapitulate the phenotype observed in Gpr151-KO mice. For this purpose, we generated lentiviruses (LV) encoding HA-tagged-Gpr151 and different shRNAs against Gpr151 (Fig. 25A). HEK293T cells were transduced with LV expressing HA-tagged-Gpr151 alone or together with bi-promoter LV expressing 5 different shRNAs (LV-shRNA). As shown in the western blot analysis in figure 25A, HA immunoreactivity is absent in cells transduced with the LV-shRNA3, indicating efficient knock down of Gpr151 expression. Importantly, *in vivo* experiments demonstrated that this shRNA effectively knocks down endogenous Gpr151 expression down to levels undetectable by immunohistochemistry. Thus, endogenous Gpr151 expression (Fig. 25B left panel) is not detected in LV-shRNA3 infected habenular neurons expressing both EGFP (Fig. 25B middle panel) and the shRNA3 directed against Gpr151 (Fig. 25B right panel).

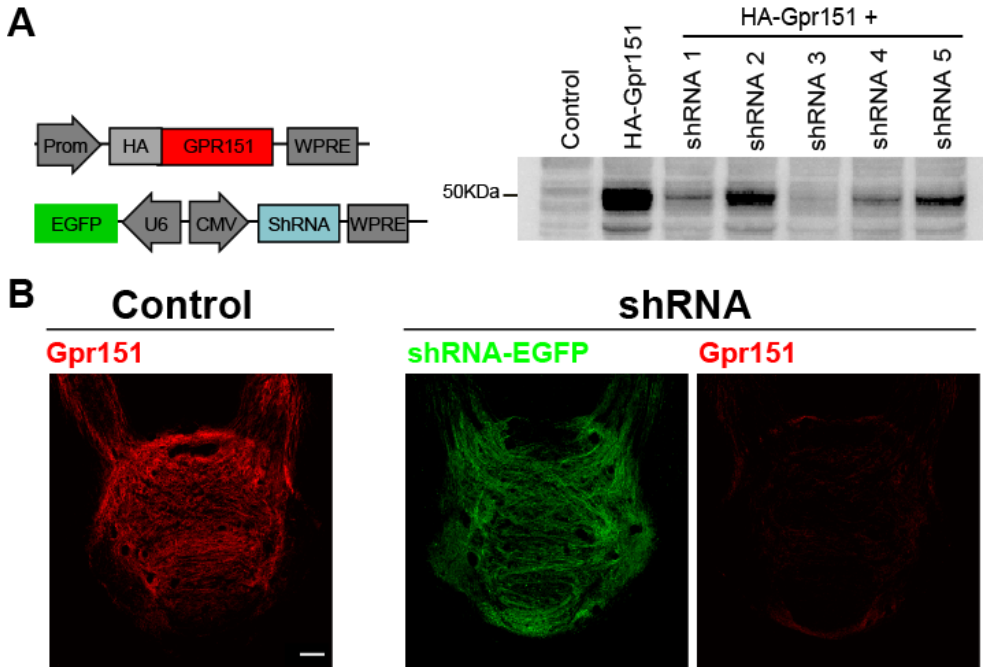

Figure 25. Validation of lentiviruses encoding shRNAs against Gpr151.

(A) Schematic representation of a lentiviral construct encoding Gpr151 with an N-terminal HA epitope and a bi-promoter construct containing shRNA against Gpr151. Western blot analysis of non-transduced HEK293Tcells (line1), transduced with LV-gpr151 alone (line 2) or together with LV containing 5 different shRNAs against Gpr151 (lines 3-7). HA immunoreactivity is evident in line 2 (47 kDa: gpr151) and is not observed in line 5, indicating that shRNA3 is able to knockdown Gpr151 in transduced cells. (B) Gpr151 expression in the IPN is almost undetectable by Gpr151 immunohistochemistry in mice injected with shRNA3 in the habenula compared to control-injected mice. Scale 100µm.

These positive knockdown results gave us the opportunity to test whether downregulation of Gpr151 in adult mice could affect nicotine-mediated behaviors. To analyze the behavioral consequences of knocking-down Gpr151, we bilaterally

injected the LV-shRNA3 into the MHb of C57Bl6 mice and employed non-coding shRNA lentivirus as a control. Two weeks after injection we analyzed the locomotor activity in the open field (Fig. 26A), anxiety-like behavior in the elevated plus maze (Fig. 26B) and sensorimotor gating by the prepulse inhibition test (Fig. 26C). No statistical differences were found between shRNA-injected mice and non-coding-shRNA-injected (control-injected) mice in any of these behaviors, as was observed in Gpr151-KO mice, indicating that the viral manipulation did not a have a deleterious effect.

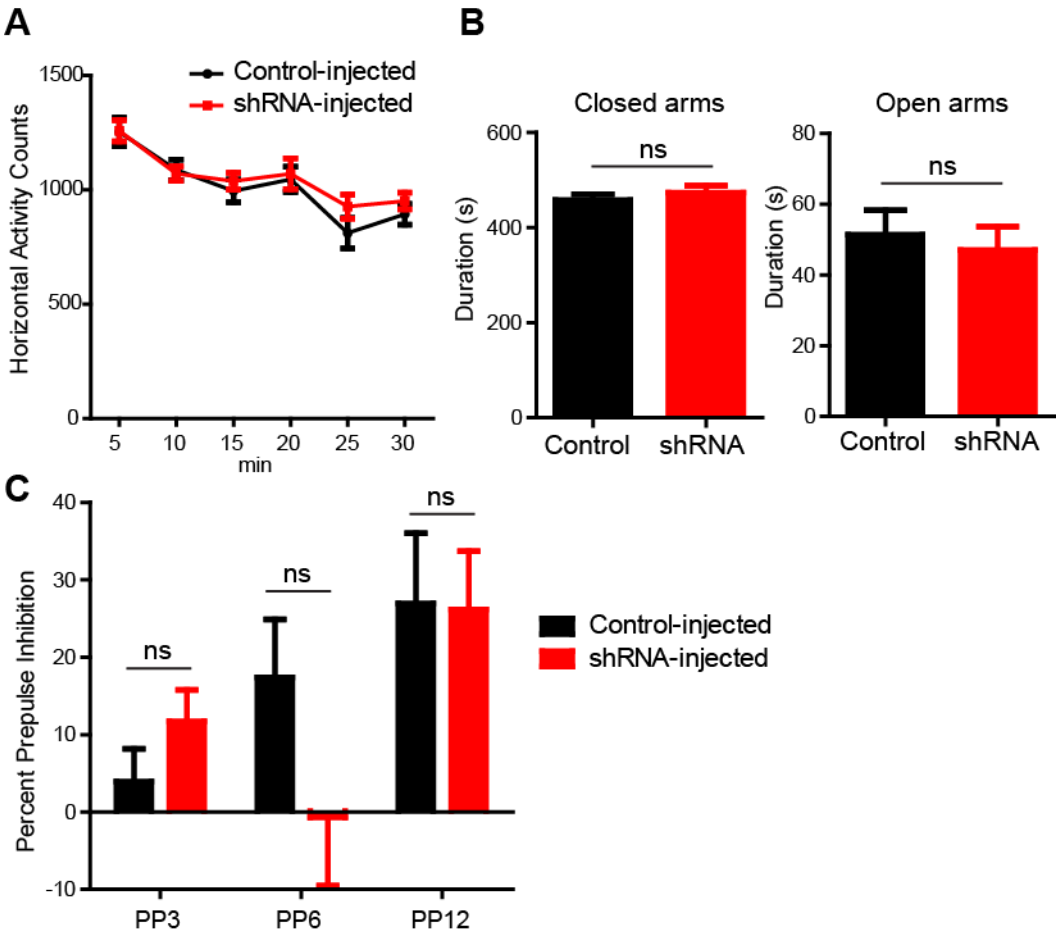

Figure 26. shRNA-injected mice showed normal locomotor activity, anxiety-like behavior and prepulse inhibition.

(A) Number of total activity counts in the open field test. Beam breaks (locomotion) are recorded in 5 min bins for 30 min. There were no significant differences between control and shRNA-injected mice (Finjection (1,29)=0.57; p=0.45; Repeated measures two-way ANOVA; n=15-16). (B) Time spent in closed and open arms in the elevated plus maze is not significantly different in shRNA-injected mice compared to control-injected (unpaired t-test, n=15-16). (C) shRNA-injected mice exhibited no differences in percent prepulse inhibition of the acoustic startle response across prepulse (PP) intensities (3, 6, 12 dB above background) compared to control-injected mice (Finjection (1,39) = 0.40; p=0.53; two-way ANOVA, n=7-8). Data are expressed as mean ± SEM (ns, not significant).

We next performed nicotine CPP at increasing concentrations of nicotine, following the same protocol used for Gpr151-KO mice. As shown in figure 27, control-injected mice showed significant preference for the nicotine-paired chamber at the concentration of 0.35 mg/kg (Fig. 27A); while shRNA-injected mice showed a tendency for nicotine preference at 0.15 mg/kg and a statistical significant preference at 0.25 mg/kg nicotine (Fig. 27B). These results demonstrate that knockdown of Gpr151 in habenula of adult mice increases nicotine sensitivity similarly to Gpr151-KO mice (Fig. 24A-B). Gpr151 is therefore necessary at adult stages for the regulation of nicotine-reward behaviors, indicating that the phenotype observed in Gpr151-KO mice is not a consequence of developmental changes induced by Gpr151 deletion.

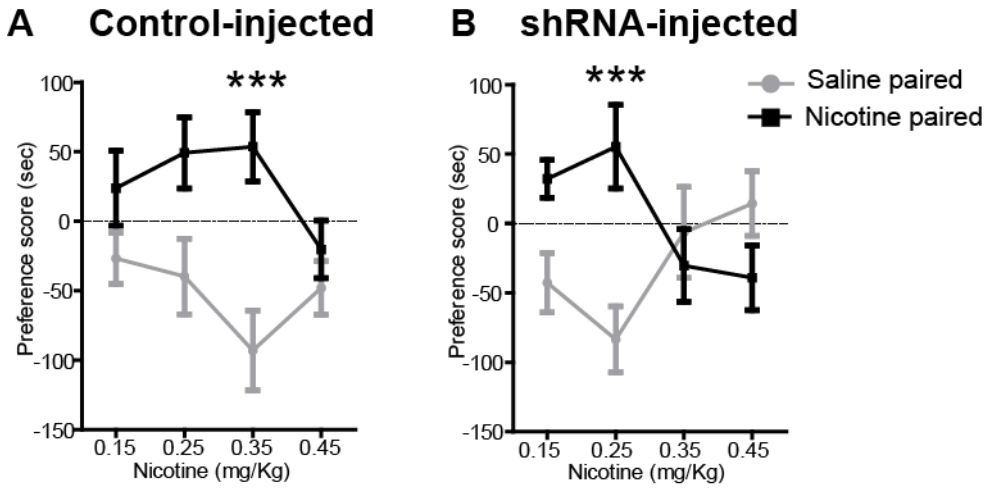

Figure 27. Downregulation of Gpr151 in the habenula increases sensitivity to nicotine.

(A-B) Nicotine conditioned place preference shows a shift to the left in the nicotine dose response curve of shRNA-injected compared to control-injected mice. (A) Control-injected mice showed nicotine CPP at 0.35 mg/kg nicotine (two-way ANOVA; ***p<0.001, Bonferroni post-hoc test). (B) shRNA-injected mice showed nicotine CPP at 0.25 mg/nicotine (two-way ANOVA;***p<0.001, Bonferroni post-hoc test) (n=12-16). Data are expressed as mean ± SEM (ns, not significant).

4. Discussion

This work identifies a novel synaptic GPCR, Gpr151, exclusively present in axonal projections of habenular neurons in the human and the mouse brain which modulates nicotine dependence and withdrawal. Therefore it provides new insights into the biology of this specific neuronal cell type and into the functional role of Gpr151. By electron microscopy, we show that Gpr151 is expressed at the presynaptic active zone in close association with synaptic vesicles. Further, we show that Gpr151 knockout mice displayed increased sensitivity to nicotine-conditioned reward as well as increased physical and affective nicotine withdrawal signs. These results highlight the importance of Gpr151 at habenular presynaptic terminals in the control of nicotine dependence and withdrawal. Targeting of Gpr151 would therefore represent a novel strategy in the development of a more effective treatment for tobacco dependence.

4.1 Gpr151 is localized at the axonal projections from habenular neurons in the mouse and the human brain.

Gpr151 expressing neurons in the habenula were localized by *in situ* hybridization in the mouse and the rat brain (Aizawa et al., 2012; Berthold et al., 2003; Ignatov et al., 2004), but the precise localization of the protein remained unknown. In this work, we show by immunohystochemistry that Gpr151 habenular neurons project to several areas in the midbrain. It is interesting to note that Gpr151 is not localized in the cell bodies, but rather in the axonal projections, suggesting that Gpr151 might be playing a role at the presynaptic terminals.

Gpr151 neurons in the vMHb project mainly to the central and intermediate subnuclei of the IPN (Fig.28). Since neurons in the vMHb are cholinergic and glutamatergic (Ren et al., 2011), we indeed observed colocalization of ChAT, VGlut1 and Gpr151 in the IPN. The MHb-IPN circuit has recently emerged as a key circuit in the regulation of nicotine reinforcement, dependence and withdrawal because of its uniquely high enrichment in α5, α3 and β4 nAChRs subunits (Fowler et al., 2011; Frahm et al., 2011; Glick et al., 2011; Salas et al., 2009). Given that the strongest Gpr151 expression was found in the IPN, we hypothesized and tested the possibility that Gpr151 modulates nicotine-related behaviors (see 4.3 and 4.4 sections in the discussion).

Gpr151 neurons in the LHb project to the rostromedial tegmental nucleus, the rhabdoid nucleus, the median raphe, the paramedian raphe, the dorsal raphe and the dorsal tegmental nucleus (Fig. 28). LHb has been shown to project predominantly to the raphe nuclei, the substantia nigra, the ventral tegmental area (Herkenham and Nauta, 1979) and the rostromedial tegmental nucleus (Fig. 2)(Goncalves et al., 2012; Jhou et al., 2009b; Kaufling et al., 2009). Interestingly we did not observe Gpr151 staining in the substantia nigra and the ventral tegmental area, indicating that Gpr151 is expressed in a subpopulation of LHb. However we observed strong Gpr151 immunostaining in the RMTg. Since the RMTg acts as an inhibitory center of the SN and the VTA (Balcita-Pedicino et al., 2011; Ferreira et al., 2008; Geisler and Zahm, 2005; Jhou et al., 2009a), it is possible that Gpr151 at habenular terminals in the RMTg modulates the inhibition of the dopaminergic neurons in the midbrain, and consequently modulates the motivational aspects of reinforcement learning and decision-making.

In addition we observed strong Gpr151 immunolabeling in the rhabdoid nucleus. Projections from LHb to the rhabdoid nucleus have not been previously described. In fact, the connections and the physiological functions of the rhabdoid nucleus have not yet been characterized. We demonstrate in this work that Gpr151 could be used as a marker to identify this nucleus and its anatomical features.

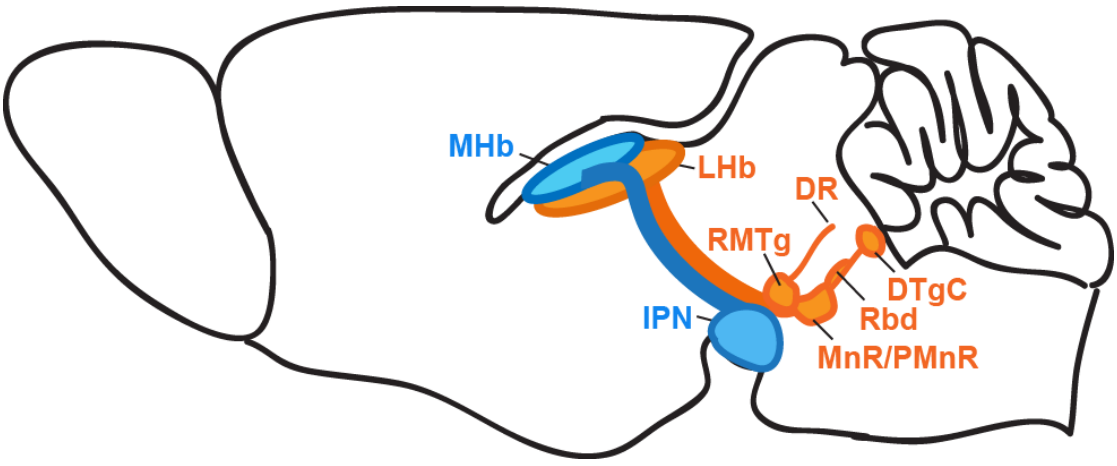

Figure 28. Gpr151 expressing habenular neurons project to the interpeduncular nucleus, rostromedial tegmental nucleus, rhabdoid nucleus, raphe nuclei and dorsal tegmental nucleus.

Schematic diagram of a sagittal mouse brain section showing the projections from MHb Gpr151 expressing neurons in blue and the projections from LHb Gpr151 expressing neurons in orange. (DTgC, dorsal tegmental nucleus centralis; DR, dorsal raphe; IPN, interpeduncular nucleus; LHb, lateral habenula; MHb, medial habenula; MnR, median raphe; PMnR, paramedian raphe; Rbd, rhabdoid nucleus, RMTg, rostromedial tegmental nucleus).

Moreover, Gpr151 expressing neurons in the LHb project to the median, paramedian and raphe nuclei. This suggests that Gpr151 could also modulate pain, stress, sleep and depression-like behavior, through its connections to the serotoninergic cells in the raphe.

Lastly, we observed that Gpr151 habenular neurons project to the dorsal tegmental nucleus, mainly to its central part in agreement with previous reports describing the projections from the LHb to the DTg (Contestabile and Flumerfelt, 1981; Groenewegen and Van Dijk, 1984; Liu et al., 1984). The DTg contains cells, which signal the animal's momentary directional heading and thus it is thought to be involved in navigation. Moreover, Sharp et al. reported that 10% of the lateral habenular cells showed a temporally precise correlation with angular head velocity or its running speed (Sharp et al., 2006). In summary, the LHb-DTg pathway appears to be important for the generation of the head direction cell signal and thus, Gpr151 might be modulating the activity of this pathway.

By staining Gpr151-KO mouse brain sections with an anti-β-galactosidase antibody, we could visualize the cell bodies of Gpr151 expressing neurons. In agreement with Aizawa et al. (Aizawa et al., 2012), Gpr151 expressing neurons were found in MHbC and MHbL, which correspond to the cholinergic population. In the LHb, Gpr151 expressing neurons were found predominantly in the LHbMS and LHbLPc. Given that Gpr151 immunostaining in WT mouse brain sections is remarkable in the LHbMPc and LHbMC, we conclude that the projections from neurons in the LHbMS and LHbLPc pass through the LHbMPc and LHbMC on the way to the fasciculus retroflexus.

Moreover, we found β-galactosidase staining in the anteromedial, anteroventral and paraventricular thalamic nuclei. These findings were unexpected as no Gpr151 immunolabeling was observed in the thalamus on sections from adult mice. It is possible that the Gpr151 antibody fails to recognize the protein expressed in the thalamus because of a hidden C-terminal domain. It is also possible that the Gpr151-KO construct containing the lacZ gene was integrated randomly in a different locus from the targeted Gpr151 locus.

In summary, Gpr151 expression in the mouse brain is very restricted to habenular neurons projecting mainly to the IPN, RMTg and raphe nuclei, suggesting that

Gpr151 could modulate the addiction circuit, reinforcement learning, pain, stress and depression-like behavior among others.

Because of the restricted expression of Gpr151 in habenula, Kobayashi et al., generated a Cre-recombinase transgenic mouse line using a bacterial artificial chromosome clone containing Gpr151 in order to examine the physiological functions of habenular neurons (Kobayashi et al., 2013). Gpr151 expressing neurons were selectively ablated using Cre-mediated expression of Eno2-STOP-DTA. The resulting mutant mice exhibited abnormalities in a wide range of behavioral effects including: hyperactivity during the early night period, maladaptation to new environments, impulsive and compulsive behavior, delay and effort aversion in decision-making, deficits in spatial memory, reduced flexibility in complex learning paradigms, and lack of susceptibility to nicotine (Kobayashi et al., 2013).

To confirm the importance of Gpr151 to human physiology, we verified Gpr151 expression in human habenula. Our results from immunohistochemical analysis of post-mortem adult human brain samples indicate that Gpr151 is indeed expressed in the habenula, the fasciculus retroflexus and the interpeduncular nucleus. We also performed immnohistochemical analysis of human brain samples with ChAT, GABAB-R1, neurofilament L&H and Substance P antibodies. We used the same antibodies as in (Diaz et al., 2011). Our aim was to investigate whether Gpr151 was being expressed in MHb and LHb by co-labeling with specific markers for both subnuclei. However, none of the antibodies mentioned above displayed specific staining in these subnuclei may be due to a difference in the fixation and post-fixation protocols used compared to (Diaz et al., 2011). Nevertheless, the fact that the Gpr151 antibody gave us a very strong signal in the habenula, fasciculus retroflexus and interpeduncular nucleus indicates that Gpr151 is being highly expressed in this axonal tract.

4.2 Ultrastructural localization of Gpr151 at habenular presynaptic terminals in the IPN

Observations at the electron microscopic level in mouse brain sections revealed that Gpr151 immunoreactivity is localized at the plasma membrane of habenular synaptic terminals in the IPN. Robust labeling was observed at the active and peri-active zone

and at the membrane of synaptic vesicles. These EM findings are critically important because they clearly identify Gpr151 as a novel presynaptic component in close proximity to the active zone and specific for habenular glutamatergic synapses. Further, the colocalization with the vesicle transporter VGlut1 in synaptic vesicles is very intriguing.

Presynaptic GPCRs that are localized at the active or peri-active zone can modulate synaptic transmission through three different mechanisms: 1) Inhibiting voltage-dependent calcium channels; 2) Regulating the exocytotic machinery (Miller, 1998); 3) Activating G protein-coupled inward rectifier K+ (GIRK) channels (Fernandez-Alacid et al., 2009). Localization of Gpr151 at the active and peri-active zone suggests that it may modulate synaptic transmission at habenular terminals in the IPN.

In addition, Gpr151 labeling was observed at the extrasynaptic plasma membrane. This result prompted us speculate about its role in modulating the R-type calcium channels ($Ca_v2.3$). The strong R-type immunoreactivity detected at MHb terminals in the IPN and the observation that no mRNA transcripts for P/Q-type and N-type calcium channels could be detected in the MHb (Ludwig et al., 1997), make the MHb terminals very unique. An ultrastructural localization study of the R-type calcium channel at MHb terminals in the IPN showed a very distinctive expression pattern. Immunogold particles were mainly observed at the extrasynaptic plasma membrane and only occasionally over the presynaptic active zone, suggesting that the R-type calcium channel may play specialized functional roles, besides its role in neurotransmitter release (Parajuli et al., 2012). Gpr151 immunoreactivity at the extrasynaptic plasma membrane at the MHb terminals in the IPN points to the possibility that Gpr151 functions as a modulator of the R-type calcium channel. Another explanation for Gpr151 localization at the extrasynaptic plasma membrane is the possibility to activate or inhibit adenylate cyclase or phospholipase Cβ by Gα proteins.

Gpr151 labeling was also observed in association with transport vesicles or cisternae inside the terminals and along the microtubules. It is well known that newly synthesized GPCR are transported from the endoplasmic reticulum through the Golgi to the plasma membrane by anterograde axoplasmic transport. Receptors located in

the membrane of the transport vesicles are later incorporated into the terminal membrane via exocytosis.
In addition, GPCR are internalized and sorted in the endosome either to the recycling endosome for return to the plasma membrane or to the lysosome for degradation (Dong et al., 2007). Therefore, we cannot exclude the possibility that vesicles or intraterminal membrane structures associated with Gpr151 labeling are involved not only in anterograde transport, but also in the recycling of the receptor.

Moreover Gpr151 labeling was found in close association with synaptic vesicles. This result suggests that Gpr151 might be integrated into the plasma membrane upon neuronal depolarization. Although GPCRs and other neurotransmitter receptors are sorted into the constitutive secretory pathway and spontaneously delivered to the plasma membrane, there is now evidence that GPCRs are translocated to the plasma membrane upon neuronal stimulation. The following GPCRs have been localized at the membrane of peptide-containing large secretory vesicles in unstimulated nerve terminals: the kappa opioid receptor (KOR) (Meshul and McGinty, 2000) (Drake et al., 1997) (Shuster et al., 1999), delta opioid receptors (DOR), serotonin 1D receptors, and serotonin 7 receptors (Doly et al., 2005; Potrebic et al., 2003). Importantly, upon stimulation, localization of the cited GPCRs decreases at the membrane of vesicles and increases at the plasma membrane. Many conditions are known to induce translocation of GPCR to the plasma membrane including brief depolarization (Bao et al., 2003), brief physiological stimuli such as swim stress (Commons, 2003) and chronic morphine treatment (Hack et al., 2005).
In summary, Gpr151 immunoreactivity associated with synaptic vesicles suggests that Gpr151 might be translocated to the plasma membrane upon stimulation of MHb neurons (for instance by nicotine). Furthermore, by performing double iEM with Gpr151 and VGlut1 antibodies, we showed that some of the glutamatergic synaptic vesicles are associated with Gpr151. MHb cholinergic neurons have been shown to co-release glutamate and acetylcholine. Brief photostimulation of ChAT-Channelrhodopsin habenular neurons generated fast excitatory postsynaptic currents in IPN neurons mediated by ionotropic glutamate receptors. In contrast, tetanic photostimulation produced slow inward currents that were largely mediated by nicotinic acetylcholine receptors (Ren et al., 2011).

In view of these results, we hypothesize that Gpr151 is translocated to the plasma membrane when MHb neurons are depolarized and glutamate-filled synaptic vesicles are released. Gpr151 receptors now at the plasma membrane would then be activated by the ligand pressumably present in the extracellular milieu, triggering a cascade of intracellular events, which could lead to the inhibition of neurotransmitter release. In summary, the stimulus-induced cell surface expression of Gpr151 may represent a feedback regulation mechanism to regulate neurotransmitter release (Fig.29).

In addition, we analyzed the ultrastructure of MHb terminals in the IPN of Gpr151-KO mice and we did not find any differences in the number, size or organization of the presynaptic terminals and synaptic vesicles compared to WT mice. The fact that Gpr151-KO mice had presynaptic terminals with normal morphology and distribution of SVs was expected as changes in the distribution of SVs have been observed only for proteins involved in the synaptic docking process, the initial association of secretory vesicles with the plasma membrane. For instance, alteration of SVs distribution have been observed in presynaptic terminals of mice null for the following proteins: Munc18 (Toonen et al., 2006; Voets et al., 2001), syntaxin-1 (de Wit et al., 2006), Snap-25 and synaptotagmin-1 (de Wit et al., 2009), RIM proteins (Kaeser et al., 2011). GPCRs are not required in the docking, thus changes in the distribution of synaptic vesicles have not been documented at the presynaptic terminals of mice null for different GPCRs at basal conditions. However, activation of the GPCR cannabinoid type 1 receptor by application of the cannabinoid agonist HU-210 reduced the number of synaptic vesicles localized close to the presynaptic membrane of synaptoneurosomes. These changes in vesicle distribution were not observed in synaptoneurosomes obtained from mice lacking CB1 receptors (Ramirez-Franco et al., 2014). Therefore it would be interesting to analyze whether ligand binding to Gpr151 promotes changes in synaptic vesicle distribution.

4.3 Gpr151 modulates nicotine conditioned reward

Given that MHb-IPN pathway regulates aversion to nicotine and nicotine withdrawal (Fowler et al., 2011; Frahm et al., 2011; Salas et al., 2009; Zhao-Shea et al., 2013) and that Gpr151 is highly expressed at habenular terminals in the IPN, we

investigated whether Gpr151 contributes to the control of these behaviors. We observed that both deletion and downregulation of Gpr151 induced a leftward shift of the nicotine dose–response curve in the CPP. These results revealed that elimination of Gpr151 increases the sensitivity to nicotine-induced reinforcement responses.

How can Gpr151 deletion or downregulation in MHb neurons enhance nicotine sensitivity? We previously demonstrated that overexpression of the β4 nAChR subunit in the MHb reduces nicotine consumption (Frahm et al., 2011; Slimak et al., 2014). This reduction is likely to be mediated by a potentiation of α3β4* nAChR currents (Frahm et al., 2011; Slimak et al., 2014). Moreover, α5 nAChR knockout mice continue to self-administer nicotine at doses that normally elicit aversion in wild-type animals. From these studies, we concluded that nicotine activation of α3β4* and α5* nAChRs in the MHb and IPN triggers an inhibitory motivational signal that limits nicotine intake. Since Gpr151 deletion and downregulation increased sensitivity to nicotine CPP, we hypothesize that the magnitude of the inhibitory signal which limits nicotine intake is enhanced in the Gpr151-KO and shRNA-injected mice. Therefore it is tempting to speculate that Gpr151 plays a role in attenuating the response of MHb neurons upon nicotine administration.

Taking together this hypothesis with the results obtained by electron microscopy, we suggest that Gpr151 may act as a feedback regulator of habenula signaling. We observed that Gpr151 was localized not only at the plasma membrane of the presynaptic terminals, but also at the membrane of synaptic vesicles as a reserve pool. Therefore it is possible that depolarization of MHb neurons induced by nicotine could cause an increase of the number of Gpr151 receptors at the plasma membrane. Gpr151 would then be accessible to bind its ligand and activate the intracellular cascade to inhibit further neurotransmitter release. In summary, Gpr151 would be reducing nicotine-induced neurotransmitter release at the MHb terminals (Fig. 29).

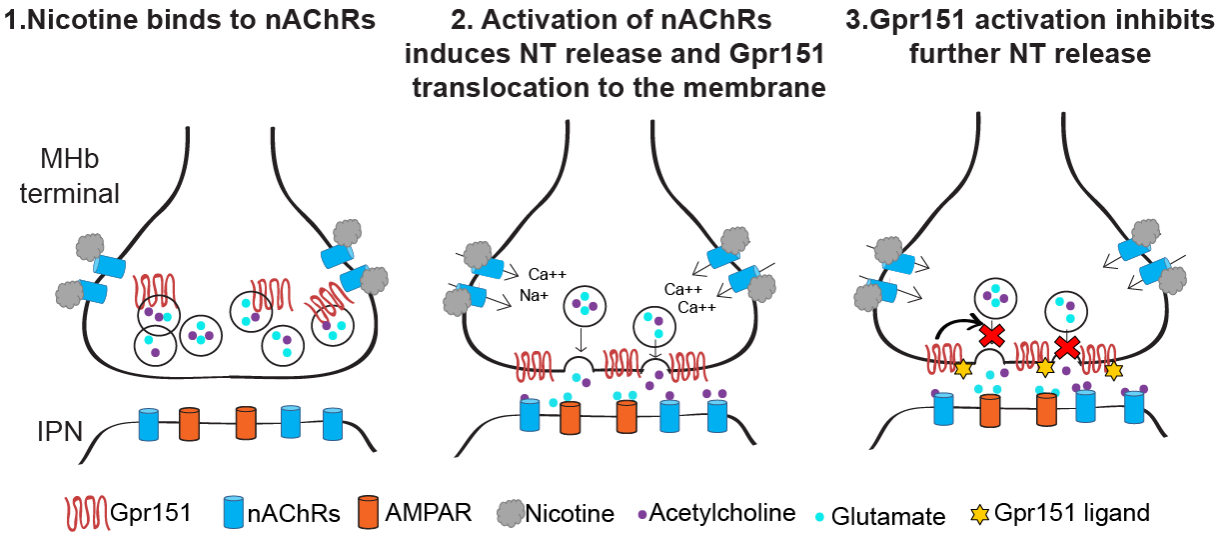

Figure 29. Nicotine-induced cell surface expression of Gpr151 as a feedback mechanism to regulate neurotransmitter release.

Nicotine binding to the nAChRs of MHb neurons induces depolarization and release of glutamate and acetylcholine. Gpr151 localized at the membrane of synaptic vesicles at the habenular terminals is translocated to the plasma membrane upon nicotine-induced depolarization. Activation of Gpr151 leads to a cascade of intracellular events to prevent further neurotransmitter release. (MHb, medial habenular; IPN, interpeduncular terminal; NT, neurotransmitter).

Therefore we hypothesize that Gpr151-KO mice and shRNA-injected mice show increased sensitivity to nicotine-induced reinforcement responses because of the lack of neurotransmission inhibition upon nicotine administration. In other words, deletion and downregulation of Gpr151 facilitates nicotine-induced neurotransmitter release at MHb terminals (Fig. 30). Moreover, the fact that deletion or downregulation of Gpr151 does not modulate other behaviors like anxiety-like behavior and sensorimotor gating in the absence of nicotine is supporting evidence for our hypothesis that Gpr151 might only be activated when habenula neurons are stimulated.

In addition to the MHb-IPN pathway, Gpr151 is also expressed at the projections from the LHb to the RMTg. Besides the MHb, a recent report suggests that the LHb may also play a role in nicotine aversion (Fowler and Kenny, 2014). LHb neurons are activated in response to aversive events such as unexpected punishments or omission of expected rewards (Bromberg-Martin and Hikosaka, 2011; Matsumoto and Hikosaka, 2007, 2009). LHb activates GABAergic neurons in the RMTg (Jhou et al., 2009a; Jhou et al., 2009b), which in turn inhibit the firing of the reward-encoding dopamine neurons in the VTA (Bromberg-Martin and Hikosaka, 2011; Matsumoto and Hikosaka, 2007, 2009). Moreover, optogenetic activation of LHb glutamatergic

terminals in the RMTg of mice promoted active, passive and conditioned behavioral avoidance (Stamatakis and Stuber, 2012). Therefore it is possible that deletion or downregulation of Gpr151 in LHb neurons projecting to the RMTg facilitates neurotransmitter release upon activation, and as a result, promotes conditioned place avoidance at nicotine doses that are still rewarding for wildtype mice (Fig. 30). We believe that the LHb might get activated upon nicotine administration through the projections from the MHb.

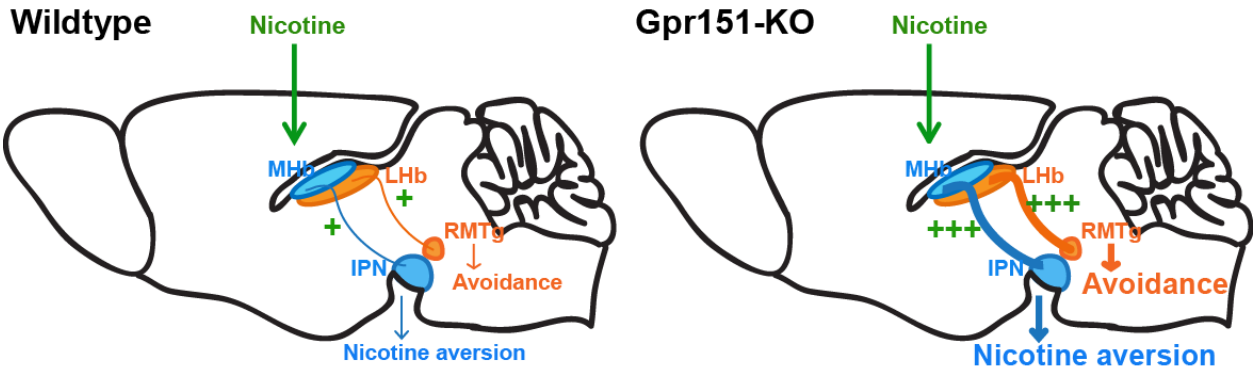

Figure 30. Deletion of Gpr151 in habenular neurons increases the sensitivity to nicotine-induced reinforcement responses.

Schematic diagram showing the neuronal pathways involved in nicotine aversion. Nicotine activates MHb-IPN pathway (blue) through the nAChRs localized in both structures. Activation of MHb-IPN pathway triggers an inhibitory signal which limits nicotine intake and leads to nicotine aversion. Activation of MHb-IPN pathway is enhanced in Gpr151-KO mice, leading to nicotine aversion at low doses of nicotine. The LHb-RMTg pathway (orange) promotes active, passive and conditioned behavioral avoidance. Deletion of Gpr151 in LHb-RMTg pathway increases the activity of the pathway and leads to avoidance of the nicotine-paired chamber in the CPP upon nicotine administration.

Another possibility is that the nicotine injection given to mice for three days to induce conditioning in the CPP paradigm is perceived as an unexpected punishment which activates the LHb and promotes avoidance to the nicotine-paired chamber. Given that deletion or downregulation of Gpr151 might increase facilitation of neurotransmitter release upon neuronal activation, Gpr151-KO mice and shRNA-injected mice develop avoidance to the nicotine-paired chamber at lower doses of nicotine. Whether Gpr151-KO mice are more susceptible to develop aversion to any other event besides the nicotine injection would be of interest in future studies.

4.4 Gpr151 modulates nicotine withdrawal

In addition to increased nicotine sensitivity, we observed that deletion of Gpr151 induces an anxiety-like response and an increase in the number of somatic signs on mice undergoing nicotine withdrawal, suggesting that Gpr151 expression in habenular terminals attenuates physical and affective signs of nicotine withdrawal.

Nicotine withdrawal has been shown to be mediated by nAChRs in the MHb-IPN tract since direct infusion of a nonspecific nAChR antagonist, mecamylamine, into the habenula and IPN can precipitate somatic withdrawal signs in nicotine-dependent mice (Salas et al., 2009). Moreover, mice lacking nAChR α5 or β4 subunits showed decreased somatic nicotine withdrawal symptoms (Salas et al., 2003; Salas et al., 2004; Salas et al., 2009).

During chronic nicotine treatment, nAChRs are upregulated (reviewed in (De Biasi and Dani, 2011)). Since nicotine is not hydrolyzed by acetylcholine esterase as ACh is, nicotine's long-lasting presence induces nAChR desensitization. The homeostatic response to desensitized receptors is upregulation. Discontinuation of nicotine intake or administration of nAChR antagonists, decreases abruptly nAChR signaling on the different neuronal types overexpressing nAChRs, which contributes to the withdrawal syndrome (reviewed in (De Biasi and Dani, 2011)).

As discussed previously, we believe that deletion of Gpr151 facilitates nicotine-induced neurotransmitter release at habenular terminals during nicotine treatment. Since MHb neurons co-release both glutamate and ACh (Ren et al., 2011), we suggest that, in addition to nicotine, increased ACh release in the IPN of Gpr151-KO mice induces upregulation of nAChRs in IPN neurons. Upregulation of nAChRs in the IPN of Gpr151-KO mice would therefore cause a stronger withdrawal-like behavior upon administration of the nAChR antagonist mecamylamine (Fig. 31).

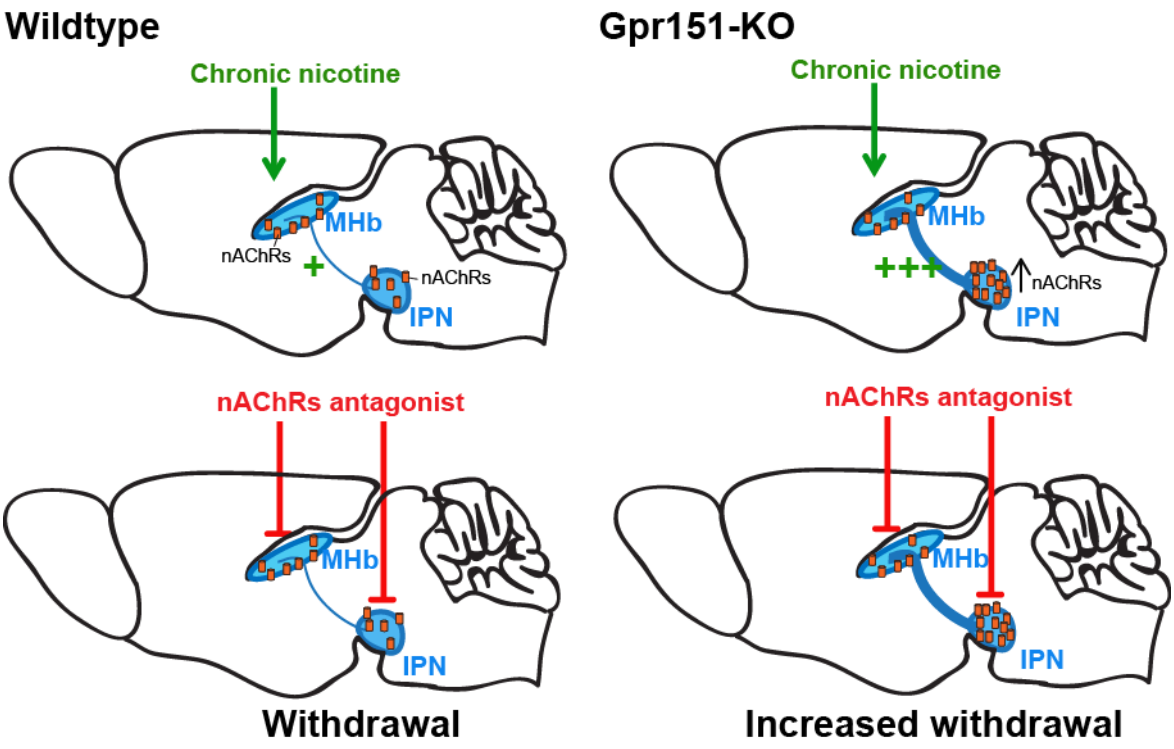

Figure 31. Deletion of Gpr151 increases somatic and affective withdrawal signs in nicotine-dependent mice.

During chronic nicotine treatment, MHb-IPN pathway is activated and as discussed in figures 29 and 30, this activation is enhanced in Gpr151-KO mice. Consequently, enhanced levels of ACh are released in the IPN of Gpr151-KO mice which induce upregulation of nAChRs in IPN neurons. Because of upregulation of nAChRs in the IPN, stronger nicotine withdrawal symptoms are observed in Gpr151-KO mice upon administration of the nAChR antagonist mecamylamine.

Recently, Zhao-Shea and colleagues have shown that optical stimulation of GABAergic neurons (GAD2-expressing) in the IPN triggers somatic signs of withdrawal in both nicotine-naive and chronic-nicotine-exposed mice, indicating that activation of these neurons is sufficient for expression of somatic withdrawal behaviors. Interestingly, activation of IPN GAD2-expressing neurons does not induce anxiety (Zhao-Shea et al., 2013). Moreover, it has been suggested that β2-containing nAChRs are involved in the affective signs of nicotine withdrawal, whereas β4 and α5 nAChRs contribute to the somatic signs (Jackson et al., 2008). Since Gpr151-KO mice display both somatic signs and increased anxiety-like behavior during nicotine withdrawal, it is possible that deletion of Gpr151 influences not only GAD2 positive neurons, but also β2-expressing neurons in the IPN.

The neurocircuitry underlying nicotine withdrawal remains to be completely elucidated and much work is still needed to reveal the different populations of GABAergic neurons in the IPN, which combinations of nAChRs they express, and

whether they act as local inhibitory interneurons or as projecting neurons. Thus it is challenging to explain the possible consequences of Gpr151 deletion in the neurocircuitry of nicotine withdrawal behavior. However it is clear from our results that Gpr151 plays an important role in the modulation of this behavior.

4.5 Gpr151 modulates cAMP levels at habenular terminals

To get insight into the Gpr151 signaling pathway, we first analyzed cAMP levels in the IPN of wildtype and Gpr151-KO mice. cAMP levels have been shown to modulate neurotransmitter release in axonal terminals of MHb neurons (Hu et al., 2012). In addition many proteins activated by cAMP are highly expressed in MHb neurons (Görlich et al., 2013). We observed that cAMP concentration was significantly increased in the IPN of Gpr151-KO mice when compared to wildtype mice, suggesting that Gpr151 couples to the Gαi/o protein, which inhibits adenylyl cyclase activity and therefore leads to a decrease of intracellular cAMP levels.
We then wanted to validate these results using cell-based second messenger assays with cells transfected with Gpr151 to measure cAMP or calcium levels. In these assays, since the Gpr151 ligand is unknown, we were testing whether overexpression of Gpr151 is sufficient to modulate the cAMP or calcium signaling by autoactivation. Expression of Gpr151 did not change either cAMP or calcium levels indicating that overexpression of Gpr151 in transfected cells does not result in autoactivation of the receptor.

The study of the Gpr151 signaling pathway is impeded by the lack of a known ligand. Therefore we are limited to studies comparing wildtype and Gpr151-KO mice. We are aware that the results of the ELISA showing increased levels of cAMP in the IPN of Gpr151-KO are not conclusive, and should be replicated and expanded using other methodologies. However it is an indication for a possible role of Gpr151 in modulating cAMP levels at the habenular terminals.

Intracellular cAMP increase activates several effectors, including cAMP-dependent protein kinase (PKA), cyclic nucleotide-gated (CNG) channels, hyperpolarization-activated cyclic nucleotide-gated (HCN) channels, and cAMP-specific guanine

nucleotide exchange factors (cAMP-GEF)/exchange proteins directly activated by cAMP (Epac) (hereafter cAMP-GEF/Epac) (reviewed in (Seino and Shibasaki, 2005)). Remarkably, the major cAMP effector, PKA, has been shown to modulate neurotransmitter release in MHb terminals (Hu et al., 2012). Hu et al. demonstrated that depletion of presynaptic cAMP levels in MHb neurons leads to a reduction of PKA activity and consequently, to the suppression of glutamate release (Hu et al., 2012). Therefore it is possible that increased levels of cAMP in the habenular terminals of Gpr151-KO facilitate nicotine-induced neurotransmitter release, leading to increased nicotine sensitivity and increased nicotine withdrawal (Fig. 32).

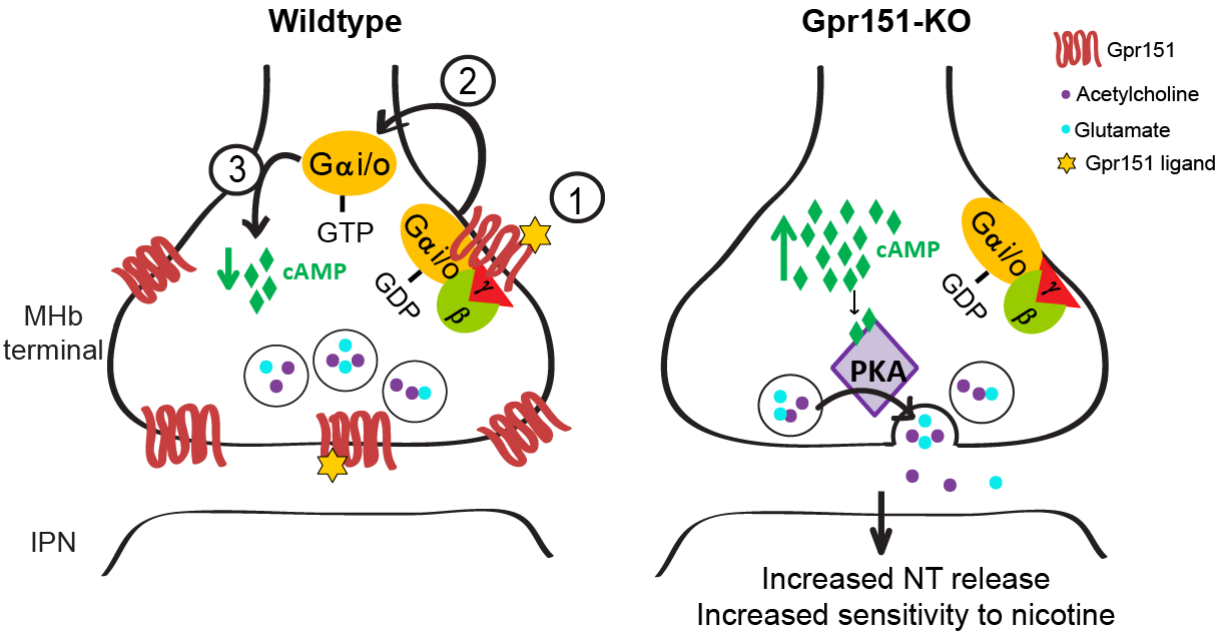

Figure 32. cAMP levels at the MHb terminals in the IPN modulate neurotransmitter release.

Activation of Gpr151 at the MHb terminals of wildtype mice leads to a decrease of cAMP levels through Gαi/o coupling. In contrast, levels of cAMP are increased at the habenular terminals of Gpr151-KO mice. cAMP activates PKA which in turn phosphorylates proteins involved in the exocytotic machinery and facilitates neurotransmitter release. (MHb, medial habenular; IPN, interpeduncular terminal; NT, neurotransmitter).

Moreover, PKA can modulate nAChRs function by phosphorylation. Specifically PKA has been shown to slow the decay of nicotine-evoked currents and accelerate nAChR recovery from desensitization in HEK293T cells expressing α3β4 nAChRs (Di Angelantonio et al., 2011). Since Gpr151 colocalizes with α3β4* nAChRs at the habenular terminals, it is tempting to speculate that PKA activated by increased cAMP levels in Gpr151-KO mice could reduce desensitization of α3β4* nAChR.

Increased levels of cAMP could also activate HCN channels. We showed that MHb neurons are equipped with HCN3 and HCN4 channels that confer them with intrinsic pacemaking activity (Gorlich et al., 2013). In addition, we demonstrated that infusion of the HCN antagonist ZD7288 into the MHb precipitates somatic and affective signs of withdrawal. The MHb pacemaking activity was increased by nicotine via activation of α3β4-containing nAChRs and was not changed in mice treated with chronic nicotine. However exposure to nicotine in mice undergoing nicotine withdrawal increased the frequency of pacemaking activity (Gorlich et al., 2013). Given that cAMP binds to the cytoplasmic site of HCN channels and enhances the intrinsic rate of HCN firing (Santoro et al., 2000), it is possible that cAMP levels at presynaptic terminals modulate habenular pacemaking activity. Increased levels of cAMP at habenular terminals of Gpr151-KO mice may accelerate rhythmogenesis of habenular neurons and lead to nicotine-related behavioral changes.

Future experiments are underway to investigate which of the possible signaling pathways is activated by Gpr151. However, either facilitation of neurotransmitter release by increased cAMP levels, decreased α3β4* nAChR desensitization or increased pacemaking activity could explain the behavioral phenotype observed in Gpr151-KO mice. Increased levels of cAMP at presynaptic terminals would in any case, increase the MHb-IPN signaling. As discussed previously, activation of the MHb-IPN pathway triggers an inhibitory motivational signal that limits nicotine intake (Fowler et al., 2011; Frahm et al., 2011). Therefore we hypothesize that deletion of Gpr151 increases the magnitude of this inhibitory motivational signal, leading to increased sensitivity to nicotine-induced reinforcement responses and increased somatic and affective signs of nicotine withdrawal.

4.6 Gpr151 as a novel target for smoking cessation therapies

According to the World Health Organization, the tobacco epidemic kills nearly six million people a year mainly from oral, esophageal, lung cancers and cardiovascular diseases. About one-third of the world's adult population smokes tobacco. In developed countries, cigarette smoking is already the leading cause of preventable death. And in less developed countries, cigarette smoking is on the rise (Benowitz, 2008). Therefore, it is one of the few causes of mortality that is increasing worldwide.

If current trends continue, tobacco is projected to be responsible for more than eight million deaths globally by 2030 (World Health Organization., 2011).
Although smoking cessation therapies are available, which include either nicotine replacement therapy (i.e., the nicotine patch and gum) or the use of nAChRs partial agonists (e.g., varenicline); the success rate of these therapies is less than 30%. In addition current therapies for nicotine addiction are hampered by serious side effects including increased risk of suicide (Crooks et al., 2014).
About 80% of those who try to quit smoking relapse within the first month, and only 3% remain abstinent at 6 months (Benowitz, 2009). The relapse is mainly driven by the avoidance of the negative states associated with withdrawal, such as dysphoria, anxiety, irritability, and to a lesser extent, the somatic symptoms of withdrawal. Thus alternative and more efficacious pharmacotherapies to target the negative states of withdrawal are needed (Crooks et al., 2014).

An important approach for the development of new therapies for circuitry-based disorders is the discovery of novel targets that: 1) are expressed specifically in cell types that contribute to the main behavior of the disorder; 2) can be pharmacologically targeted using current approaches for drug development, and 3) can modulate the activity of the cells that express the target.
Gpr151 fulfills these prerequisites. It is exclusively localized at the axonal projections from habenular neurons. Moreover behavioral experiments in mice demonstrated that Gpr151 plays an important role in regulating nicotine dependence and nicotine withdrawal. By electron microscopy, we showed that Gpr151 is localized at the presynaptic terminal, at the plasma membrane close to the active zone and also in association with synaptic vesicles, supporting the hypothesis that Gpr151 modulates neurotransmission. To confirm the importance of Gpr151 to human physiology, we analyzed Gpr151 expression on human brain sections and found that the human Gpr151 expression pattern matches the one observed in mice.
Importantly, Gpr151-KO mice display increased somatic and affective signs of nicotine withdrawal. This suggests that a Gpr151 agonist could decrease the magnitude of the negative states associated with nicotine withdrawal such as anxiety and somatic symptoms. Altogether, these results allow the conclusion that modulation of this receptor which is present in smokers, might be an important objective for the treatment of tobacco addiction.

4.7 Deorphanizing Gpr151

In addition to its restricted localization to habenular neurons and its role in nicotine dependence and withdrawal, Gpr151 has the potential to become a drug target as it belongs to the highly druggable Class A family of GPCR. It is estimated that more than 40% of all drugs, including those under development, exert their effects by acting on GPCRs. Gpr151 is one of the approximately 100 GPCR that still remains orphan. We are aware that many pharmaceutical companies, besides us, are currently searching for compounds to interfere or modulate the function of Gpr151.

We attempted to uncover the Gpr151 ligand using three different approaches. First, since Gpr151 shows high homology with galanin and tachykinin receptors, we tested the activity of galanin-like and tachykinin-like peptides on cell-base second messenger assays. Second, we tested the hypothesis that Gpr151 ligand could be release by Gpr151-expressing neurons upon stimulation. Third, we performed an *in silico* homology modeling of Gpr151 followed by high throughput screening of a chemical database.

The primary challenge in the deorphanization of Gpr151 is that its signaling pathway remains unknown. Given that the levels of cAMP were increased in the IPN of Gpr151-KO mice, we used a cAMP cell-based assay to test different compounds. We also employed a calcium cell-based assay because calcium signaling is the other major second messenger involved in GPCR signal transduction. However, it is possible that cAMP or calcium signaling gets activated by Gpr151 in the presence of G-protein subunits and/or auxiliary adaptors that are not expressed in the HEK293 cells and therefore, cAMP or calcium assays would be inadequate to screen for Gpr151 ligands, unless these specific G-protein subunits and adaptors are identified. Indeed some G-protein subunits including Gαo, Gαo2, Gα14, Gα15, Gγ7 and Gγ8 are not expressed in HEK293 cells (Atwood et al., 2011). In addition, it is possible that the *in silico* screening of a virtual chemical library likely failed due to poor homology modeling of Gpr151 by the MOA software.

Although progress to deorphanize Gpr151 has been challenging, we will continue searching for ligands and modulators. We are currently optimizing a new strategy to find Gpr151 binding partners by performing immunoprecipitations followed by mass-spectrometry analysis. We will focus on Gpr151 binding partners because of the possibility that Gpr151 forms heterodimers with another GPCR and functions in a

ligand-independent manner. This working model has been shown for GABABR1 and GABABR2, and GPR50 and Melatonin receptors 1 or 2. Regarding GABAB heterodimers, GABABR1 provides ligand-binding and GABABR2 promotes efficient transport of GABABR1 to the cell surface and G protein coupling (Galvez et al., 2001; Jones et al., 1998; Robbins et al., 2001).

Another possibility is that Gpr151 requires accessory proteins for its activity. Several cases have been shown where coexpression of an orphan GPCR with an accessory protein is required for the functional expression of the orphan GPCR. One example is the calcitonin receptor-like receptor (CRLR), which requires RAMPs (receptor activity-modifying proteins) for efficient transport to the cell surface. Interestingly, the properties of CRLR are regulated in a cell type-specific manner depending on the differential interaction with one of the three RAMPs. When CRLR associates with RAMP1, it functions as calcitonin gene-related peptide; whereas when it associates with RAMP2 or 3, it acts as an adrenomedulin receptor (Hay et al., 2006; McLatchie et al., 1998).
Another example is the orphan GPR56, which has been shown to associate with the membrane-bound tetraspanin molecules CD9 and CD81 in vitro, and CD9/CD81/GPR56 complexes facilitate association with Gαq/11 and Gβ subunits (Little et al., 2004). Another orphan GPCR, GPR37, has been shown to interact with the dopamine transporter (DAT) and to modulate its activity. GPR37 and DAT were found to colocalize in mouse striatal presynaptic membranes and *Gpr37*-null mutant mice showed enhanced DAT-mediated dopamine uptake in striatal membrane samples (Marazziti et al., 2007).

Thus we should keep in mind the possibility that Gpr151 transduces the signal independently from G proteins. If Gpr151 requires accessory proteins for its activity, the classical deorphanization strategies, which rely on monitoring changes at the second messenger level will not be useful to identify its ligands or modulators. Huge efforts need to be made to develop new screening assays, which consider accessory proteins and other possible signaling mechanisms. We are confident that our future immunoprecipitations studies using IPN samples from wildtype and Gpr151-KO mice will contribute to identify Gpr151 interactors and understand the mechanism of action of Gpr151 at habenular terminals. Therefore these future studies will provide critical

information for the understanding of the signaling and binding partners of Gpr151 necessary for the development of a novel treatment for nicotine cessation.

5. Conclusions

This work identifies a novel synaptic G protein-coupled receptor, Gpr151, present only in habenular neurons in the human and mouse brain, as a novel target for the development of smoking cessation therapies. Therefore it provides new insights into the biology of this specific neuronal cell type and into the functional role of Gpr151.

This study was prompted: first, by our discovery of the habenula as a key brain area controlling nicotine consumption and withdrawal (Frahm et al., 2011; Gorlich et al., 2013; Slimak et al., 2014) and second, by the identification of Gpr151 as highly and specifically enriched in cholinergic neurons of the medial habenula using the TRAP methodology when compared to previously collected TRAP data from different cell types in the CNS (Gorlich et al., 2013).

Three main conclusions can be drawn from this work:

First, I show that Gpr151 is exclusively localized at the axonal projections of habenular neurons where it plays a key role in regulating nicotine dependence and nicotine withdrawal. Gpr151-expressing neurons of the medial and lateral habenula project mainly to the interpeduncular nucleus (IPN), the rostromedial tegmental nucleus (RMTg) and the raphe nuclei. Respectively, the MHb-IPN tract modulates nicotine-related behaviors, the RMTg regulates negative reward and the raphe nuclei are responsible for releasing serotonin to other parts of the brain, suggesting that Gpr151 could modulate the nicotine addiction circuit, reinforcement learning, pain, stress and depression-like behavior among others.

I demonstrate that Gpr151 deletion or shRNA-mediated downregulation increased the sensitivity to nicotine-conditioned reward. In addition, deletion of Gpr151 induced an anxiety-like response and an increase in the number of somatic signs in mice undergoing nicotine withdrawal, indicating that Gpr151 expression in habenular terminals attenuates physical and affective signs of nicotine withdrawal.

Second, I show by electron microscopy that Gpr151 is localized at habenular presynaptic terminals in the interpeduncular nucleus, specifically at the plasma membrane close to the active zone and also in association with synaptic vesicles. These findings are critically important because they clearly identify Gpr151 as a novel

presynaptic component in close proximity to the active zone and specific for habenular synapses. Further, the colocalization with the transporter VGlut1 in synaptic vesicles indicates that Gpr151 might be translocated from the synaptic vesicles to the plasma membrane when habenular neurons are depolarized and glutamate-filled synaptic vesicles are released. These results together with the behavioral analysis, suggest that Gpr151 at the plasma membrane of habenular presynaptic terminals may act as an inhibitory feedback regulator of habenula signaling.

Third, analysis of the Gpr151 signaling pathway indicates that Gpr151 couples to the Gαi/o protein. I observed an increase of cAMP levels in the habenular terminals of Gpr151 knockout mice. Remarkably cAMP at the habenular terminals has been shown to modulate neurotransmitter release (Hu et al., 2012). Depletion of presynaptic cAMP levels in medial habenular neurons led to a reduction of protein kinase A activity and consequently to a suppression of glutamate release (Hu et al., 2012). These data together with the behavioral analysis suggest that increased levels of cAMP in the habenular terminals of Gpr151-KO mice facilitate nicotine-induced neurotransmitter release. Activation of the MHb-IPN pathway triggers an inhibitory motivational signal that limits nicotine intake (Fowler et al., 2011; Frahm et al., 2011). Therefore I hypothesize that increased levels of cAMP in the MHb terminals of Gpr151-KO increases the magnitude of this inhibitory signal, leading to increased sensitivity to nicotine-induced reinforcement responses and increased somatic and affective signs of nicotine withdrawal.

Altogether these results highlight the importance of Gpr151 for smoking-related diseases. Current therapies for nicotine addiction are hampered by serious side effects since they act on nicotinic and/or dopamine targets in the mesocorticolimbic reward system. In addition the success rate of these therapies is less than 30% (Crooks et al., 2014). Thus alternative and more efficacious pharmacotherapies to target the negative states of withdrawal are required. Human genetics studies have identified several loci associated with heavy smoking and lung cancer in relation to nicotinic acetylcholine receptors. Importantly, although α4β2 and α7 nAChRs are the major subtypes present in the brain, genome wide association studies (GWAS) have not linked these genes to nicotine abuse. Rather, they have established a strong

association between SNPs in the CHRNB4-A3-A5 gene cluster and smoking dependence, indicating that α3β4α5 nAChRs, which are mostly restricted to the MHb-IPN pathway in the CNS, are critical for acquisition of nicotine dependence and difficulties in smoking cessation. However because α3β4α5 receptors are also expressed in ganglia in the PNS, antagonists of these cholinergic receptors are expected to have undesired side effects. Therefore an ideal candidate for such therapies is Gpr151 as the habenula-interpeduncular nucleus tract has never been previously targeted. The studies presented here favor the hypothesis that a Gpr151 agonist would be a very valuable therapeutic target not only for smoking cessation, as it could decrease the magnitude of the negative states associated with nicotine withdrawal such as anxiety, but also as a deterrent to become nicotine dependent, since a Gpr151 agonist would decrease the sensitivity to nicotine reward.

5. Zusammenfassung

In dieser Arbeit wurde der neue G-Protein-gekoppelte Rezeptor Gpr151, der im Menschen- und Mäusehirn nur in Neuronen der Habenula zu finden ist, als neuer potentieller Angriffspunkt für die Rauchentwöhnungstherapie entdeckt. Damit bietet diese Arbeit neue Einblicke in die Biologie und die Funktion dieses spezifischen, neuronalen Zelltyps und von Gpr151.

Als Grundlage für diese Arbeit dienen erstens Befunde welcher der Habenula Schlüsselfunktionen im Nikotinkonsum sowie Nikotinentzug zuweisen (Frahm et al., 2011; Görlich et al., 2013; Slimak et al., 2014), und zweitens Befunde aus vergleichenden TRAP-Analysen (Görlich et al., 2013), die Gpr151 als hoch prominent und spezifisch in cholinergen Neuronen der medialen Habenula ausweisen.

Drei Hauptaussagen können aus dieser Arbeit getroffen werden:

Erstens: Gpr151 ist ausschließlich in axonalen Projektionen der Habenula zu finden und spielt dort eine Schlüsselrolle in der Regulation von Nikotinabhängigkeit und Nikotinentzug. Gpr151 exprimierende Neurone der medialen und lateralen Habenula projizieren hauptsächlich zum interpeduncular nucleus (IPN), dem rostromedialen tegmental nucleus (RMTg) und den raphe Kernen. Verhalten, das mit Nikotinkosum in Bezug gesetzt wird, ist durch den MHb-IPN Signalweg, Vermeidungsverhalten durch den RMTg, und Serotonin-Ausschüttung von den raphe Kernen moduliert. Dies lässt vermuten, dass Gpr151 unter anderem Nikotinabhängigkeit, bestärkendes Lernen, Schmerz, Stress und depressives Verhalten beeinflusst.
In dieser Arbeit konnte ich zeigen, dass eine Gpr151 Gendeletion oder eine shRNA-vermittelte Expressionsreduktion, die Sensitivität von Nikotin-konditioniertem Belohnungsverhalten erhöht. Zudem induziert die Gendeletion von Gpr151 in Mäusen ein Angst-ähnliches Verhalten sowie eine erhöhte Zahl an somatischen Symptomen im Nikotinentzug woraus zu schließen ist, dass die Gpr151 Expression in Terminalen der Habenula physische und somatische Entzugserscheinungen vermindert.

Zweitens: Mit elektronenmikroskopischen Aufnahmen konnte ich zeigen, dass Gpr151 im IPN in Axonterminalen der Habenula vor allem an der Plasmamembran

der aktiven Zone sowie vereinzelt an synaptische Vesikel assoziiert ist. Da diese Ergebnisse Gpr151 klar als neue präsynaptische Komponente in der aktiven Zone der habenula Terminalen zeigt, sind sie von besonderer Bedeutung,
Da meine Ergebnisse zudem eine Kolokalisation von Gpr151 mit dem vesikulärem Glutamat Transporter VGlut1 in synaptischen Vesikeln zeigt, vermute ich, dass Gpr151 durch Depolarisation von Habenulaneuronen und folgender Glutamatausschüttung in die Plasmamembran eingebracht wird. Dies lässt zusammen mit meinen Verhaltensexperimenten vermuten, dass Gpr151 an der präsynaptischen Membran die Habenula-IPN Signalübertragung reguliert.

Drittens: Meine Analysen deuten darauf hin, das Gpr151 mit dem Gαi Protein gekoppelt ist. In habenula Terminalen von Gpr151 knockout (KO) Mäusen konnte ich eine Erhöhung des cAMP Levels erkennen. Ein verringerter cAMP Spiegel in präsynaptischen Terminalen der medialen Habenula führt zu einer Reduktion der Proteinkinase A Aktivität und folglich zu einer verminderten Glutamatausschüttung (Hu et al., 2012). Zusammen mit meinen Verhaltensexperimenten deuten diese Ergebnisse darauf hin, dass ein erhöhter cAMP Level in habenula Terminalen von Gpr151-KO Tieren die nikotin-induzierte Neurotransmitterfreisetzung erhöht. Durch Aktivierung des MHb-IPN Trakts wird die Nikotin-Einnahme auf Grund Demotivation reduziert (Fowler et al., 2011; Frahm et al., 2011). Ich vermute daher, dass der erhöhte cAMP Level in MHb Terminalen von Gpr151-KO Mäusen inhibitorische Signale potenziert, somit die Reaktion auf Nikotin verstärkt und zu erhöhten somatischen und affektiven Signalen des Nikotinentzugs führt.

Zusammengefasst unterstreichen meine Ergebnisse die wichtige Bedeutung von Gpr151 für durch Rauchen verursachte Krankheiten. Da derzeitige Therapien zur Rauchentwöhnung an nikotinergen und/oder dopaminergen Rezeptoren im mesocorticolimbischen System agieren, bedingen sie schwerwiegende Nebenwirkungen und sind daher unbefriedigend. Hinzu kommt, dass weniger als 30% der derzeitigen Therapien erfolgreich sind (Crooks et al., 2014). Alternative, effektivere pharmakologische Therapien mit reduzierten Nebenwirkungen sind notwendig.
Humane Genanalysen haben starkes Rauchen und das Risiko an Lungenkrebs zu erkranken mit nikotinergen Acetylcholin Rezeptoren (nAChR) in Verbindung

gebracht. Obwohl α4β2 und α7 nAChRs die Haupt-Rezeptoruntereinheiten des CNS sind, konnten sie in genomweiten Assoziationsstudien (GWAS) nicht mit Nikotinmissbrauch in Verbindung gesetzt werden. Nikotinabhängigkeit wurde vielmehr mit SNPs im CHRNB4-A3-A5 Gen-Cluster und damit mit α3β4α5 nAChRs welche vor allem im MHb-IPN Trakt im CNS vorkommen, assoziiert. Da α3β4α5 nAChRs auch in Ganglien des PNS exprimiert sind, ist zu vermuten, dass Antagonisten gegen diesen Rezeptor unerwünschte Nebeneffekte mit sich bringen.

Die hier dargelegten Ergebnisse favorisieren die Hypothese, dass ein Gpr151 Agonist eine sehr nützliche Alternative zu derzeitig praktizierten Rauchentwöhnungstherapien seien kann. Da Gpr151 zudem die belohnenden Effekte von Nikotin verringert, ist ein Agonist auch als Präventionsmittel zur Nikotinabhängigkeit denkbar.

6. Appendix

6.1 Abbreviations

3V	Third ventricle
5-HT3	5-hydroxytryptamine receptor 3A
AbdNu	Abducens nucleus
AC	Anterior commissure
ACh	Acetylcholine
AntNu	Anterior nucleus of thalamus
Aq	Aqueduct
BAC	Bacterial Artificial Chromosome
BLAST	Basic Local Alignment Search Tool
BP	Basilar pons
BSA	Bovine serum albumin
BST	Bed Nucleus of Stria Terminalis
Cav2.3	R-type voltage-gated calcium channel
cDNA	Complementary DNA
ChAT	Acetylcholine transferase
CLi	Caudal linear nucleus of the raphe
CNS	Central nervous system
CorCI	Corpus callosum
CPP	Conditioned place preference
CPu	Caudate and putamen
DA	Dopamine
DAPI	4′,6-Diamidino-2-phenylindol
DBB	Diagonal band of Broca
DIV	Days in vitro
DMEM	Dulbecco’s modified Eagle’s medium
dMHb	Dorsal medial habenula
DMNu	Dorsomedial nucleus of thalamus
DMSO	Dimethyl sulfoxide
DNA	Deoxyribonucleic acid
dNTP	Deoxynucleotidetriphosphate
DR	Dorsal raphe
DRI	Dorsal raphe interfascicular
DRV	Dorsal raphe ventral part
DRVL	Dorsal raphe ventrolateral
DTgC	Dorsal tegmental nucleus central
DTgP	Dorsal tegmental nucleus pericent
DTT	Dithiothreitol
EDTA	Ethylenediaminetetraacetic acid
EGFP	Enhanced green fluorescent protein
EM	Electron microscopy
EPM	Elevated plus maze

FBS	Fetal bovine serum
FNu	Fastigial nucleus
For	Fornix
FR	Fasciculus retroflexus
GABA	γ-aminobutyric acid
GABABR1	GABA B Receptor 1
GABABR2	GABA B Receptor 2
GAD	Glutamate decarboxylase
GIRK	G protein-coupled inwardly-rectifying potassium channels
Glu	Glutamate
Gng8	Guanine nucleotide binding protein gamma 8
GPCR	G-protein coupled receptor
GPi	Globus pallidus internus
HA	Hemagglutinin
Hab	Habenular nuclei
hbc	Habenular commissure
HCN	Hyperpolarization-activated cyclic nucleotide-gated channels
HyNu	Hypoglossal nucleus
HyTh	Hypothalamus
i.p.	Intraperitoneal
IC	Inferior colliculus
IPC	Interpeduncular nucleus caudal
IPN	Interpeduncular nucleus
IPR	Interpeduncular nucleus rostral
Kd	Dissociation constant
KO	Knock-out
LCsp	Lateral corticospinal tract
LDNu	Lateral dorsal nucleus
LDTg	Laterodorsal tegmental nucleus
LH	Lateral hypothalamus
LHb	Lateral habenula
LHbLB	Basal part of the lateral division of LHb
LHbLMc	Magnocellular part of the lateral division of LHb
LHbLMg	Marginal part of the lateral division of LHb
LHbLO	Oval part of the lateral division of LHb
LHbLPc	Parvocellular part of the lateral division of LHb
LHbMC	Central part of the medial division of LHb
LHbMMg	Marginal part of the medial division of LHb
LHbMPc	Parvocellular part of the medial division of LHb
LHbMS	Superior part of the medial division of LHb
LPO	Lateral preoptic area
LV	Lentivirus
MB	Mammillary body
MHb	Medial habenula
MHbC	Central part of MHb

MHbI	Inferior part of MHb
MHbL	Lateral part of MHb
MHbS	Superior part of MHb
ML	Medial lemniscus
MLF	Medial longitudinal fasciculus
MnR	Median raphe
MOI	Multiplicity of infection (virus particles/cell)
MQ	Type-I ultrapure water (from Barnstead E-pure system)
mRNA	Messenger ribonucleic acid
MtTr	Mammillothalamic tract
n.s	Not significant
nAChR	Nicotinic acetylcholine receptor
NaCl	Sodium chloride
NaOH	Sodium hydroxide
NCBI	National Center for Biotechnology Information
NF-H	Neurofilament H
NuGr	Nucleus gracilis
o/n	Over night
OcNr	Oculomotor nerve
OD	Optical density
OpNr	Optic nerve
PBS	Phosphate-buffered saline
PBT	PBS-Tween-20
PCR	Polymerase chain reaction
PDTg	Posterodorsal tegmental nucleus
PFA	Paraformaldehyde
PFC	Prefrontal cortex
pH	Potentium hydrogenii
PKA	Protein kinase A
PLC	Phospholipase C
PMnR	Paramedian raphe
PNS	Peripheral nervous system
PO	Principal olivary nucleus
PoCom	Posterior commissure
PPI	Prepulse Inhibition
PrTecNu	Pretectal nuclei
Py	Pyramid
Rbd	Rhabdoid nucleus
RMTg	Rostromedial tegmental nucleus
RNase	Ribonuclease
RNu	Red nucleus
rpm	Revolutions per minute
RT	Room temperature
s.e.m	Standard error of the mean
SC	Superior colliculus

scp	Superior cerebellar peduncle
SD	Standard deviation
SDS	Sodium dodecyl sulphate
shRNA	Short hairpin RNA
sm	Stria medullaris
SNc	Substantia nigra pars compacta
SP	Substance P
TAE	Tris-acetate EDTA
TE	Tris-EDTA
TH	Tyrosine hydroxylase
TpH	Tryptophan hydroxylase
Tris	Tris-(hydroxymethyl-) aminoethane
t-RNA	Transfer ribonucleic acid
TroNr	Trochlear nerve
TU	Transducing unit
VGlut1	Vesicular glutamate transporter 1
vMHb	Ventral medial habenula
VTA	Ventral tegmental area
WPRE	Woodchuck hepatitis post-transcriptional regulatory element
WT	Wildtype
xscp	Decussation superior cerebellar peduncle
βGal	Beta-galactosidase

Units

bp	base pairs
°C	Degrees Celsius
d	Days
g	Gram
h	Hour
kb	Kilobase
kDa	Kilodalton
l	Liter
M	Molar
mg	Milligram
min	Minute
ml	Milliliter
mM	Millimolar
µg	Microgram
ng	Nanogram
s	Second
RFU	Relative Fluorescence Units
RLU	Relative Luminescence Units
U	Unit (for enzyme activity)

6.2 Plasmid maps

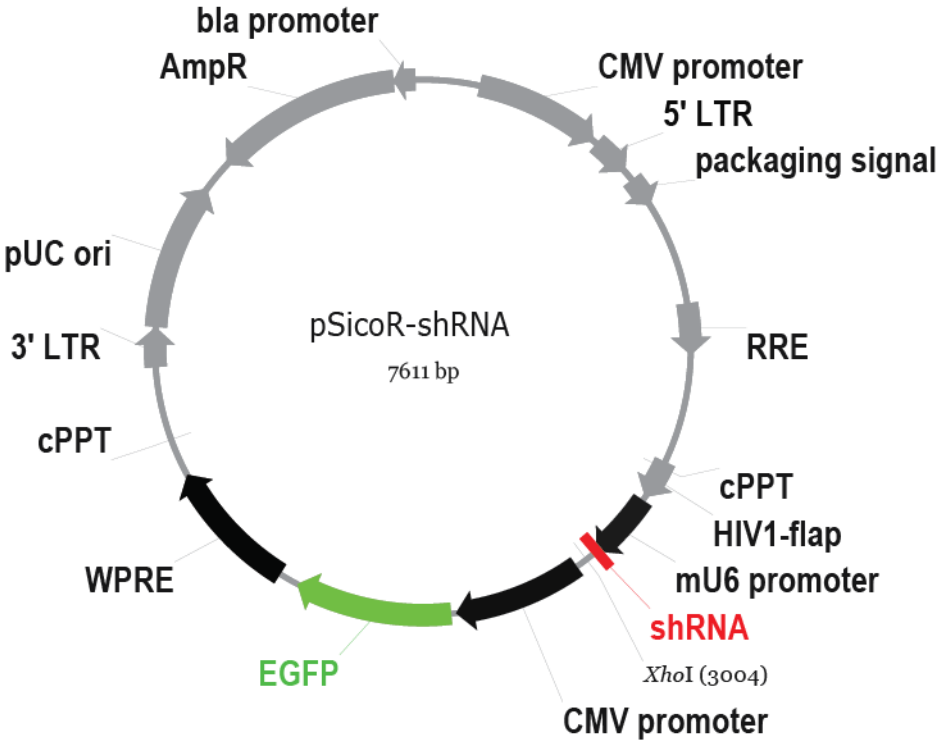

atccgacgccgccatctctaggcccgcgccggccccctcgcacagacttgtgggagaagctcggctactcccctgccccggttaatttgcatat
aatatttcctagtaactatagaggcttaatgtgcgataaaagacagataatctgttcttttaatactagctacattttacatgataggcttggatttctat
aacttcgtatagcatacattatacgaagttataaacagcacaaaaggaaactcaccctaactgtaaagtaattgtgtgttttgagactataaatatc
ccttggagaaaagccttgtttgccaagagcttgacatttgttttcaagagaaacaaatgtcaagctcttggctttttctcgagtactaggatccattag
gcggccgcgtggataaccgtattaccgccatgcattagttattaatagtaatcaattacggggtcattagttcatagcccatatatggagttccgcgt
tacataacttacggtaaatggcccgcctggctgaccgcccaacgacccccgcccattgacgtcaataatgacgtatgttcccatagtaacgcca
atagggactttccattgacgtcaatgggtggagtatttacggtaaactgcccacttggcagtacatcaagtgtatcatatgccaagtacgccccta
ttgacgtcaatgacggtaaatggcccgcctggcattatgcccagtacatgaccttatgggactttcctacttggcagtacatctacgtattagtcatc
gctattaccatggtgatgcggttttggcagtacatcaatgggcgtggatagcggtttgactcacggggatttccaagtctccaccccattgacgtca
atgggagtttgttttggcaccaaaatcaacgggactttccaaaatgtcgtaacaactccgccccattgacgcaaatgggcggtaggcgtgtacg
gtgggaggtctatataagcagagctggtttagtgaaccgtcagatccgctagcgctaccggtcgccaccatggtgagcaagggcgaggagct
gttcaccggggtggtgcccatcctggtcgagctggacggcgacgtaaacggccacaagttcagcgtgtccggcgagggcgagggcgatgcc
acctacggcaagctgaccctgaagttcatctgcaccaccggcaagctgcccgtgccctggcccaccctcgtgaccaccctgacctacggcgtg
cagtgcttcagccgctaccccgaccacatgaagcagcacgacttcttcaagtccgccatgcccgaaggctacgtccaggagcgcaccatcttc
ttcaaggacgacggcaactacaagacccgcgccgaggtgaagttcgagggcgacaccctggtgaaccgcatcgagctgaagggcatcga
cttcaaggaggacggcaacatcctggggcacaagctggagtacaactacaacagccacaacgtctatatcatggccgacaagcagaagaa
cggcatcaaggtgaacttcaagatccgccacaacatcgaggacggcagcgtgcagctcgccgaccactaccagcagaacacccccatcgg
cgacggccccgtgctgctgcccgacaaccactacctgagcacccagtccgccctgagcaaagaccccaacgagaagcgcgatcacatggt
cctgctggagttcgtgaccgccgccgggatcactctcggcatggacgagctgtacaagtaggaattcgtcgagggacctaataacttcgtatag
catacattatacgaagttatacatgtttaagggttccggttccactaggtacaattcgatatcaagcttatcgataatcaacctctggattacaaaattt
gtgaaagattgactggtattcttaactatgttgctccttttacgctatgtggatacgctgctttaatgcctttgtatcatgctattgcttcccgtatggctttca
ttttctcctccttgtataaatcctggttgctgtctctttatgaggagttgtggcccgttgtcaggcaacgtggcgtggtgtgcactgtgtttgctgacgcaa
cccccactggttggggcattgccaccacctgtcagctcctttccgggactttcgctttcccctccctattgccacggcggaactcatcgccgcctg
ccttgcccgctgctggacaggggctcggctgttgggcactgacaattccgtggtgttgtcggggaaatcatcgtcctttccttggctgctcgcctgtgt
tgccacctggattctgcgcgggacgtccttctgctacgtcccttcggccctcaatccagcggaccttccttcccgcggcctgctgccggctctgcgg
cctcttccgcgtcttcgccttcgccctcagacgagtcggatctccctttgggccgcctccccgcatcgataccgtcgacc

Figure 33. Plasmid map of shRNA (sequence 1) in the pSicoR vector.

Genetic code shows mU6 promoter, shRNA1, CMV promoter, EGFP and WPRE sequences. Sequences for shRNA 2, 3, 4, 5 can be found in Materials and Methods (Table 11).

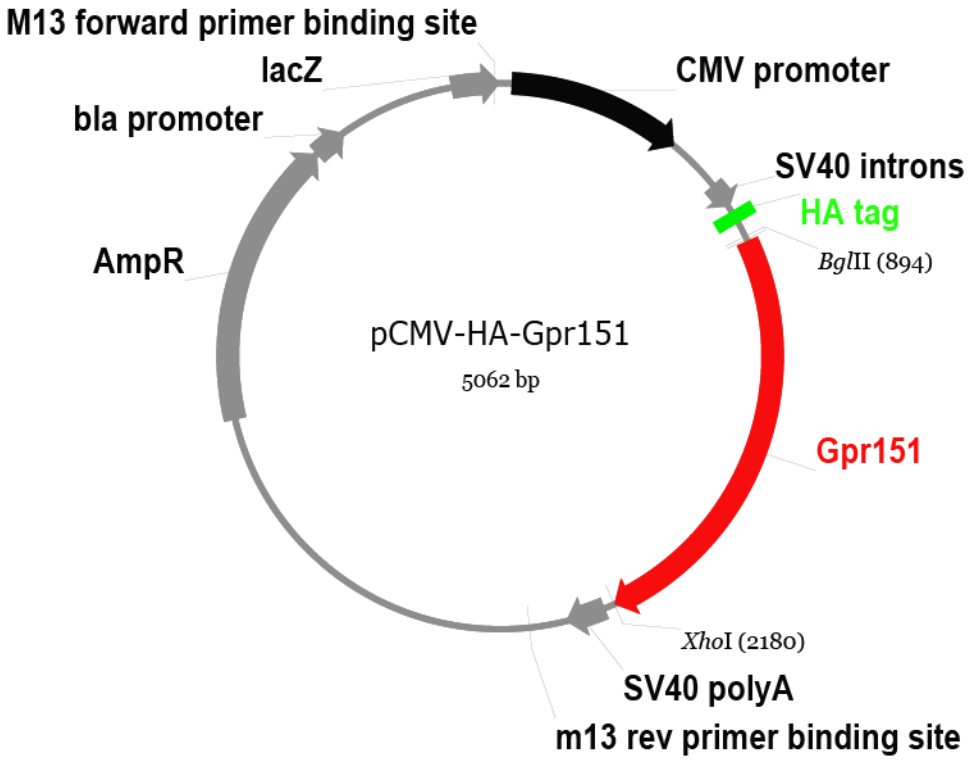

cgttacataacttacggtaaatggcccgcctggctgaccgcccaacgacccccgcccattgacgtcaataatgacgtatgttcccatagtaacg
ccaatagggactttccattgacgtcaatgggtggagtatttacggtaaactgcccacttggcagtacatcaagtgtatcatatgccaagtacgccc
cctattgacgtcaatgacggtaaatggcccgcctggcattatgcccagtacatgaccttatgggactttcctacttggcagtacatctacgtattagt
catcgctattaccatggtgatgcggttttggcagtacatcaatgggcgtggatagcggtttgactcacggggatttccaagtctccaccccattgac
gtcaatgggagtttgttttggcaccaaaatcaacgggactttccaaaatgtcgtaacaactccgccccattgacgcaaatgggcggtaggcgtgt
acggtgggaggtctatataagcagagctcgtttagtgaaccgtcagatcgcctggagacgccatccacgctgttttgacctccatagaagacac
cgggaccgatccagcctccggactctagaggatccggtactagaggaactgaaaaaccagaaagttaactggtaagtttagtctttttgtcttttat
ttcaggtcccggatccggtggtggtgcaaatcaaagaactgctcctcagtggatgttgcctttacttctaggcctgtacggaagtgttacttctgctct
aaaagctgcggaattgtacccgcgggcccaccatgtacccatacgatgttccagattacgcttatggccatggaggcccgaattcggtcgac
cgagatctcatagatctccatgggaaaggcaatgctgagagctgggtttgccgacaccaattccagcaacatgaacgagtcgtttgctcgcctc
cactttgcaggaggctacctgccgtctgactccaaggactggaggaccatcattccgtctctcttgatggccgtgtgcctggtgggtctcgtggga
aacctgtgtgtgattggcattctccttcatggcgtttggaaaagaaagccatccacgatccactccctgattctgaatctaagcctggctgacttctct
ctcctgctcttctctgcacctgtccgagcggcagcatactccaagggcgtttgggatctcggctggttcatctgcaagtcctctgactggttcaccca
cgtgtgcatggcagccaagagcttgacatttgttgtggtagccaaagcatgcttcgcgtatgcaagtgacccagccaagcaagagagtatccac
agccgcaccatctggtcagtgctggcgggcatctgggttgtagccagcctgcttcccctgccagaatggctctttagcaccaccagacgtcacgc
aggtgtggaaatgtgcctcgtggatgtgccagctgtggcagaagaattcatgtccatgttcggtaagctctaccctctgctggtgttctgccttccttta
cttctggctggcgtttatttctggcgagcttatgaccaatgtaagacacgatgtacgaaaactcgaaatctgagagaccagatgcgttcaaagca
actcacagtgatgctgctaagcactgcaatcatctctgctcttctgtggctcccagagtggatagcctggctgtgggtatggcatgtgaaggctgga
gggccgatgccaccacaggggttcatagccctgtctcaagttctcatgtttttcacctccacagcaaaccctctcatttttctagttatgtctgaagagt
tcaaggcaggcttgaaaggcctatggaaatggatgataaccagaaagccagcagttacttcagaggttcaggaggcacctgctggaaacac
agaggcccttcccggaaaggctccatcaccagagacccaaacatgcatcctagacacagacggacgtgggtctcctgatgacagcaaaga
gaaatctggtaaggtggtggctcccatcctccctgacgtggagcagttttggcacgagagggatgctgtcccttcagcacaagacaatgaccct
ataccctgggaacacgaaggccaagagacagagggctgcaattaa

Figure 34. Plasmid map of Gpr151 in the pCMV-HA vector.

Genetic code shows CMV promoter, HA tag and Gpr151 sequences.

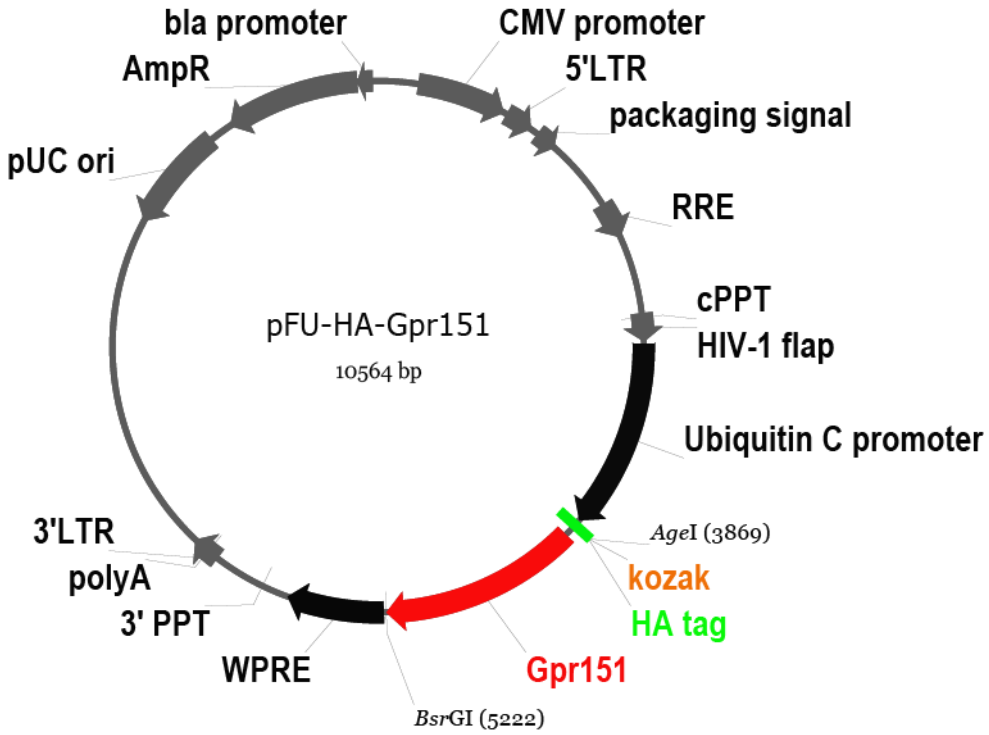

gatctggcctccgcgccgggttttggcgcctcccgcgggcgcccccctcctcacggcgagcgctgccacgtcagacgaagggcgcagcgag
cgtcctgatccttccgcccggacgctcaggacagcggcccgctgctcataagactcggccttagaaccccagtatcagcagaaggacatttta
ggacgggacttgggtgactctagggcactggttttctttccagagagcggaacaggcgaggaaaagtagtcccttctcggcgattctgcggagg
gatctccgtggggcggtgaacgccgatgattatataaggacgcgccgggtgtggcacagctagttccgtcgcagccgggatttgggtcgcggtt
cttgtttgtggatcgctgtgatcgtcacttggtgagtagcgggctgctgggctggccggggctttcgtggccgccgggccgctcggtgggacggaa
gcgtgtggagagaccgccaagggctgtagtctgggtccgcgagcaaggttgccctgaactgggggttgggggagcgcagcaaaatggcg
gctgttcccgagtcttgaatggaagacgcttgtgaggcgggctgtgaggtcgttgaaacaaggtgggggcatggtgggcggcaagaaccca
aggtcttgaggccttcgctaatgcgggaaagctcttattcgggtgagatgggctggggcaccatctggggaccctgacgtgaagtttgtcactga
ctggagaactcgggtttgtcgtctggttgcgggggcggcagttatgcggtgccgttgggcagtgcacccgtacctttgggagcgcgcgcctcgtc
gtgtcgtgacgtcacccgttctgttggcttataatgcagggtggggccacctgccggtaggtgtgcggtaggcttttctccgtcgcaggacgcagg
gttcgggcctagggtaggctctcctgaatcgacaggcgccggacctctggtgaggggagggataagtgaggcgtcagtttctttggtcggttttat
gtacctatcttcttaagtagctgaagctccggttttgaactatgcgctcggggttggcgagtgtgttttgtgaagttttttaggcacctttgaaatgtaat
catttgggtcaatatgtaattttcagtgttagactagtaaattgtccgctaaattctggccgtttttggcttttttgttagacgaagcttgggctgcaggtcg
actctagaggatccccgggtaccggtgccaccatgtacccatacgatgttccagattacgcttatggccatggaggcccgaattcggtcgacc
gagatctccatgggaaaggcaatgctgagagctgggtttgccgacaccaattccagcaacatgaacgagtcgtttgctcgcctccactttgcag
gaggctacctgccgtctgactccaaggactggaggaccatcattccgtctctcttgatggccgtgtgcctggtgggtctcgtgggaaacctgtgtgt
gattggcattctccttcatggcgtttggaaaagaaagccatccacgatccactccctgattctgaatctaagcctggctgacttctctctcctgctcttc
tctgcacctgtccgagcggcagcatactccaagggcgtttgggatctcggctggttcatctgcaagtcctctgactggttcacccacgtgtgcatgg
cagccaagagcttgacatttgttgtggtagccaaagcatgcttcgcgtatgcaagtgacccagccaagcaagagagtatccacagccgcacc
atctggtcagtgctggcgggcatctgggttgtagccagcctgcttcccctgccagaatggctctttagcaccaccagacgtcacgcaggtgtgga
aatgtgcctcgtggatgtgccagctgtggcagaagaattcatgtccatgttcggtaagctctaccctctgctggtgttctgccttcctttacttctggctg
gcgtttatttctggcgagcttatgaccaatgtaagacacgatgtacgaaaactcgaaatctgagagaccagatgcgttcaaagcaactcacagt
gatgctgctaagcactgcaatcatctctgctcttctgtggctcccagagtggatagcctggctgtgggtatggcatgtgaaggctggagggccgat
gccaccacaggggttcatagccctgtctcaagttctcatgtttttcacctccacagcaaaccctctcatttttctagttatgtctgaagagttcaaggca
ggcttgaaaggcctatggaaatggatgataaccagaaagccagcagttacttcagaggttcaggaggcacctgctggaaacacagaggccc
ttcccggaaaggctccatcaccagagacccaaacatgcatcctagacacagacggacgtgggtctcctgatgacagcaaagagaaatctgg
taaggtggtggctcccatcctccctgacgtggagcagttttggcacgagagggatgctgtcccttcagcacaagacaatgaccctataccctgg
gaacacgaaggccaagagacagagggctgcaattaatgtacaagtaagaattcgatatcaagcttatcgataatcaacctctggattacaaa
atttgtgaaagattgactggtattcttaactatgttgctccttttacgctatgtggatacgctgctttaatgccttgtatcatgctattgcttcccgtatggctt
tcattttctcctccttgtataaatcctggttgctgtctctttatgaggagttgtggcccgttgtcaggcaacgtggcgtggtgtgcactgtgtttgctgacgc
aacccccactggttggggcattgccaccacctgtcagctcctttccgggactttcgctttcccctccctattgccacggcggaactcatcgccgcc
tgccttgcccgctgctggacaggggctcggctgttgggcactgacaattccgtggtgttgtcggggaaatcatcgtcctttccttggctgctcgcctgt
gttgccacctggattctgcgcgggacgtccttctgctacgtcccttcggccctcaatccagcggaccttccttcccgcggcctgctgccggctctgc
ggcctcttccgcgtcttcgccttcgccctcagacgagtcggatctccctttgggccgcctccccgcatcgataccgtcgacc

Figure 35. Plasmid map of HA-Gpr151 in the lentiviral pFUGW vector.

Genetic code shows UbiquitinC promoter, kozak, HA tag, Gpr151 and WPRE sequences.

6.3 Index of figures

Figure 1. Habenula neuroanatomy. 9
Figure 2. Connectivity of the habenula. 11
Figure 3. Representation of the classical model of GPCR signaling. 19
Figure 4. Non-canonical GPCR signaling mechanisms..... 21
Figure 5. Schematic diagram of the mouse Gpr151 indicating sites or domains required for protein folding and activation. 25
Figure 6. Gpr151 is localized at the axonal projections of habenular neurons. 56
Figure 7. Gpr151 expression in the medial habenula. 58
Figure 8. Gpr151 expression in the lateral habenula. 59
Figure 9. Gpr151 habenular neurons project to the IPN. 60
Figure 10. Gpr151 habenular neurons project to the IPN, tegmental nuclei and raphe nuclei 61
Figure 11. Gpr151 habenular neurons project to the RMTg, raphe and rhabdoid nucleus. 62
Figure 12. Gpr151 expressing neurons are labeled with β-galactosidase in the thalamus and habenula in Gpr151-KO mouse coronal sections. 63
Figure 13. Gpr151 is expressed in the human MHb-IPN pathway. 65
Figure 14. Gpr151 is localized at habenular terminals in the IPN. 67
Figure 15. Distribution of Gpr151 immunogold particles in habenular terminals in the IPN. 69
Figure 16. Ultrastructure of the IPN is not altered in Gpr151-KO mice. 71
Figure 17. Gpr151 is likely to couple to Gαi/o. 72
Figure 18. Gpr151 overexpression does not activate cAMP or calcium signaling. 74
Figure 19. Galanin does not activate cAMP or calcium signaling on HEK293 cells expressing Gpr151. 76
Figure 20. Different galanin-like and tachykinin-like peptides do not activate cAMP or calcium signaling on HEK293 cells expressing Gpr151. 77
Figure 21. Application of the supernatant of light-stimulated habenular cultures does not result on activation of cAMP signaling on HEK293T cells expressing Gpr151. 79
Figure 22. Docking of Gpr151 model against Asinex Platinum database using Molecular Operating Environment software. 81
Figure 23. Gpr151-KO mice showed normal locomotor activity, anxiety-like behavior and prepulse inhibition. 83
Figure 24. Increased sensitivity to nicotine and withdrawal manifestations in Gpr151-KO mice. 85
Figure 25. Validation of lentiviruses encoding shRNAs against Gpr151. 86
Figure 26. shRNA-injected mice showed normal locomotor activity, anxiety-like behavior and prepulse inhibition. 87
Figure 27. Downregulation of Gpr151 in the habenula increases sensitivity to nicotine. 88
Figure 28. Gpr151 expressing habenular neurons project to the interpeduncular nucleus, rostromedial tegmental nucleus, rhabdoid nucleus, raphe nuclei and dorsal tegmental nucleus. 90
Figure 29. Nicotine-induced cell surface expression of Gpr151 as a feedback mechanism to regulate neurotransmitter release. 97
Figure 30. Deletion of Gpr151 in habenular neurons increases the sensitivity to nicotine-induced reinforcement responses. 98
Figure 31. Deletion of Gpr151 increases somatic and affective withdrawal signs in nicotine-dependent mice. 100
Figure 32. cAMP levels at the MHb terminals in the IPN modulate neurotransmitter release. 102
Figure 33. Plasmid map of shRNA (sequence 1) in the pSicoR vector. 118
Figure 34. Plasmid map of Gpr151 in the pCMV-HA vector. 119
Figure 35. Plasmid map of HA-Gpr151 in the lentiviral pFUGW vector. 120

6.4 Index of tables

Table 1. List of the primary downstream effectors activated or inhibited by each of the main G-protein subunits. 20
Table 2. Selected transcripts enriched in cholinergic MHb neurons. 26
Table 3. List of chemicals used in this work 30
Table 4. Composition of buffers and solutions 32
Table 5. Culture media used in this work 33
Table 6. Solutions used for chronic nicotine treatment experiments 33
Table 7. Bacteria strains used in this work 33
Table 8. Cell lines used in this work 33
Table 9. Plasmids used in this work 33
Table 10. Primers used in this work 34
Table 11. Oligonucleotides used for shRNA knockdown of Gpr151 34
Table 12. Enzymes used in this work 35
Table 13. List of the kits used in this work 35
Table 14. Antibodies used in this work. 35
Table 15. Peptides tested in cell-based second messenger assays 36
Table 16. Equipment used in this work 36
Table 17. Standard PCR mix for one reaction 40
Table 18. Standard PCR program 40

Erklärung

Hiermit versichere ich, Beatriz Antolin Fontes, dass ich die vorgelegte Dissertation mit dem Titel “Identification of a novel synaptic G protein-coupled receptor controlling nicotine dependence and withdrawal” selbstständig, ohne unerlaubte Hilfe angefertigt habe.

Ort, Datum

Unterschrift

6.5 Publication and presentation list

Publications

Slimak, M.A., Ables, J.L., Frahm, S., **Antolin-Fontes, B.**, Santos-Torres, J., Moretti, M., Gotti, C., and Ibanez-Tallon, I. (2014). Habenular expression of rare missense variants of the beta4 nicotinic receptor subunit alters nicotine consumption. Frontiers in human neuroscience 8, 12.

Gorlich, A., **Antolin-Fontes, B.**, Ables, J.L., Frahm, S., Slimak, M.A., Dougherty, J.D., and Ibanez-Tallon, I. (2013). Reexposure to nicotine during withdrawal increases the pacemaking activity of cholinergic habenular neurons. Proc Natl Acad Sci U S A 110, 17077-17082.

Frahm, S., Slimak, M.A., Ferrarese, L., Santos-Torres, J., **Antolin-Fontes, B.**, Auer, S., Filkin, S., Pons, S., Fontaine, J.F., Tsetlin, V., et al. (2011). Aversion to nicotine is regulated by the balanced activity of beta4 and alpha5 nicotinic receptor subunits in the medial habenula. Neuron 70, 522-535.

Poster presentations

Gorlich, A., Antolin-Fontes, B., Ables, J.L., Frahm, S., Slimak, M.A., Dougherty, J.D., and Ibanez-Tallon, I. Reexposure to nicotine during withdrawal increases the pacemaking activity of cholinergic habenular neurons. Society for Neuroscience 2013 Meeting, San Diego, CA, USA, 9-13.11.2013

Slimak, M.A., Frahm, S., Santos-Torres, J., Antolin-Fontes, B., Ables, J.L., and Ibanez-Tallon, I. Functional analysis of single nucleotide polymorphisms (SNPs) in the coding region of the β4 subunit of nAChR. Society for Neuroscience 2012 Meeting, New Orleans, LA, USA, 13-17.10.2012

Antolin-Fontes B., and Ibanez-Tallon, I. Dissecting the midbrain habenular circuit and its contribution to addictive behaviors. SFB665: Developmental disturbances in the nervous system 2011. Seminaris SeeHotel Potsdam, Germany, 27-29.10.2011

Slimak MA., Antolin-Fontes B., Santos-Torres J, Ables J., Ferrarese L., Ibañez-Tallon I. Functional analysis of the single nucleotide polymorphisms in the coding region of the β4 subunit of nAChR. SFB665: Developmental disturbances in the nervous system 2011. Seminaris SeeHotel Potsdam, Germany, 27-29.10.2011

Slimak MA., Antolin-Fontes B., Frahm S., Santos-Torres J., Ferrarese L., Sebastian Auer, Filkin S., Maskos U., Tsetlin V., Ibañez-Tallon I. Genetic and molecular studies to dissect the contribution of nAChRs in the habenular circuit to brain function and behavior. Society for Neuroscience 2010 Meeting, San Diego, CA, USA,13-17.11.2010

6.6 Curriculum Vitae

For reasons of data protection, the curriculum vitae is not included in the online version.

For reasons of data protection, the curriculum vitae is not included in the online version.

7. References

Ahmari, S.E., Buchanan, J., and Smith, S.J. (2000). Assembly of presynaptic active zones from cytoplasmic transport packets. Nature neuroscience *3*, 445-451.

Aizawa, H., Bianco, I.H., Hamaoka, T., Miyashita, T., Uemura, O., Concha, M.L., Russell, C., Wilson, S.W., and Okamoto, H. (2005). Laterotopic representation of left-right information onto the dorso-ventral axis of a zebrafish midbrain target nucleus. Current biology : CB *15*, 238-243.

Aizawa, H., Kobayashi, M., Tanaka, S., Fukai, T., and Okamoto, H. (2012). Molecular characterization of the subnuclei in rat habenula. J Comp Neurol *520*, 4051-4066.

Aizawa, H., Yanagihara, S., Kobayashi, M., Niisato, K., Takekawa, T., Harukuni, R., McHugh, T.J., Fukai, T., Isomura, Y., and Okamoto, H. (2013). The synchronous activity of lateral habenular neurons is essential for regulating hippocampal theta oscillation. J Neurosci *33*, 8909-8921.

Andres, K.H., von During, M., and Veh, R.W. (1999). Subnuclear organization of the rat habenular complexes. J Comp Neurol *407*, 130-150.

Atwood, B.K., Lopez, J., Wager-Miller, J., Mackie, K., and Straiker, A. (2011). Expression of G protein-coupled receptors and related proteins in HEK293, AtT20, BV2, and N18 cell lines as revealed by microarray analysis. BMC genomics *12*, 14.

Auer, S., Sturzebecher, A.S., Juttner, R., Santos-Torres, J., Hanack, C., Frahm, S., Liehl, B., and Ibanez-Tallon, I. (2010). Silencing neurotransmission with membrane-tethered toxins. Nat Methods *7*, 229-236.

Balcita-Pedicino, J.J., Omelchenko, N., Bell, R., and Sesack, S.R. (2011). The inhibitory influence of the lateral habenula on midbrain dopamine cells: ultrastructural evidence for indirect mediation via the rostromedial mesopontine tegmental nucleus. J Comp Neurol *519*, 1143-1164.

Bao, L., Jin, S.X., Zhang, C., Wang, L.H., Xu, Z.Z., Zhang, F.X., Wang, L.C., Ning, F.S., Cai, H.J., Guan, J.S*., et al.* (2003). Activation of delta opioid receptors induces receptor insertion and neuropeptide secretion. Neuron *37*, 121-133.

Benowitz, N.L. (2008). Clinical pharmacology of nicotine: implications for understanding, preventing, and treating tobacco addiction. Clinical pharmacology and therapeutics *83*, 531-541.

Benowitz, N.L. (2009). Pharmacology of nicotine: addiction, smoking-induced disease, and therapeutics. Annu Rev Pharmacol Toxicol *49*, 57-71.

Berrettini, W., Yuan, X., Tozzi, F., Song, K., Francks, C., Chilcoat, H., Waterworth, D., Muglia, P., and Mooser, V. (2008). Alpha-5/alpha-3 nicotinic receptor subunit alleles increase risk for heavy smoking. Mol Psychiatry *13*, 368-373.

Berthold, M., Collin, M., Sejlitz, T., Meister, B., and Lind, P. (2003). Cloning of a novel orphan G protein-coupled receptor (GPCR-2037): in situ hybridization reveals high mRNA expression in rat brain restricted to neurons of the habenular complex. Brain Res Mol Brain Res *120*, 22-29.

Bianco, I.H., and Wilson, S.W. (2009). The habenular nuclei: a conserved asymmetric relay station in the vertebrate brain. Philos Trans R Soc Lond B Biol Sci *364*, 1005-1020.

Bierut, L.J., Stitzel, J.A., Wang, J.C., Hinrichs, A.L., Grucza, R.A., Xuei, X., Saccone, N.L., Saccone, S.F., Bertelsen, S., Fox, L*., et al.* (2008). Variants in nicotinic receptors and risk for nicotine dependence. Am J Psychiatry *165*, 1163-1171.

Bond, R.A., Leff, P., Johnson, T.D., Milano, C.A., Rockman, H.A., McMinn, T.R., Apparsundaram, S., Hyek, M.F., Kenakin, T.P., Allen, L.F*., et al.* (1995). Physiological effects of inverse agonists in transgenic mice with myocardial overexpression of the beta 2-adrenoceptor. Nature *374*, 272-276.

Braff, D.L., and Geyer, M.A. (1990). Sensorimotor gating and schizophrenia. Human and animal model studies. Arch Gen Psychiatry *47*, 181-188.

Bridges, T.M., and Lindsley, C.W. (2008). G-protein-coupled receptors: from classical modes of modulation to allosteric mechanisms. ACS chemical biology *3*, 530-541.

Bromberg-Martin, E.S., and Hikosaka, O. (2011). Lateral habenula neurons signal errors in the prediction of reward information. Nature neuroscience *14*, 1209-1216.
Buijs, R.M. (1978). Intra- and extrahypothalamic vasopressin and oxytocin pathways in the rat. Pathways to the limbic system, medulla oblongata and spinal cord. Cell and tissue research *192*, 423-435.
Buzsaki, G. (2002). Theta oscillations in the hippocampus. Neuron *33*, 325-340.
Caldecott-Hazard, S., Mazziotta, J., and Phelps, M. (1988). Cerebral correlates of depressed behavior in rats, visualized using 14C-2-deoxyglucose autoradiography. J Neurosci *8*, 1951-1961.
Calver, A.R., Michalovich, D., Testa, T.T., Robbins, M.J., Jaillard, C., Hill, J., Szekeres, P.G., Charles, K.J., Jourdain, S., Holbrook, J.D.*, et al.* (2003). Molecular cloning and characterisation of a novel GABAB-related G-protein coupled receptor. Brain Res Mol Brain Res *110*, 305-317.
Caputo, A., Ghiringhelli, L., Dieci, M., Giobbio, G.M., Tenconi, F., Ferrari, L., Gimosti, E., Prato, K., and Vita, A. (1998). Epithalamus calcifications in schizophrenia. European archives of psychiatry and clinical neuroscience *248*, 272-276.
Christoph, G.R., Leonzio, R.J., and Wilcox, K.S. (1986). Stimulation of the lateral habenula inhibits dopamine-containing neurons in the substantia nigra and ventral tegmental area of the rat. J Neurosci *6*, 613-619.
Commons, K.G. (2003). Translocation of presynaptic delta opioid receptors in the ventrolateral periaqueductal gray after swim stress. J Comp Neurol *464*, 197-207.
Concha, M.L., and Wilson, S.W. (2001). Asymmetry in the epithalamus of vertebrates. Journal of anatomy *199*, 63-84.
Contestabile, A., and Flumerfelt, B.A. (1981). Afferent connections of the interpeduncular nucleus and the topographic organization of the habenulo-interpeduncular pathway: an HRP study in the rat. J Comp Neurol *196*, 253-270.
Contestabile, A., and Fonnum, F. (1983). Cholinergic and GABAergic forebrain projections to the habenula and nucleus interpeduncularis: surgical and kainic acid lesions. Brain Res *275*, 287-297.
Contestabile, A., Villani, L., Fasolo, A., Franzoni, M.F., Gribaudo, L., Oktedalen, O., and Fonnum, F. (1987). Topography of cholinergic and substance P pathways in the habenulo-interpeduncular system of the rat. An immunocytochemical and microchemical approach. Neuroscience *21*, 253-270.
Corrigall, W.A., Franklin, K.B., Coen, K.M., and Clarke, P.B. (1992). The mesolimbic dopaminergic system is implicated in the reinforcing effects of nicotine. Psychopharmacology (Berl) *107*, 285-289.
Courtoy, P.J., Picton, D.H., and Farquhar, M.G. (1983). Resolution and limitations of the immunoperoxidase procedure in the localization of extracellular matrix antigens. The journal of histochemistry and cytochemistry : official journal of the Histochemistry Society *31*, 945-951.
Crooks, P.A., Bardo, M.T., and Dwoskin, L.P. (2014). Nicotinic receptor antagonists as treatments for nicotine abuse. Advances in pharmacology *69*, 513-551.
Cuello, A.C., Emson, P.C., Paxinos, G., and Jessell, T. (1978). Substance P containing and cholinergic projections from the habenula. Brain Res *149*, 413-429.
Dadda, M., Domenichini, A., Piffer, L., Argenton, F., and Bisazza, A. (2010). Early differences in epithalamic left-right asymmetry influence lateralization and personality of adult zebrafish. Behavioural brain research *206*, 208-215.
Damaj, M.I., Kao, W., and Martin, B.R. (2003). Characterization of spontaneous and precipitated nicotine withdrawal in the mouse. J Pharmacol Exp Ther *307*, 526-534.
Dani, J.A., and De Biasi, M. (2013). Mesolimbic dopamine and habenulo-interpeduncular pathways in nicotine withdrawal. Cold Spring Harbor perspectives in medicine *3*.
Davenport, A.P., and Harmar, A.J. (2013). Evolving pharmacology of orphan GPCRs: IUPHAR Commentary. British journal of pharmacology *170*, 693-695.
De Biasi, M., and Dani, J.A. (2011). Reward, addiction, withdrawal to nicotine. Annu Rev Neurosci *34*, 105-130.

de Wit, H., Cornelisse, L.N., Toonen, R.F., and Verhage, M. (2006). Docking of secretory vesicles is syntaxin dependent. PLoS One *1*, e126.
de Wit, H., Walter, A.M., Milosevic, I., Gulyas-Kovacs, A., Riedel, D., Sorensen, J.B., and Verhage, M. (2009). Synaptotagmin-1 docks secretory vesicles to syntaxin-1/SNAP-25 acceptor complexes. Cell *138*, 935-946.
Di Angelantonio, S., Piccioni, A., Moriconi, C., Trettel, F., Cristalli, G., Grassi, F., and Limatola, C. (2011). Adenosine A2A receptor induces protein kinase A-dependent functional modulation of human (alpha)3(beta)4 nicotinic receptor. J Physiol *589*, 2755-2766.
Diaz, E., Bravo, D., Rojas, X., and Concha, M.L. (2011). Morphologic and immunohistochemical organization of the human habenular complex. J Comp Neurol *519*, 3727-3747.
Doly, S., Fischer, J., Brisorgueil, M.J., Verge, D., and Conrath, M. (2005). Pre- and postsynaptic localization of the 5-HT7 receptor in rat dorsal spinal cord: immunocytochemical evidence. J Comp Neurol *490*, 256-269.
Dong, C., Filipeanu, C.M., Duvernay, M.T., and Wu, G. (2007). Regulation of G protein-coupled receptor export trafficking. Biochimica et biophysica acta *1768*, 853-870.
Doyle, J.P., Dougherty, J.D., Heiman, M., Schmidt, E.F., Stevens, T.R., Ma, G., Bupp, S., Shrestha, P., Shah, R.D., Doughty, M.L.*, et al.* (2008). Application of a translational profiling approach for the comparative analysis of CNS cell types. Cell *135*, 749-762.
Drake, C.T., Chavkin, C., and Milner, T.A. (1997). Kappa opioid receptor-like immunoreactivity is present in substance P-containing subcortical afferents in guinea pig dentate gyrus. Hippocampus *7*, 36-47.
Eberini, I., Daniele, S., Parravicini, C., Sensi, C., Trincavelli, M.L., Martini, C., and Abbracchio, M.P. (2011). In silico identification of new ligands for GPR17: a promising therapeutic target for neurodegenerative diseases. J Comput Aided Mol Des *25*, 743-752.
Ferguson, S.S., Downey, W.E., 3rd, Colapietro, A.M., Barak, L.S., Menard, L., and Caron, M.G. (1996). Role of beta-arrestin in mediating agonist-promoted G protein-coupled receptor internalization. Science *271*, 363-366.
Fernandez-Alacid, L., Aguado, C., Ciruela, F., Martin, R., Colon, J., Cabanero, M.J., Gassmann, M., Watanabe, M., Shigemoto, R., Wickman, K.*, et al.* (2009). Subcellular compartment-specific molecular diversity of pre- and post-synaptic GABA-activated GIRK channels in Purkinje cells. J Neurochem *110*, 1363-1376.
Ferreira, J.G., Del-Fava, F., Hasue, R.H., and Shammah-Lagnado, S.J. (2008). Organization of ventral tegmental area projections to the ventral tegmental area-nigral complex in the rat. Neuroscience *153*, 196-213.
Flanagan, C.A. (2005). A GPCR that is not "DRY". Mol Pharmacol *68*, 1-3.
Foord, S.M., and Marshall, F.H. (1999). RAMPs: accessory proteins for seven transmembrane domain receptors. Trends Pharmacol Sci *20*, 184-187.
Fowler, C.D., and Kenny, P.J. (2014). Nicotine aversion: Neurobiological mechanisms and relevance to tobacco dependence vulnerability. Neuropharmacology *76 Pt B*, 533-544.
Fowler, C.D., Lu, Q., Johnson, P.M., Marks, M.J., and Kenny, P.J. (2011). Habenular alpha5 nicotinic receptor subunit signalling controls nicotine intake. Nature *471*, 597-601.
Frahm, S., Slimak, M.A., Ferrarese, L., Santos-Torres, J., Antolin-Fontes, B., Auer, S., Filkin, S., Pons, S., Fontaine, J.F., Tsetlin, V.*, et al.* (2011). Aversion to nicotine is regulated by the balanced activity of beta4 and alpha5 nicotinic receptor subunits in the medial habenula. Neuron *70*, 522-535.
Galvez, T., Duthey, B., Kniazeff, J., Blahos, J., Rovelli, G., Bettler, B., Prezeau, L., and Pin, J.P. (2001). Allosteric interactions between GB1 and GB2 subunits are required for optimal GABA(B) receptor function. The EMBO journal *20*, 2152-2159.
Geisler, S., Andres, K.H., and Veh, R.W. (2003). Morphologic and cytochemical criteria for the identification and delineation of individual subnuclei within the lateral habenular complex of the rat. J Comp Neurol *458*, 78-97.
Geisler, S., and Zahm, D.S. (2005). Afferents of the ventral tegmental area in the rat-anatomical substratum for integrative functions. J Comp Neurol *490*, 270-294.

Geyer, M.A., Krebs-Thomson, K., Braff, D.L., and Swerdlow, N.R. (2001). Pharmacological studies of prepulse inhibition models of sensorimotor gating deficits in schizophrenia: a decade in review. Psychopharmacology (Berl) *156*, 117-154.
Glick, S.D., Sell, E.M., McCallum, S.E., and Maisonneuve, I.M. (2011). Brain regions mediating alpha3beta4 nicotinic antagonist effects of 18-MC on nicotine self-administration. Eur J Pharmacol *669*, 71-75.
Goncalves, L., Sego, C., and Metzger, M. (2012). Differential projections from the lateral habenula to the rostromedial tegmental nucleus and ventral tegmental area in the rat. J Comp Neurol *520*, 1278-1300.
Goodman, O.B., Jr., Krupnick, J.G., Santini, F., Gurevich, V.V., Penn, R.B., Gagnon, A.W., Keen, J.H., and Benovic, J.L. (1996). Beta-arrestin acts as a clathrin adaptor in endocytosis of the beta2-adrenergic receptor. Nature *383*, 447-450.
Gorlich, A., Antolin-Fontes, B., Ables, J.L., Frahm, S., Slimak, M.A., Dougherty, J.D., and Ibanez-Tallon, I. (2013). Reexposure to nicotine during withdrawal increases the pacemaking activity of cholinergic habenular neurons. Proc Natl Acad Sci U S A *110*, 17077-17082.
Goto, M., Swanson, L.W., and Canteras, N.S. (2001). Connections of the nucleus incertus. J Comp Neurol *438*, 86-122.
Gottesfeld, Z. (1983). Origin and distribution of noradrenergic innervation in the habenula: a neurochemical study. Brain Res *275*, 299-304.
Grabus, S.D., Martin, B.R., Batman, A.M., Tyndale, R.F., Sellers, E., and Damaj, M.I. (2005). Nicotine physical dependence and tolerance in the mouse following chronic oral administration. Psychopharmacology (Berl) *178*, 183-192.
Grady, S.R., Salminen, O., Laverty, D.C., Whiteaker, P., McIntosh, J.M., Collins, A.C., and Marks, M.J. (2007). The subtypes of nicotinic acetylcholine receptors on dopaminergic terminals of mouse striatum. Biochem Pharmacol *74*, 1235-1246.
Greatrex, R.M., and Phillipson, O.T. (1982). Demonstration of synaptic input from prefrontal cortex to the habenula i the rat. Brain Res *238*, 192-197.
Groenewegen, H.J., and Van Dijk, C.A. (1984). Efferent connections of the dorsal tegmental region in the rat, studied by means of anterograde transport of the lectin Phaseolus vulgaris-leucoagglutinin (PHA-L). Brain Res *304*, 367-371.
Gruber, C., Kahl, A., Lebenheim, L., Kowski, A., Dittgen, A., and Veh, R.W. (2007). Dopaminergic projections from the VTA substantially contribute to the mesohabenular pathway in the rat. Neurosci Lett *427*, 165-170.
Grucza, R.A., Wang, J.C., Stitzel, J.A., Hinrichs, A.L., Saccone, S.F., Saccone, N.L., Bucholz, K.K., Cloninger, C.R., Neuman, R.J., Budde, J.P.*, et al.* (2008). A risk allele for nicotine dependence in CHRNA5 is a protective allele for cocaine dependence. Biol Psychiatry *64*, 922-929.
Hack, S.P., Bagley, E.E., Chieng, B.C., and Christie, M.J. (2005). Induction of delta-opioid receptor function in the midbrain after chronic morphine treatment. J Neurosci *25*, 3192-3198.
Haines, D.E. (2000). Neuroanatomy : an atlas of structures, sections, and systems, 5th edn (Philadelphia: Lippincott Williams & Wilkins).
Hamill, G.S., and Lenn, N.J. (1984). The subnuclear organization of the rat interpeduncular nucleus: a light and electron microscopic study. J Comp Neurol *222*, 396-408.
Hay, D.L., Poyner, D.R., and Sexton, P.M. (2006). GPCR modulation by RAMPs. Pharmacol Ther *109*, 173-197.
Heimer, L., Záborszky, L., Wouterlood, F.G., and Lanciego, J.L. (2006). Neuroanatomical tract-tracing 3 : molecules, neurons, and systems, [3rd edn (New York: Springer).
Herkenham, M., and Nauta, W.J. (1977). Afferent connections of the habenular nuclei in the rat. A horseradish peroxidase study, with a note on the fiber-of-passage problem. J Comp Neurol *173*, 123-146.
Herkenham, M., and Nauta, W.J. (1979). Efferent connections of the habenular nuclei in the rat. J Comp Neurol *187*, 19-47.
Hikosaka, O. (2010). The habenula: from stress evasion to value-based decision-making. Nat Rev Neurosci *11*, 503-513.

Hong, S., Jhou, T.C., Smith, M., Saleem, K.S., and Hikosaka, O. (2011). Negative reward signals from the lateral habenula to dopamine neurons are mediated by rostromedial tegmental nucleus in primates. J Neurosci *31*, 11457-11471.
Howard, A.D., McAllister, G., Feighner, S.D., Liu, Q., Nargund, R.P., Van der Ploeg, L.H., and Patchett, A.A. (2001). Orphan G-protein-coupled receptors and natural ligand discovery. Trends Pharmacol Sci *22*, 132-140.
Hsu, Y.W., Tempest, L., Quina, L.A., Wei, A.D., Zeng, H., and Turner, E.E. (2013). Medial habenula output circuit mediated by alpha5 nicotinic receptor-expressing GABAergic neurons in the interpeduncular nucleus. J Neurosci *33*, 18022-18035.
Hu, F., Ren, J., Zhang, J.E., Zhong, W., and Luo, M. (2012). Natriuretic peptides block synaptic transmission by activating phosphodiesterase 2A and reducing presynaptic PKA activity. Proc Natl Acad Sci U S A *109*, 17681-17686.
Huang da, W., Sherman, B.T., and Lempicki, R.A. (2009). Bioinformatics enrichment tools: paths toward the comprehensive functional analysis of large gene lists. Nucleic Acids Res *37*, 1-13.
Ide, J.S., and Li, C.S. (2011). Error-related functional connectivity of the habenula in humans. Frontiers in human neuroscience *5*, 25.
Ignatov, A., Hermans-Borgmeyer, I., and Schaller, H.C. (2004). Cloning and characterization of a novel G-protein-coupled receptor with homology to galanin receptors. Neuropharmacology *46*, 1114-1120.
Ikemoto, S., Qin, M., and Liu, Z.H. (2006). Primary reinforcing effects of nicotine are triggered from multiple regions both inside and outside the ventral tegmental area. J Neurosci *26*, 723-730.
Iyaniwura, T.T., Wright, A.E., and Balfour, D.J. (2001). Evidence that mesoaccumbens dopamine and locomotor responses to nicotine in the rat are influenced by pretreatment dose and strain. Psychopharmacology (Berl) *158*, 73-79.
Jaakola, V.P., and Ijzerman, A.P. (2010). The crystallographic structure of the human adenosine A2A receptor in a high-affinity antagonist-bound state: implications for GPCR drug screening and design. Current opinion in structural biology *20*, 401-414.
Jackson, K.J., Martin, B.R., Changeux, J.P., and Damaj, M.I. (2008). Differential role of nicotinic acetylcholine receptor subunits in physical and affective nicotine withdrawal signs. J Pharmacol Exp Ther *325*, 302-312.
Jhou, T.C., Fields, H.L., Baxter, M.G., Saper, C.B., and Holland, P.C. (2009a). The rostromedial tegmental nucleus (RMTg), a GABAergic afferent to midbrain dopamine neurons, encodes aversive stimuli and inhibits motor responses. Neuron *61*, 786-800.
Jhou, T.C., Geisler, S., Marinelli, M., Degarmo, B.A., and Zahm, D.S. (2009b). The mesopontine rostromedial tegmental nucleus: A structure targeted by the lateral habenula that projects to the ventral tegmental area of Tsai and substantia nigra compacta. J Comp Neurol *513*, 566-596.
Ji, H., and Shepard, P.D. (2007). Lateral habenula stimulation inhibits rat midbrain dopamine neurons through a GABA(A) receptor-mediated mechanism. J Neurosci *27*, 6923-6930.
Jones, K.A., Borowsky, B., Tamm, J.A., Craig, D.A., Durkin, M.M., Dai, M., Yao, W.J., Johnson, M., Gunwaldsen, C., Huang, L.Y*., et al.* (1998). GABA(B) receptors function as a heteromeric assembly of the subunits GABA(B)R1 and GABA(B)R2. Nature *396*, 674-679.
Kaeser, P.S., Deng, L., Wang, Y., Dulubova, I., Liu, X., Rizo, J., and Sudhof, T.C. (2011). RIM proteins tether Ca2+ channels to presynaptic active zones via a direct PDZ-domain interaction. Cell *144*, 282-295.
Kaufling, J., Veinante, P., Pawlowski, S.A., Freund-Mercier, M.J., and Barrot, M. (2009). Afferents to the GABAergic tail of the ventral tegmental area in the rat. J Comp Neurol *513*, 597-621.
Kawaja, M.D., Flumerfelt, B.A., and Hrycyshyn, A.W. (1989). Glutamate decarboxylase immunoreactivity in the rat interpeduncular nucleus: a light and electron microscope investigation. Neuroscience *30*, 741-753.
Kim, U., and Chang, S.Y. (2005). Dendritic morphology, local circuitry, and intrinsic electrophysiology of neurons in the rat medial and lateral habenular nuclei of the epithalamus. J Comp Neurol *483*, 236-250.

Klemm, W.R. (2004). Habenular and interpeduncularis nuclei: shared components in multiple-function networks. Medical science monitor : international medical journal of experimental and clinical research *10*, RA261-273.
Kobayashi, Y., Sano, Y., Vannoni, E., Goto, H., Suzuki, H., Oba, A., Kawasaki, H., Kanba, S., Lipp, H.P., Murphy, N.P.*, et al.* (2013). Genetic dissection of medial habenula-interpeduncular nucleus pathway function in mice. Frontiers in behavioral neuroscience *7*, 17.
Lagerstrom, M.C., and Schioth, H.B. (2008). Structural diversity of G protein-coupled receptors and significance for drug discovery. Nat Rev Drug Discov *7*, 339-357.
Lammel, S., Lim, B.K., Ran, C., Huang, K.W., Betley, M.J., Tye, K.M., Deisseroth, K., and Malenka, R.C. (2012). Input-specific control of reward and aversion in the ventral tegmental area. Nature *491*, 212-217.
Lecourtier, L., Defrancesco, A., and Moghaddam, B. (2008). Differential tonic influence of lateral habenula on prefrontal cortex and nucleus accumbens dopamine release. Eur J Neurosci *27*, 1755-1762.
Lecourtier, L., and Kelly, P.H. (2007). A conductor hidden in the orchestra? Role of the habenular complex in monoamine transmission and cognition. Neurosci Biobehav Rev *31*, 658-672.
Lecourtier, L., Neijt, H.C., and Kelly, P.H. (2004). Habenula lesions cause impaired cognitive performance in rats: implications for schizophrenia. Eur J Neurosci *19*, 2551-2560.
Lee, E.H., and Huang, S.L. (1988). Role of lateral habenula in the regulation of exploratory behavior and its relationship to stress in rats. Behavioural brain research *30*, 265-271.
Lenn, N.J. (1976). Synapses in the interpeduncular nucleus: electron microscopy of normal and habenula lesioned rats. J Comp Neurol *166*, 77-99.
Levoye, A., Dam, J., Ayoub, M.A., Guillaume, J.L., Couturier, C., Delagrange, P., and Jockers, R. (2006). The orphan GPR50 receptor specifically inhibits MT1 melatonin receptor function through heterodimerization. The EMBO journal *25*, 3012-3023.
Li, C.S., Yan, P., Chao, H.H., Sinha, R., Paliwal, P., Constable, R.T., Zhang, S., and Lee, T.W. (2008). Error-specific medial cortical and subcortical activity during the stop signal task: a functional magnetic resonance imaging study. Neuroscience *155*, 1142-1151.
Li, Y.Q., Takada, M., and Mizuno, N. (1993). Demonstration of habenular neurons which receive afferent fibers from the nucleus accumbens and send their axons to the midbrain periaqueductal gray. Neurosci Lett *158*, 55-58.
Lips, E.H., Gaborieau, V., McKay, J.D., Chabrier, A., Hung, R.J., Boffetta, P., Hashibe, M., Zaridze, D., Szeszenia-Dabrowska, N., Lissowska, J.*, et al.* (2010). Association between a 15q25 gene variant, smoking quantity and tobacco-related cancers among 17 000 individuals. Int J Epidemiol *39*, 563-577.
Lisoprawski, A., Herve, D., Blanc, G., Glowinski, J., and Tassin, J.P. (1980). Selective activation of the mesocortico-frontal dopaminergic neurons induced by lesion of the habenula in the rat. Brain Res *183*, 229-234.
Little, K.D., Hemler, M.E., and Stipp, C.S. (2004). Dynamic regulation of a GPCR-tetraspanin-G protein complex on intact cells: central role of CD81 in facilitating GPR56-Galpha q/11 association. Molecular biology of the cell *15*, 2375-2387.
Liu, J.Z., Tozzi, F., Waterworth, D.M., Pillai, S.G., Muglia, P., Middleton, L., Berrettini, W., Knouff, C.W., Yuan, X., Waeber, G.*, et al.* (2010). Meta-analysis and imputation refines the association of 15q25 with smoking quantity. Nat Genet *42*, 436-440.
Liu, R., Chang, L., and Wickern, G. (1984). The dorsal tegmental nucleus: an axoplasmic transport study. Brain Res *310*, 123-132.
Ludwig, A., Flockerzi, V., and Hofmann, F. (1997). Regional expression and cellular localization of the alpha1 and beta subunit of high voltage-activated calcium channels in rat brain. J Neurosci *17*, 1339-1349.
Luttrell, L.M. (2008). Reviews in molecular biology and biotechnology: transmembrane signaling by G protein-coupled receptors. Molecular biotechnology *39*, 239-264.
Magalhaes, A.C., Dunn, H., and Ferguson, S.S. (2012). Regulation of GPCR activity, trafficking and localization by GPCR-interacting proteins. British journal of pharmacology *165*, 1717-1736.

Marazziti, D., Mandillo, S., Di Pietro, C., Golini, E., Matteoni, R., and Tocchini-Valentini, G.P. (2007). GPR37 associates with the dopamine transporter to modulate dopamine uptake and behavioral responses to dopaminergic drugs. Proc Natl Acad Sci U S A *104*, 9846-9851.
Maskos, U., Molles, B.E., Pons, S., Besson, M., Guiard, B.P., Guilloux, J.P., Evrard, A., Cazala, P., Cormier, A., Mameli-Engvall, M.*, et al.* (2005). Nicotine reinforcement and cognition restored by targeted expression of nicotinic receptors. Nature *436*, 103-107.
Mathuru, A.S., and Jesuthasan, S. (2013). The medial habenula as a regulator of anxiety in adult zebrafish. Frontiers in neural circuits *7*, 99.
Matsumoto, M., and Hikosaka, O. (2007). Lateral habenula as a source of negative reward signals in dopamine neurons. Nature *447*, 1111-1115.
Matsumoto, M., and Hikosaka, O. (2009). Representation of negative motivational value in the primate lateral habenula. Nature neuroscience *12*, 77-84.
Matta, S.G., Balfour, D.J., Benowitz, N.L., Boyd, R.T., Buccafusco, J.J., Caggiula, A.R., Craig, C.R., Collins, A.C., Damaj, M.I., Donny, E.C.*, et al.* (2007). Guidelines on nicotine dose selection for in vivo research. Psychopharmacology (Berl) *190*, 269-319.
McCudden, C.R., Hains, M.D., Kimple, R.J., Siderovski, D.P., and Willard, F.S. (2005). G-protein signaling: back to the future. Cellular and molecular life sciences : CMLS *62*, 551-577.
McLatchie, L.M., Fraser, N.J., Main, M.J., Wise, A., Brown, J., Thompson, N., Solari, R., Lee, M.G., and Foord, S.M. (1998). RAMPs regulate the transport and ligand specificity of the calcitonin-receptor-like receptor. Nature *393*, 333-339.
Meshul, C.K., and McGinty, J.F. (2000). Kappa opioid receptor immunoreactivity in the nucleus accumbens and caudate-putamen is primarily associated with synaptic vesicles in axons. Neuroscience *96*, 91-99.
Miller, R.J. (1998). Presynaptic receptors. Annu Rev Pharmacol Toxicol *38*, 201-227.
Morris, J.S., Smith, K.A., Cowen, P.J., Friston, K.J., and Dolan, R.J. (1999). Covariation of activity in habenula and dorsal raphe nuclei following tryptophan depletion. NeuroImage *10*, 163-172.
Murphy, C.A., DiCamillo, A.M., Haun, F., and Murray, M. (1996). Lesion of the habenular efferent pathway produces anxiety and locomotor hyperactivity in rats: a comparison of the effects of neonatal and adult lesions. Behavioural brain research *81*, 43-52.
Nelson, G., Chandrashekar, J., Hoon, M.A., Feng, L., Zhao, G., Ryba, N.J., and Zuker, C.S. (2002). An amino-acid taste receptor. Nature *416*, 199-202.
Nelson, G., Hoon, M.A., Chandrashekar, J., Zhang, Y., Ryba, N.J., and Zuker, C.S. (2001). Mammalian sweet taste receptors. Cell *106*, 381-390.
Nisell, M., Marcus, M., Nomikos, G.G., and Svensson, T.H. (1997). Differential effects of acute and chronic nicotine on dopamine output in the core and shell of the rat nucleus accumbens. Journal of neural transmission *104*, 1-10.
Nishikawa, T., Fage, D., and Scatton, B. (1986). Evidence for, and nature of, the tonic inhibitory influence of habenulointerpeduncular pathways upon cerebral dopaminergic transmission in the rat. Brain Res *373*, 324-336.
Noonan, M.P., Mars, R.B., and Rushworth, M.F. (2011). Distinct roles of three frontal cortical areas in reward-guided behavior. J Neurosci *31*, 14399-14412.
Novikoff, A.B. (1980). DAB cytochemistry: artifact problems in its current uses. The journal of histochemistry and cytochemistry : official journal of the Histochemistry Society *28*, 1036-1038.
Olucha-Bordonau, F.E., Teruel, V., Barcia-Gonzalez, J., Ruiz-Torner, A., Valverde-Navarro, A.A., and Martinez-Soriano, F. (2003). Cytoarchitecture and efferent projections of the nucleus incertus of the rat. J Comp Neurol *464*, 62-97.
Ozawa, A., Lindberg, I., Roth, B., and Kroeze, W.K. (2010). Deorphanization of novel peptides and their receptors. The AAPS journal *12*, 378-384.
Parajuli, L.K., Nakajima, C., Kulik, A., Matsui, K., Schneider, T., Shigemoto, R., and Fukazawa, Y. (2012). Quantitative regional and ultrastructural localization of the Ca(v)2.3 subunit of R-type calcium channel in mouse brain. J Neurosci *32*, 13555-13567.
Park, M.R. (1987). Monosynaptic inhibitory postsynaptic potentials from lateral habenula recorded in dorsal raphe neurons. Brain research bulletin *19*, 581-586.

Paxinos, G., and Franklin, K.B.J. (2001). The mouse brain in stereotaxic coordinates, 2nd edn (San Diego, Calif.: Academic Press).
Phillipson, O.T., and Pycock, C.J. (1982). Dopamine neurones of the ventral tegmentum project to both medial and lateral habenula. Some implications for habenular function. Experimental brain research *45*, 89-94.
Picciotto, M.R. (2003). Nicotine as a modulator of behavior: beyond the inverted U. Trends Pharmacol Sci *24*, 493-499.
Picciotto, M.R., Zoli, M., Rimondini, R., Lena, C., Marubio, L.M., Pich, E.M., Fuxe, K., and Changeux, J.P. (1998). Acetylcholine receptors containing the beta2 subunit are involved in the reinforcing properties of nicotine. Nature *391*, 173-177.
Pontieri, F.E., Tanda, G., Orzi, F., and Di Chiara, G. (1996). Effects of nicotine on the nucleus accumbens and similarity to those of addictive drugs. Nature *382*, 255-257.
Potrebic, S., Ahn, A.H., Skinner, K., Fields, H.L., and Basbaum, A.I. (2003). Peptidergic nociceptors of both trigeminal and dorsal root ganglia express serotonin 1D receptors: implications for the selective antimigraine action of triptans. J Neurosci *23*, 10988-10997.
Qin, C., and Luo, M. (2009). Neurochemical phenotypes of the afferent and efferent projections of the mouse medial habenula. Neuroscience *161*, 827-837.
Quina, L.A., Wang, S., Ng, L., and Turner, E.E. (2009). Brn3a and Nurr1 mediate a gene regulatory pathway for habenula development. J Neurosci *29*, 14309-14322.
Ramirez-Franco, J., Bartolome-Martin, D., Alonso, B., Torres, M., and Sanchez-Prieto, J. (2014). Cannabinoid type 1 receptors transiently silence glutamatergic nerve terminals of cultured cerebellar granule cells. PLoS One *9*, e88594.
Ranft, K., Dobrowolny, H., Krell, D., Bielau, H., Bogerts, B., and Bernstein, H.G. (2010). Evidence for structural abnormalities of the human habenular complex in affective disorders but not in schizophrenia. Psychological medicine *40*, 557-567.
Rask-Andersen, M., Almen, M.S., and Schioth, H.B. (2011). Trends in the exploitation of novel drug targets. Nat Rev Drug Discov *10*, 579-590.
Reisine, T.D., Soubrie, P., Artaud, F., and Glowinski, J. (1982). Involvement of lateral habenula-dorsal raphe neurons in the differential regulation of striatal and nigral serotonergic transmission cats. J Neurosci *2*, 1062-1071.
Ren, J., Qin, C., Hu, F., Tan, J., Qiu, L., Zhao, S., Feng, G., and Luo, M. (2011). Habenula "cholinergic" neurons co-release glutamate and acetylcholine and activate postsynaptic neurons via distinct transmission modes. Neuron *69*, 445-452.
Riobo, N.A., Lu, K., and Emerson, C.P., Jr. (2006). Hedgehog signal transduction: signal integration and cross talk in development and cancer. Cell cycle *5*, 1612-1615.
Ritter, S.L., and Hall, R.A. (2009). Fine-tuning of GPCR activity by receptor-interacting proteins. Nature reviews Molecular cell biology *10*, 819-830.
Robbins, M.J., Calver, A.R., Filippov, A.K., Hirst, W.D., Russell, R.B., Wood, M.D., Nasir, S., Couve, A., Brown, D.A., Moss, S.J.*, et al.* (2001). GABA(B2) is essential for g-protein coupling of the GABA(B) receptor heterodimer. J Neurosci *21*, 8043-8052.
Robertson, S.J., and Edwards, F.A. (1998). ATP and glutamate are released from separate neurones in the rat medial habenula nucleus: frequency dependence and adenosine-mediated inhibition of release. J Physiol *508 (Pt 3)*, 691-701.
Ronnekleiv, O.K., and Moller, M. (1979). Brain-pineal nervous connections in the rat: an ultrastructure study following habenular lesion. Experimental brain research *37*, 551-562.
Rosenkilde, M.M., Benned-Jensen, T., Andersen, H., Holst, P.J., Kledal, T.N., Luttichau, H.R., Larsen, J.K., Christensen, J.P., and Schwartz, T.W. (2006). Molecular pharmacological phenotyping of EBI2. An orphan seven-transmembrane receptor with constitutive activity. J Biol Chem *281*, 13199-13208.
Rosenkilde, M.M., Kledal, T.N., and Schwartz, T.W. (2005). High constitutive activity of a virus-encoded seven transmembrane receptor in the absence of the conserved DRY motif (Asp-Arg-Tyr) in transmembrane helix 3. Mol Pharmacol *68*, 11-19.
Ross, E.M., and Wilkie, T.M. (2000). GTPase-activating proteins for heterotrimeric G proteins: regulators of G protein signaling (RGS) and RGS-like proteins. Annual review of biochemistry *69*, 795-827.

Salas, R., Baldwin, P., de Biasi, M., and Montague, P.R. (2010). BOLD Responses to Negative Reward Prediction Errors in Human Habenula. Frontiers in human neuroscience *4*, 36.
Salas, R., Orr-Urtreger, A., Broide, R.S., Beaudet, A., Paylor, R., and De Biasi, M. (2003). The nicotinic acetylcholine receptor subunit alpha 5 mediates short-term effects of nicotine in vivo. Mol Pharmacol *63*, 1059-1066.
Salas, R., Pieri, F., and De Biasi, M. (2004). Decreased signs of nicotine withdrawal in mice null for the beta4 nicotinic acetylcholine receptor subunit. J Neurosci *24*, 10035-10039.
Salas, R., Sturm, R., Boulter, J., and De Biasi, M. (2009). Nicotinic receptors in the habenulo-interpeduncular system are necessary for nicotine withdrawal in mice. J Neurosci *29*, 3014-3018.
Sandyk, R. (1992). Pineal and habenula calcification in schizophrenia. Int J Neurosci *67*, 19-30.
Santoro, B., Chen, S., Luthi, A., Pavlidis, P., Shumyatsky, G.P., Tibbs, G.R., and Siegelbaum, S.A. (2000). Molecular and functional heterogeneity of hyperpolarization-activated pacemaker channels in the mouse CNS. J Neurosci *20*, 5264-5275.
Sartorius, A., and Henn, F.A. (2007). Deep brain stimulation of the lateral habenula in treatment resistant major depression. Medical hypotheses *69*, 1305-1308.
Seino, S., and Shibasaki, T. (2005). PKA-dependent and PKA-independent pathways for cAMP-regulated exocytosis. Physiol Rev *85*, 1303-1342.
Sharp, P.E., Turner-Williams, S., and Tuttle, S. (2006). Movement-related correlates of single cell activity in the interpeduncular nucleus and habenula of the rat during a pellet-chasing task. Behavioural brain research *166*, 55-70.
Sheffield, E.B., Quick, M.W., and Lester, R.A. (2000). Nicotinic acetylcholine receptor subunit mRNA expression and channel function in medial habenula neurons. Neuropharmacology *39*, 2591-2603.
Shelton, L., Becerra, L., and Borsook, D. (2012). Unmasking the mysteries of the habenula in pain and analgesia. Prog Neurobiol *96*, 208-219.
Shepard, P.D., Holcomb, H.H., and Gold, J.M. (2006). Schizophrenia in translation: the presence of absence: habenular regulation of dopamine neurons and the encoding of negative outcomes. Schizophrenia bulletin *32*, 417-421.
Shumake, J., Edwards, E., and Gonzalez-Lima, F. (2003). Opposite metabolic changes in the habenula and ventral tegmental area of a genetic model of helpless behavior. Brain Res *963*, 274-281.
Shumake, J., and Gonzalez-Lima, F. (2003). Brain systems underlying susceptibility to helplessness and depression. Behavioral and cognitive neuroscience reviews *2*, 198-221.
Shuster, S.J., Riedl, M., Li, X., Vulchanova, L., and Elde, R. (1999). Stimulus-dependent translocation of kappa opioid receptors to the plasma membrane. J Neurosci *19*, 2658-2664.
Simon, M.I., Strathmann, M.P., and Gautam, N. (1991). Diversity of G proteins in signal transduction. Science *252*, 802-808.
Slimak, M.A., Ables, J.L., Frahm, S., Antolin-Fontes, B., Santos-Torres, J., Moretti, M., Gotti, C., and Ibanez-Tallon, I. (2014). Habenular expression of rare missense variants of the beta4 nicotinic receptor subunit alters nicotine consumption. Frontiers in human neuroscience *8*, 12.
Sodhi, A., Montaner, S., and Gutkind, J.S. (2004). Viral hijacking of G-protein-coupled-receptor signalling networks. Nature reviews Molecular cell biology *5*, 998-1012.
Sofroniew, M.V., and Weindl, A. (1978). Projections from the parvocellular vasopressin- and neurophysin-containing neurons of the suprachiasmatic nucleus. The American journal of anatomy *153*, 391-429.
Sparks, J.A., and Pauly, J.R. (1999). Effects of continuous oral nicotine administration on brain nicotinic receptors and responsiveness to nicotine in C57Bl/6 mice. Psychopharmacology (Berl) *141*, 145-153.
Stables, J., Green, A., Marshall, F., Fraser, N., Knight, E., Sautel, M., Milligan, G., Lee, M., and Rees, S. (1997). A bioluminescent assay for agonist activity at potentially any G-protein-coupled receptor. Analytical biochemistry *252*, 115-126.

Staines, W.A., Yamamoto, T., Dewar, K.M., Daddona, P.E., Geiger, J.D., and Nagy, J.I. (1988). Distribution, morphology and habenular projections of adenosine deaminase-containing neurons in the septal area of rat. Brain Res *455*, 72-87.
Stamatakis, A.M., Jennings, J.H., Ung, R.L., Blair, G.A., Weinberg, R.J., Neve, R.L., Boyce, F., Mattis, J., Ramakrishnan, C., Deisseroth, K.*, et al.* (2013). A unique population of ventral tegmental area neurons inhibits the lateral habenula to promote reward. Neuron *80*, 1039-1053.
Stamatakis, A.M., and Stuber, G.D. (2012). Activation of lateral habenula inputs to the ventral midbrain promotes behavioral avoidance. Nature neuroscience *15*, 1105-1107.
Stead, L.F., Perera, R., Bullen, C., Mant, D., and Lancaster, T. (2008). Nicotine replacement therapy for smoking cessation. Cochrane Database Syst Rev, CD000146.
Stevens, R.C., Cherezov, V., Katritch, V., Abagyan, R., Kuhn, P., Rosen, H., and Wuthrich, K. (2013). The GPCR Network: a large-scale collaboration to determine human GPCR structure and function. Nat Rev Drug Discov *12*, 25-34.
Stevens, V.L., Bierut, L.J., Talbot, J.T., Wang, J.C., Sun, J., Hinrichs, A.L., Thun, M.J., Goate, A., and Calle, E.E. (2008). Nicotinic receptor gene variants influence susceptibility to heavy smoking. Cancer epidemiology, biomarkers & prevention : a publication of the American Association for Cancer Research, cosponsored by the American Society of Preventive Oncology *17*, 3517-3525.
Sudhof, T.C. (2004). The synaptic vesicle cycle. Annu Rev Neurosci *27*, 509-547.
Sutherland, R.J. (1982). The dorsal diencephalic conduction system: a review of the anatomy and functions of the habenular complex. Neurosci Biobehav Rev *6*, 1-13.
Swanson, L.W., and Cowan, W.M. (1979). The connections of the septal region in the rat. J Comp Neurol *186*, 621-655.
Tapper, A.R., McKinney, S.L., Nashmi, R., Schwarz, J., Deshpande, P., Labarca, C., Whiteaker, P., Marks, M.J., Collins, A.C., and Lester, H.A. (2004). Nicotine activation of alpha4* receptors: sufficient for reward, tolerance, and sensitization. Science *306*, 1029-1032.
Thompson, M.D., Percy, M.E., McIntyre Burnham, W., and Cole, D.E. (2008). G protein-coupled receptors disrupted in human genetic disease. Methods in molecular biology *448*, 109-137.
Tomar, N.R., Singh, V., Marla, S.S., Chandra, R., Kumar, R., and Kumar, A. (2010). Molecular docking studies with rabies virus glycoprotein to design viral therapeutics. Indian J Pharm Sci *72*, 486-490.
Toonen, R.F., Kochubey, O., de Wit, H., Gulyas-Kovacs, A., Konijnenburg, B., Sorensen, J.B., Klingauf, J., and Verhage, M. (2006). Dissecting docking and tethering of secretory vesicles at the target membrane. The EMBO journal *25*, 3725-3737.
Ullsperger, M., and von Cramon, D.Y. (2003). Error monitoring using external feedback: specific roles of the habenular complex, the reward system, and the cingulate motor area revealed by functional magnetic resonance imaging. J Neurosci *23*, 4308-4314.
Vertes, R.P., Fortin, W.J., and Crane, A.M. (1999). Projections of the median raphe nucleus in the rat. J Comp Neurol *407*, 555-582.
Vischer, H.F., Leurs, R., and Smit, M.J. (2006). HCMV-encoded G-protein-coupled receptors as constitutively active modulators of cellular signaling networks. Trends Pharmacol Sci *27*, 56-63.
Voets, T., Toonen, R.F., Brian, E.C., de Wit, H., Moser, T., Rettig, J., Sudhof, T.C., Neher, E., and Verhage, M. (2001). Munc18-1 promotes large dense-core vesicle docking. Neuron *31*, 581-591.
Wagner, F., Stroh, T., and Veh, R.W. (2014). Correlating habenular subnuclei in rat and mouse using topographical, morphological and cytochemical criteria. J Comp Neurol.
Waldhoer, M., Kledal, T.N., Farrell, H., and Schwartz, T.W. (2002). Murine cytomegalovirus (CMV) M33 and human CMV US28 receptors exhibit similar constitutive signaling activities. Journal of virology *76*, 8161-8168.
Wang, R.Y., and Aghajanian, G.K. (1977). Physiological evidence for habenula as major link between forebrain and midbrain raphe. Science *197*, 89-91.

Ware, J.J., van den Bree, M.B., and Munafo, M.R. (2011). Association of the CHRNA5-A3-B4 gene cluster with heaviness of smoking: a meta-analysis. Nicotine Tob Res *13*, 1167-1175.

World Health Organization. (2011). WHO report on the global tobacco epidemic, 2011 warning about the dangers of tobacco (Geneva: World Health Organization,), pp. 1 online resource.

Xie, Q., Itoh, M., Miki, T., Dong, Y.Y., and Takeuchi, Y. (1998). Occlusion of the femoral artery induced fos-like immunoreactive neurons in the lateral habenular nucleus projecting to the midbrain periaqueductal gray in the rat. Okajimas folia anatomica Japonica *75*, 167-172.

Xu, H., Staszewski, L., Tang, H., Adler, E., Zoller, M., and Li, X. (2004). Different functional roles of T1R subunits in the heteromeric taste receptors. Proc Natl Acad Sci U S A *101*, 14258-14263.

Yamaguchi, T., Danjo, T., Pastan, I., Hikida, T., and Nakanishi, S. (2013). Distinct roles of segregated transmission of the septo-habenular pathway in anxiety and fear. Neuron *78*, 537-544.

Yang, L.M., Hu, B., Xia, Y.H., Zhang, B.L., and Zhao, H. (2008). Lateral habenula lesions improve the behavioral response in depressed rats via increasing the serotonin level in dorsal raphe nucleus. Behavioural brain research *188*, 84-90.

Zhao-Shea, R., Liu, L., Pang, X., Gardner, P.D., and Tapper, A.R. (2013). Activation of GABAergic neurons in the interpeduncular nucleus triggers physical nicotine withdrawal symptoms. Current biology : CB *23*, 2327-2335.

Zhao, S., Ting, J.T., Atallah, H.E., Qiu, L., Tan, J., Gloss, B., Augustine, G.J., Deisseroth, K., Luo, M., Graybiel, A.M.*, et al.* (2011). Cell type-specific channelrhodopsin-2 transgenic mice for optogenetic dissection of neural circuitry function. Nat Methods *8*, 745-752.